1 **Orogenic lithosphere and slabs in the greater Alpine area - Interpretation of mantle structure in**
2 **the Alps-Apennines-Pannonian region from teleseismic V_p studies**
3
4 Mark R. Handy[1], Stefan M. Schmid[2], Marcel Paffrath[3], Wolfgang Friederich[3] and the AlpArray
5 Working Group[+]
6
7 [1] Institut für Geologische Wissenschaften, Freie Universität Berlin, Malteserstr. 74-100, 12249
8   Berlin, Germany; Institut für Geologie, ETH-Zürich, Sonneggstr. 5, 8092 Zürich
9 [2] Institut für Geophysik, ETH-Zürich, Sonneggstr. 5, 8092 Zürich
10 [3] Institut für Geologie, Mineralogie, Geophysik, Ruhr-Universität Bochum, 44780 Bochum, Germany
11 [+] For the complete team list visit the link at the end of the paper
12
13

15 **Abstract**
16 Based on recent results of AlpArray, we propose a new model of Alpine collision that involves
17 subduction and detachment of anomolously thick (180-200 km) European lithosphere. Our
18 approach combines teleseismic P-wave tomography and existing Local Earthquake Tomography
19 (LET) allowing us to image the Alpine slabs and their connections with the overlying orogenic
20 lithosphere at an unprecedented resolution. The images call into question the conventional notion
21 that slabs comprise only seismically fast lithosphere and suggest that the mantle of parts of the
22 downgoing European Plate is heterogeneous, containing both positive and negative V_p anomalies of
23 up to 5-6%. We attribute these to seismic anisotropy and/or compositional differences inherited
24 from the Variscan and pre-Variscan orogenic cycle, rather than to thermal anomalies. In contrast,
25 the lithosphere of the Adriatic Plate is thinner (100-120 km) and has a lower boundary
26 approximately at the interface between positive and negative V_p anomalies.
27   Horizontal and vertical tomographic slices reveal that beneath the Central and Western Alps, the
28 European slab dips steeply to the S and SE and is only locally still attached to the Alpine lithosphere.
29 However, in the Eastern Alps and Carpathians, this slab is completely detached from the orogenic
30 crust and dips steeply to the N-NE. This along-strike change in attachment coincides with an abrupt
31 decrease in Moho depth below the Tauern Window, the Moho being underlain by a pronounced
32 negative V_p anomaly that reaches eastward into the Pannonian Basin area. This negative V_p anomaly
33 is interpreted to represent hot upwelling asthenosphere that heated the overlying crust, allowing it
34 to accommodate Neogene orogen-parallel lateral extrusion and thinning of the ALCAPA tectonic
35 unit (upper plate crustal edifice of Alps and Carpathians) to the east. A European origin of the
36 northward-dipping, detached slab segment beneath the Eastern Alps is likely since its imaged down-
37 dip length matches estimated Tertiary shortening in the Eastern Alps accommodated by originally
38 south-dipping subduction of European lithosphere.
39   A slab anomaly beneath the Dinarides is of Adriatic origin and dips to the northeast. There is no
40 evidence that this slab dips beneath the Alps. The slab anomaly beneath the northern Apennines,
41 also of Adriatic origin, hangs subvertically and is detached from the Apenninic orogenic crust and
42 foreland. Except for its northernmost segment where it locally overlies the southern end of the
43 European slab of the Alps, this slab is clearly separated from the latter by a broad zone of low V_p
44 velocities located south of the Alpine slab beneath the Po Basin. Considered as a whole, the slabs of
45 the Alpine chain are interpreted as highly attenuated, largely detached sheets of continental margin
46 and Alpine Tethyan oceanic lithosphere that locally reach down to a slab graveyard in the Mantle
47 Transition Zone (MTZ).

50 **1   Introduction**
51 The prevailing paradigm of mountain building in the greater Alpine area (Fig. 1) involves subduction
52 of European continental lithosphere that is some 100-120 km thick beneath the upper Adriatic
53 Plate, lithosphere thickness being based largely on seismological criteria (Jones et al., 2010; Geissler
54 et al., 2010, Kissling et al., 2006). We refer to this as the *standard lithosphere model* of continental
55 subduction to distinguish it from a new model here involving the subduction and partial
56 delamination of much thicker, compositionally heterogeneous European mantle. We base this
57 model on recent P-wave images of the AlpArray seismological campaign (Paffrath et al., 2021b)
58 presented below.
59   We use the terms *plate* and *slab* in a strictly structural-kinematic sense to refer to bodies of
60 compositionally heterogeneous mantle and crust that have moved coherently with respect to
61 markers in both the mantle and at the surface. As pointed out by Artemieva (2011), different

geophysical techniques have given rise to a multitude of definitions of the lithosphere based on seismic, thermal, electrical, rheological, and petrological properties. Our definition therefore differs from strictly seismological definitions, which treat plates as seismically fast mantle lithosphere (e.g., Piromallo & Morelli, 2003; Wortel & Spakman, 2000). Implicit in the structural-kinematic definition of lithosphere we use is that the base of the lithosphere is a shear zone that accommodates the relative motion of plates.
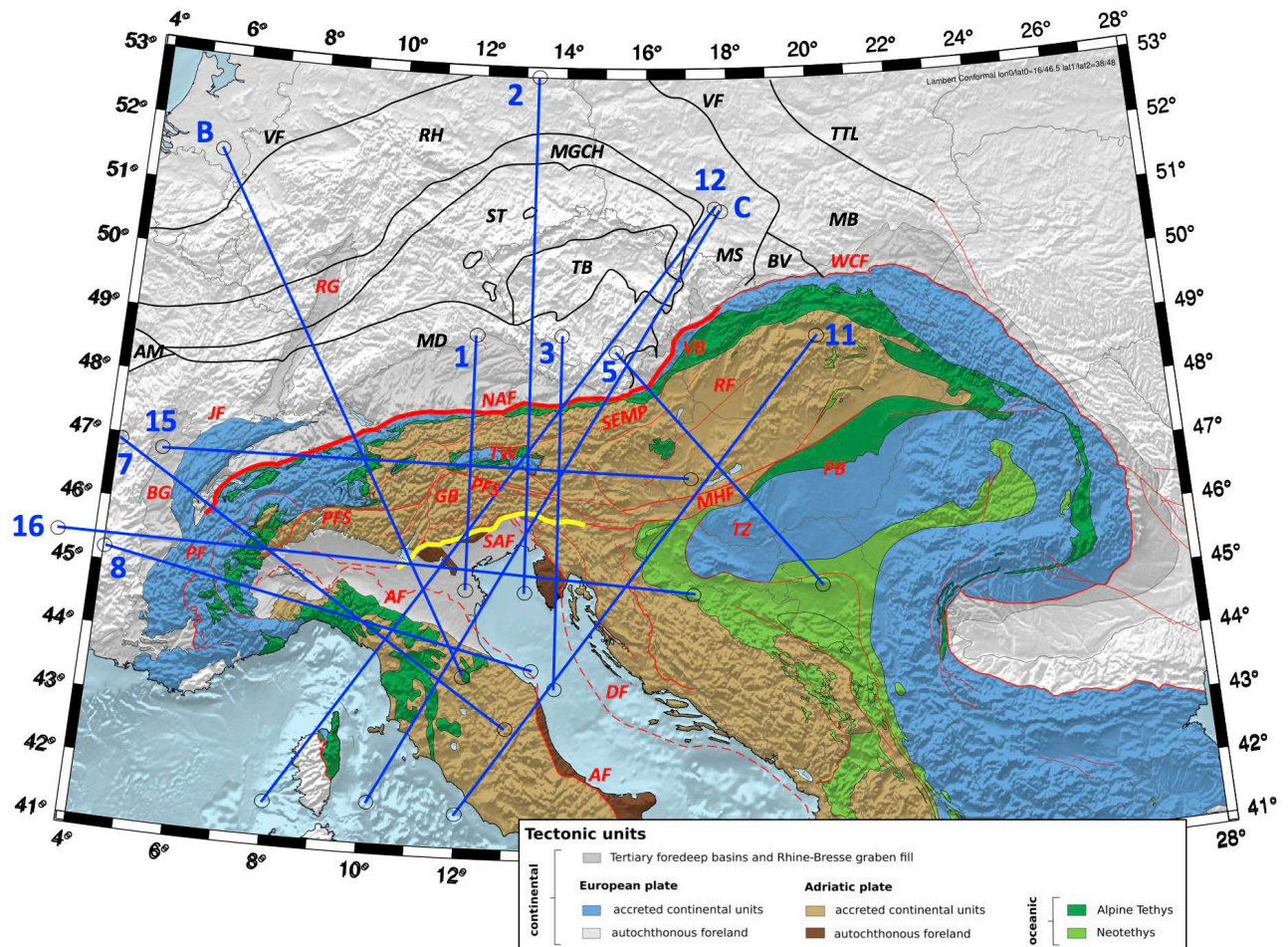
Figure 1: Tectonic map of the Alpine chain and its foreland, including Variscan units. Thin red lines – main Tertiary tectonic faults after Schmid et al. (2004) and (2008); Thin black lines –tectonic lineaments separating Variscan tectonometamorphic domains after Franke (2017, 2000), Mazur et al. (2020), and Schulmann et al. (2014). Blue lines are traces of vertical tomographic profiles in Figs. 3-7. The numbers of the traces are in accordance with their appearance in Appendix A. Thick red line along the NAF marks the Oligo-Miocene plate boundary in the Alps; Yellow line along the SAF marks the presently active plate boundary in the Alps; Green units are the Adria-Europe suture marking the Late Cretaceous-to-late Eocene plate boundary.

Alpine faults and related structures: NAF - North Alpine Front, SAF – Southern Alps Front; PFS - Periadriatic Fault System, GB – Giudicarie Belt, JF – Jura Front, PF – Penninic Front, RG – Rhein Graben, BG – Bresse Graben, TW – Tauern Window, SEMP – Salzach-Ennstal –Mariazell-Puch Fault, MHF – Mid-Hungarian Fault Zone, VB – Vienna Basin, PB – Pannonian Basin, RF – Raba Fault, WCF – Western Carpathian Front, DF – Dinaric Front
Variscan tectonic domains and faults: VF – Variscan orogenic front, RH – Rheno-Hercynian, MGCH – Mid-German Crystalline High, ST – Saxo-Thuringian, MD – Moldanubian, TB – Tepla-Barrandian, AM – Armorican Massif, BV – Bruno-Vistulian, MB – Malopolska Block, MS – Moravo-Silesian. Other faults: TTL - Teysseyre-Thornquist Line

As in other orogenic belts, the standard model of lithospheric subduction in the Alps was initially supported by teleseismic body-wave studies showing fast seismic velocity anomalies dipping

87 beneath the Alpine-Mediterranean mountain belts (Wortel and Spakman, 2000). They are often
88 inclined in the same direction as the dipping Mohos that define the base of the orogenic crust
89 (Waldhauser et al., 2002; Lippitsch et al., 2003; Spada et al., 2013). These seismically fast domains
90 are inferred to reflect negative temperature anomalies that mark descending slabs of cold
91 subcontinental lithospheric mantle, whereas positive anomalies at the base of, and surrounding,
92 these seismically fast domains are often interpreted as warm asthenospheric mantle (e.g., Spakman
93 and Wortel, 2004). In the Alps, the base of the subducting European Plate has thus been taken to be
94 the boundary between seismically fast and slow domains (respectively, blue and red domains in
95 most tomographic slices), whereas its top is the interface with the upper Adriatic Plate.
96 Seismological studies in the Western Alps have shown that this interface includes subducted crust
97 down to depths of > 90 km (Lippitsch et al., 2003; Zhao et al., 2015, 2016), corroborating geological
98 evidence of deeply subducted and exhumed fragments of oceanic and continental crust (e.g.,
99 Chopin, 1984; Schertl et al., 1991) and mantle (Brenker and Brey, 1997) preserved in the Alps (Agard
100 and Handy, 2021).
101   When assessing the geometry of subduction and plate boundaries in the Alps, it is important
102 to distinguish the Late Cretaceous-Paleogene Adria-Europe subduction plate boundary represented
103 by the Tethyan ophiolite belt along the Alps (Fig. 1) from the Oligo-Miocene collisional boundary
104 exposed along the northern Alpine orogenic front (labeled NAF in Fig. 1). Both of these boundaries
105 differ from the Pliocene-to-active plate boundary along the Southern Alpine Front (SAF in Fig. 1). In
106 the analysis below, these differently aged boundaries provide important kinematic and time
107 constraints for the tectonic interpretation of mantle anomalies. None of these geological
108 boundaries coincide at the surface, nor are they expected to merge at depth given that the Alps
109 have experience changes in the amount and direction of shortening with time (Schmid et al., 2004;
110 Handy et al., 2010). This is especially true of the eastern part of the Alps, where Paleogene N-S
111 shortening and subduction has given way to Mio-Pliocene eastward lateral extrusion of orogenic
112 crust and possibly upper mantle (e.g., Ratschbacher et al., 1991) that is still ongoing during
113 continued Adria-Europe N-S convergence (e.g., Grenerzcy et al., 2005; Serpelloni et al., 2016).
114   Controversy on Alpine subduction has arisen because the SE dip of the Alpine slab anomaly
115 in the Central and Western Alps (Lippitsch et al., 2003; Zhao et al., 2015, Lyu et al. 2017) indicating
116 "classical" SE-directed subduction of the European slab (e.g., Argand, 1924; Pfiffner et al., 1997;
117 Schmid et al., 1996) contrasts with a dip to the NE of a positive V_p slab anomaly in the eastern part
118 of the chain, i.e., east of 12-13°E in Fig. 1 (Lippitsch et al., 2003; Mitterbauer et al., 2011; Karousová
119 et al., 2013, Zhao et al. 2016). This NE dip is inconsistent with SE-directed Alpine subduction inferred
120 from the uniformly S-dip and N- to NW-directed shear sense indicators of sutured oceanic
121 lithosphere and crustal nappes all along the Alps (e.g., Schmid et al., 2004), including the Eastern
122 Alps (e.g., Handy et al., 2010 and refs. therein). The plate tectonic affinity of this part of the slab
123 beneath the Eastern Alps therefore remains unclear and debated. Proponents of a European origin
124 propose the existence of a very steeply NE-dipping overturned to subvertically oriented slab that
125 detached from the crust east of the Tauern Window (Mitterbauer et al., 2011; Rosenberg et al.,
126 2018). Proponents of an Adriatic origin of this slab based their interpretation on the tomographic
127 images of Lippitsch et al. (2013; their Fig. 13c) that depict a moderately NE-dipping slab still
128 attached to the still undeformed parts of the Adriatic Plate. They therefore proposed a late-stage
129 reversal of subduction polarity (Schmid et al., 2004; Kissling et al., 2006; Handy et al., 2015). A
130 recent review by Kästle et al. (2020) that also takes surface wave tomography into consideration
131 considers the possibility that this slab has a combined European-Adriatic origin, as discussed in
132 Handy et al. (2015).

133   In this paper, we interpret vertical and horizontal tomographic slices of the Alps generated by
134   integrating crustal and mantle tomographic P-wave models gleaned from the AlpArray seismological
135   network (Hetényi et al., 2018). This new method, described in the next section and in detail in
136   Paffrath et al. (2021b), employs teleseismic tomography and integrates the crustal/uppermost
137   mantle models of Diehl et al. (2009) and Tesauro et al. (2008) as *a priori* information into the
138   teleseismic inversion, weighted according to its reliability. This allows us to image the Alpine slabs
139   and their potential connections with the orogenic edifice as well as the fore- and hinterland
140   lithospheres at an unprecedented resolution. The images presented in sections 3 and 4 call into
141   question the conventional notion based on seismological criteria that slabs comprise only
142   seismically fast mantle lithosphere that is some 100-120 km thick. Instead, they suggest that the
143   down-going European Plate in the Alps is much thicker and contains positive and negative seismic
144   anomalies inherited from pre-Alpine (Variscan) events that, given their age, are likely to be of
145   structural and compositional, rather than thermal nature. In section 5, we showcase evidence for
146   large-scale delamination of the slabs in the Alps and northern Apennines, with slabs that have been
147   partly to entirely detached from their orogenic edifices. The discussion in section 6 revisits the
148   debate on subduction polarity in light of the new data and touches on some implications of
149   widespread delamination and slab detachment for crustal seismicity and foreland basin evolution.
150   We conclude with a conceptual 3-D visualization of mantle structure beneath the Alps and
151   Apennines that serves as a vehicle for assessing the interaction of slabs and asthenosphere at
152   depths down to the Mantle Transition Zone (MTZ).
153
154

2. Methodology

156   The images of velocity anomalies in this paper are derived from a 3D-model of P-wave velocity in
157   the crust and mantle below the greater Alpine region (Paffrath et al., 2021b). This is obtained by
158   tomographic inversion of teleseismic P-wave travel-time residuals measured on records of the
159   AlpArray Seismic Network (Paffrath et al., 2021a). Travel time residual is the difference between the
160   observed and a theoretical travel time calculated for a standard earth model. Calculation of the
161   travel-time residuals and the inversion procedure are described here in turn, as outlined in Paffrath
162   et al. (2021b, their chapt. 2 and Appendix A1).
163   The travel-time database comprises 162366 onsets of 331 teleseismic earthquakes of
164   magnitude 5.5 or higher at epicentral distances between 35 and 135 degrees occurring between
165   January 2015 and July 2019. Paffrath et al. (2021b) subtracted the array average from these
166   residuals on an event-to-event basis. This procedure avoids errors in earthquake origin time and
167   reduces influences of heterogeneities in earth structure outside the inversion domain (see Paffrath
168   et al., 2021a on obtaining highly accurate travel-time residuals suitable for teleseismic inversion).
169   Inversion of the travel-time residuals to obtain the P-wave velocity perturbations in the
170   depth slices and profiles of Vp anomalies below is a complex process. The aim of inversion is to find
171   a model that reduces the misfit between the observations and predictions of travel times to a
172   certain threshold value. Iteration of the inversion ends if either the observations fit within their
173   uncertainties or if the misfit reduction stagnates when executing further iterations.
174   Because teleseismic waves propagate subvertically through the crust, the resolution of
175   strongly heterogeneous crust is poor. Correcting for heterogeneities requires a velocity model of
176   the crust, termed an *a priori* model (e.g., Kissling, 1993), that is based on independent data, e.g.,
177   reflection and refraction seismics, receiver functions, local earthquake tomography. The standard
178   correction method involves computing travel-time residuals for the crustal model on the
179   assumption of idealized wave fronts, then subtracting these residuals from the observed residuals.

180   This oversimplifies the true ray paths, which are refracted in the crust and underlying mantle
181   depending on vertical and azimuthal incidence.
182   The novel approach of Paffrath et al. (2012b) entails creating a starting model for inversion
183   iteration by superposing a 1-D standard earth model (here taken to be model AK135 of Kennett et
184   al., 1995) and a 3-D *a priori* model of the crust and uppermost mantle, then damping the inversion
185   according to the reliability of the *a priori* model (see below and Paffrath et al., 2021b on inversion
186   regularisation). The purpose of the *a priori* model is to account for strongly heterogeneous velocity
187   structure, particularly in the crust. In constructing their *a priori* crustal model, Paffrath et al. (2021b)
188   discretize the EuCRUST-07 model of Tesauro et al. (2008) and the fully three-dimensional, high-
189   resolution P-wave velocity model of Diehl et al. (2009) for the central Alpine region. In addition,
190   information on Moho depth in the Alpine region is refined using the study of Spada et al. (2013).
191   The P-wave velocity at a given point in the *a priori* model is a weighted average of the Diehl
192   and Tesauro models, with weights depending on the reliability of Diehl's model as measured by the
193   values of the diagonal elements of the resolution matrix (RDE). For values of RDE above 0.15 the
194   crustal model is dominated by Diehl's model, whereas for values below, the model of Tesauro et al.
195   (2008) takes over smoothly (see Paffrath et al. 2001b, their Fig. 2 for the areas in which these
196   models dominate). For regions of the inversion domain beyond the extent of the *a priori* crustal
197   model, Paffrath et al. (2021b) assume the modified standard earth model AK135 of Kennett et al.
198   (1995) and the 1D-reference model used by Diehl et al. (2009). The advantage of this multifaceted
199   approach is that it provides a comprehensive model of crust and mantle structure that allows for
200   refined interpretation of the orogenic crust and its transition to the underlying mantle lithosphere,
201   including subducted slabs.
202   Paffrath et al. (2021b) assess the resolution of mantle structures imaged in this study by
203   employing different general tests, as well as very specific resolution tests that focus on crucial,
204   smaller scale structures in the Alps, e.g., gaps and different dip directions of slabs. Among the general
205   tests are two checkerboard tests which regularly alter the velocity of the mantle in a synthetic model
206   by applying a perturbation of +/- 10% in P-wave velocity on different cell sizes of 2 x 2 x 3 grid points
207   and 3 x 3 x 4 grid points (Fig. 7 in Paffrath et al. 2021b). Gaps between the cells remain unperturbed
208   in order to analyse smearing throughout the irradiated model domain.
209   Checkerboard tests show that, due to the uneven event distribution, smearing is more
210   prominent in the NW-SE direction (Paffrath et al. 2021b, their Figs. 8-9). Hence, velocity anomalies in
211   cross sections of slabs that dip in this vertical plane tend to be elongated in a down dip direction and
212   lose amplitude, whereas structures trending perpendicular to this direction tend to be broadened
213   along strike of the slab (Paffrath et al. 2021b, their Fig. 10). Generally, vertical smearing is greater at
214   shallow depths and horizontal smearing increases with depth. Whereas the general recovery of the
215   positions of the coarse checkerboard anomalies (75 x 75 x 60 km) is excellent down to the bottom of
216   the inversion domain at 600 km, the amount of smearing increases with depth, decreasing the
217   resolution below ~400 km to several tens of kilometers.
218   For smaller scale anomalies (50 x 50 x 45 km), recovery of the pattern in checkerboard tests is
219   impeded already below ~300 km depth, where smearing in the NW-SE direction as well as with depth
220   becomes more significant. Also, the amplitude of these smaller anomalies decreases strongly at
221   greater depths. Paffrath et al. (2021b) state that anomalies below the 600 km depth marking the
222   lower boundary of their inversion domain may be amplified and thus appear to lie above this
223   boundary. This is due to the hybrid approach of their tomography which only accounts for three-
224   dimensional velocity perturbations within the inversion domain. To conclude this section, Paffrath et
225   al. (2021b) show that their source-receiver setup is able to distinguish fundamental differences in the

226 geometry of slabs on the scale of tens to hundreds of km, thus aiding us in interpreting these
227 structures.
228
229

230 ## 3. Mantle velocity structure

231 For highlighting and interpreting the major mantle structures, we found it useful to trace contours
232 of both positive and negative velocity anomalies in horizontal tomographic depth slices, then
233 superpose these traces on the tectonic map of the Alps (Fig. 2) and compare them with anomaly
234 contours in profiles across the orogen (Figs. 3-6). The surface location of the aforementioned plate
235 boundaries on these profiles are used as markers (e.g., Fig. 7). Also included in the profiles is the
236 trace of the 7.25 km/s iso-velocity contour from the P-wave local earthquake tomography images of
237 Diehl (2009). We use this contour as a proxy for the Moho in the entire Alps in lieu of other Moho
238 models which are either local in their coverage (e.g., Behm et al., 2007; Brückl et al., 2007 in the
239 Eastern Alps) or were found to provide inconsistent estimates of the Moho depth (Spada et al.,
240 2013, e.g., in the Apennines and Ligurian region). The reader is referred to Kind et al. (2021) for a re-
241 assessment of Moho depth. The crustal structure in the profiles is taken from Alpine cross sections
242 of Schmid et al. (2004, 2013, 2017) and Cassano et al. (1986), whereas schematic Variscan crustal
243 cross sections are from Franke et al. (2017), Franke (2020), Mazur et al. (2020) and Schulmann et al.
244 (2014).
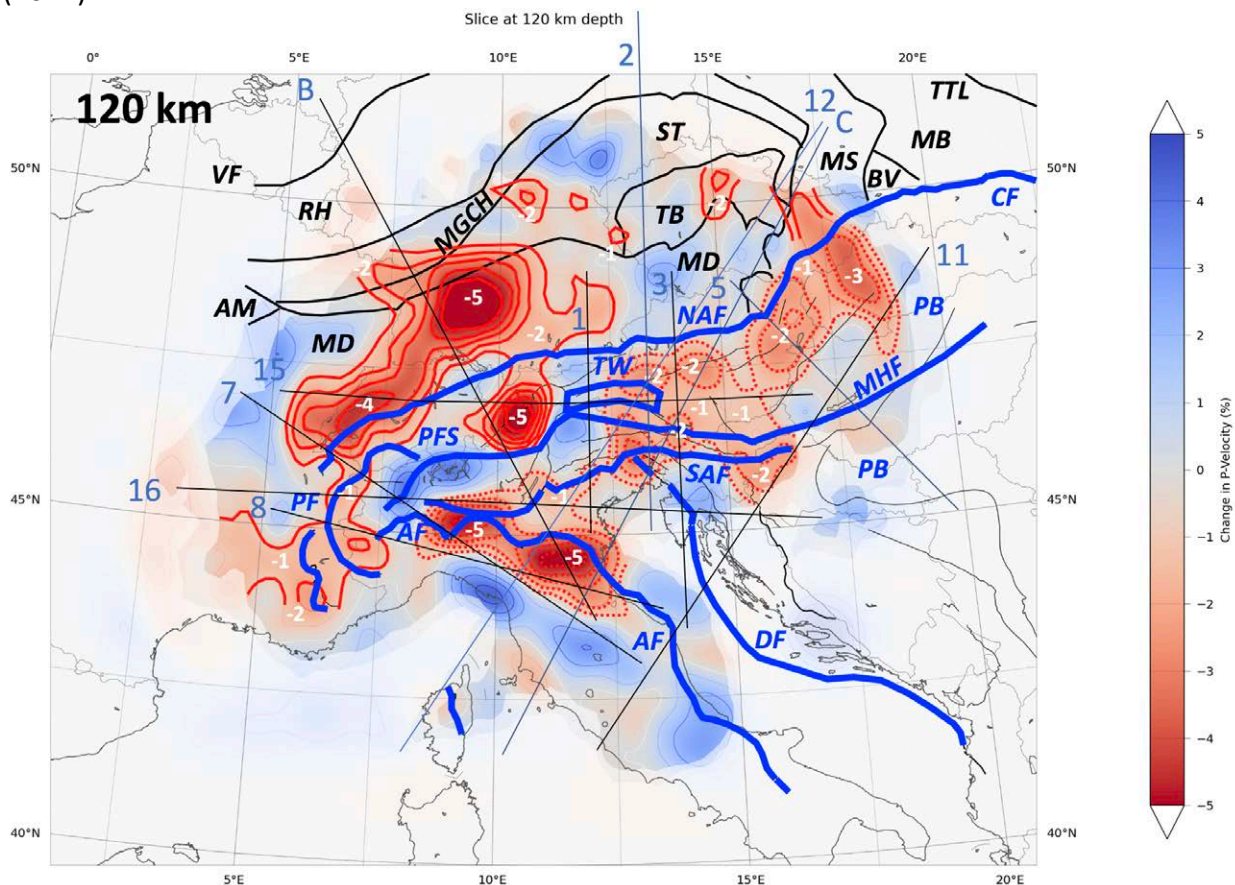
245
246 **Figure 2**: Horizontal V_p tomographic slice at 120 km depth in rhe mantle. Blue and red areas represent positive
247 (+V_p) and negative (-V_p) anomalies, respectively. Contours of slow anomalies emphasized with thick red lines. Solid
248 red contours - negative velocity anomalies interpreted to correspond to pre-Alpine compositional domains;
249 dashed red lines - negative velocity anomalies interpreted to correspond to positive thermal anomalies in the
250 mantle (see text for explanation). Thin black lines indicate the traces of all the profiles displayed in Figures 3 to 6.
251 Thick blue lines – main Alpine structures: NAF - North Alpine Front, SAF – Southern Alpine Front; Other Alpine

252 structures and related features: PFS - Periadriatic Fault System, PF – Penninic Front, TW – Tauern Window, PB –
253 Pannonian Basin, MHF – Mid-Hungarian Fault Zone, WCF – Western Carpathian Front. Thin black lines – Variscan
254 boundaries: VF – Variscan orogenic front, RH – Rheno-Hercynian, MGCH – Mid-German Crystalline High, ST – Saxo-
255 Thuringian, MD – Moldanubian, TB – Tepla-Barrandian, AM – Armorican Massif, BR – Bruno-Vistulian, MB –
256 Malopolska Block, MS – Moravo-Silesian. Other faults: TTL - Teysseyre-Thornquist Line.
257
258 A striking feature in horizontal slices at 100 to 220 km depth is the lateral continuity of $-V_p$
259 anomalies of up to 5-6% which reaches from the northern Alpine foreland across the Alpine
260 orogenic front to beneath the Western and Central Alps, as well as the westernmost part of the
261 Eastern Alps (Fig. 2, solid red contours). In three profiles crossing these parts (profiles B, 1 of Figs.
262 3B, 3C, 4A), $+V_p$ and $-V_p$ anomalies in the 100-220 depth interval form coherent, inclined layers and
263 together outline a package that dips beneath the Alpine front to below the center of the orogen.
264 The base of this package is interpreted to be the base of the lithosphere, or lithosphere-
265 asthenosphere boundary, LAB, which corresponds to the base of the moving plate and/or slab in a
266 strictly structural-kinematic sense. The layered structure making up the European lithosphere (see
267 next chapter below) continues down-dip to the SE and beneath the core of the orogen, where it is
268 interrupted, marking a slab tear (Figs. 3B, 4A). The putative location of the Alpine Tethys suture
269 projected downward into the mantle in all profiles (dashed green line) is hypothetical and drawn in
270 all profiles merely to show the affinity of the former Adria-Europe plate boundary to the European
271 slab (see chapter 5). Profile 8 across the foreland of the southernmost Western Alps (Fig. 3A)
272 contains part of the Moldanubian core of the Variscan orogen (Franke et al., 2017) and differs from
273 other profiles across the Alps in featuring only a high velocity layer to some 150 km depth and
274 dipping slightly beneath the front of the Alps.
275

Section 8 – W. Alps - N. Apennines
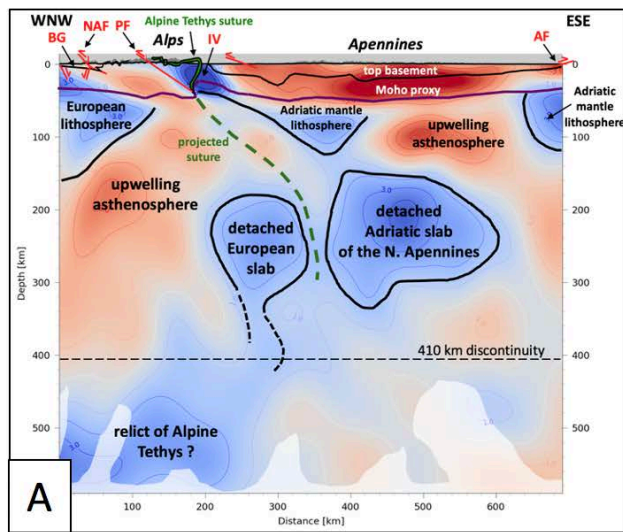
Section 7 – W. Alps – Apennines
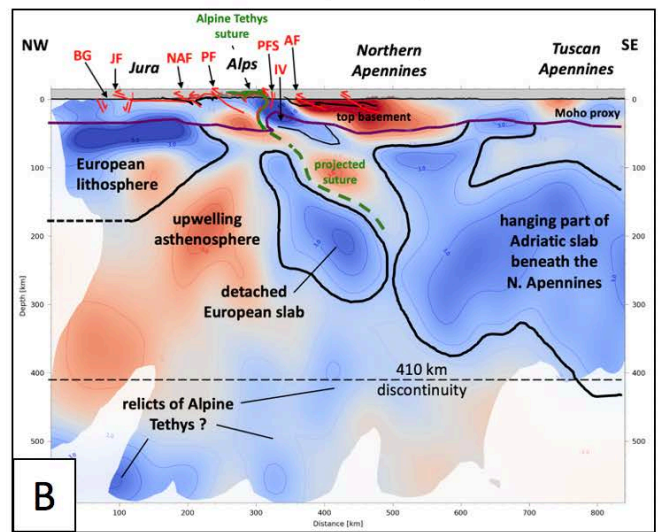
Section B – C. Alps – N. Apeninnes
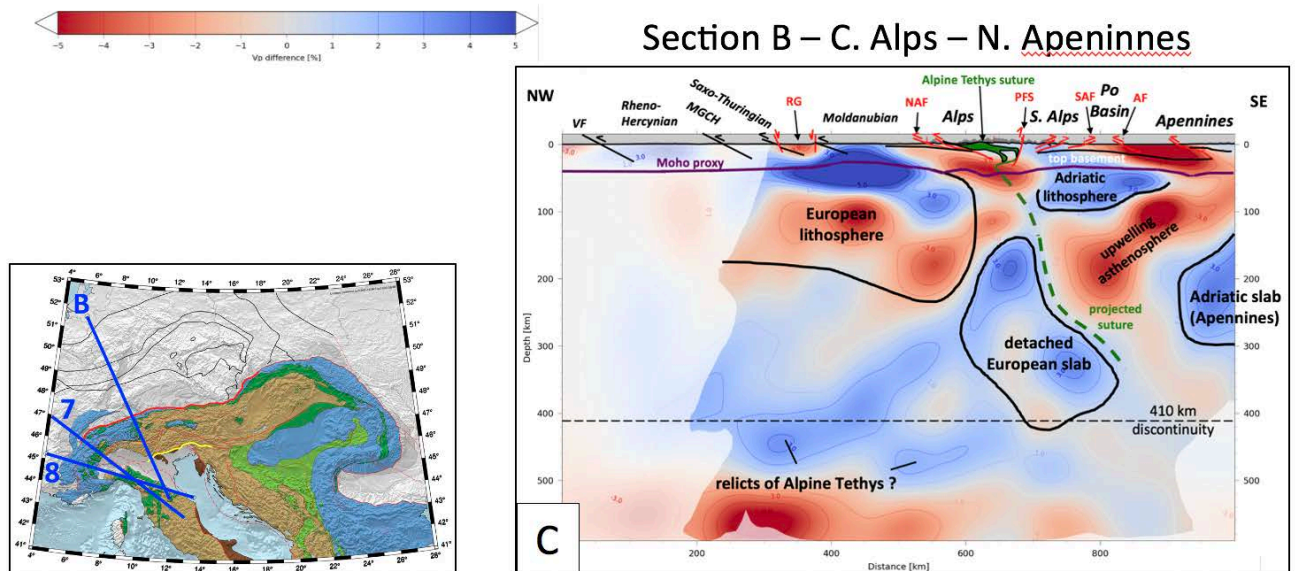
Figure 3: Cross sections of the Western and Central Alps along traces of profiles 8, 7 and B shown in inset: (A) Western Alps; (B) Western Alps from the Bresse Graben to the Northern Apennines, parallel to profile B of Lippitsch et al. 2003; (C) Central Alps from the Variscan Belt to the Po Basin and Northern Apennines. Black solid lines: outlines of the European lithosphere, Adriatic lithosphere and detached to semi-detached slab material. Green dashed line – putative trace of Alpine Tethys suture based on the location of this suture in the schematic crustal cross sections depicted above the Moho proxy. The Moho proxy follows the V_p contour of 7.25 sec^{-1} obtained from the 3D crustal model of Diehl et al. (2009), part of the *a priori* model for obtaining crustal correction that was incorporated into the tomographic model (Section 2). Geological cross sections largely after Schmid et al. (2004, 2013, 2017) and Cassano et al. (1986); Variscan crustal cross sections after Franke (2017, 2000), Mazur et al. (2020), and Schulmann et al. (2014).

Strong -V_p anomalies of 3-5% (contoured solid red in Fig. 2) generally underlie the central and western parts of the Moldanubian domain in the Alpine foreland, and run somewhat oblique to the Variscan domain boundaries. They are not aligned with the Tertiary Bresse and Rhine Grabens of Oligocene age (Fig. 1). Further to the east, in the area traversed by profiles 2 and 3 (Fig. 2), the subhorizontally oriented European lithosphere is characterized by dominantly positive velocity anomalies that cross beneath the front of the Alps and abut a low velocity area in the central part of the Alps (see Figs. 4B & 4C; stippled red contours in Fig. 2). A large 2% positive anomaly underlies

the Moldanubian and Tepla-Barrandean domains beneath the foreland of the Eastern Alps, but does not extend beneath the orogenic front of the Eastern Alps (Fig. 2; profiles 2 and 3 in Figs. 4B, 4C).
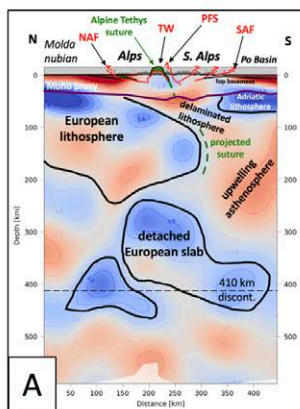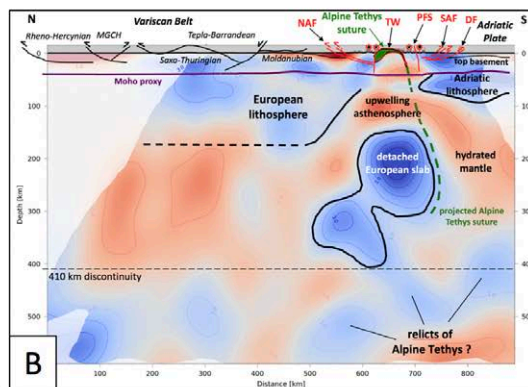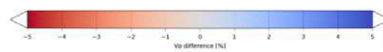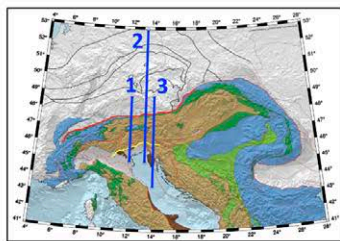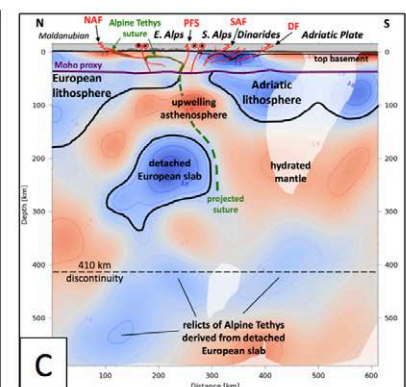
Figure 4: Cross sections of the Eastern Alps along traces 1, 2 and 3 shown in inset: (A) profile 1 (TRANSALP profile) from the Variscan foreland to the Po Basin. The thick European lithosphere has the same structure as beneath the Central Alps (Fig. 3) and is partly detached; (B) Profile 2 (EASI profile) from the Variscan Belt to the Dinaric Front and Adriatic Plate. The base of the European lithosphere is mostly undefined seismically and the European slab is detached; (C) Profile 3 (ALP01 profile) from the Variscan Belt to the Adriatic Plate. See legend of Fig. 3 for further explanations. Alpine and related structures: NAF - North Alpine Front, SAF – Southern Alps Front; PFS - Periadriatic Fault System, TW – Tauern Window, DF – Dinaride Front

In the Eastern Alps, the negative anomaly contours at 120 km depth in Fig. 2 (dashed red contours) form a broad maximum of 2-5% in map view located between the Northern and Southern Alpine fronts, and extending eastward from beneath the middle of the Tauern Window to the Pannonian Basin. Beneath the Eastern Alpine foreland, the upper 80-100 km are characterized by a broad, moderately positive V_p anomaly of 1-2%. This eastern area shows no horizontal layering of $+V_p$ and $-V_p$ anomalies (profiles 2 and 3 of Figs. 4B, 4C), in contrast to the layering seen beneath the foreland in the profile immediately to the west (profile 1, Fig. 4A). The mantle structure beneath the core of the Eastern Alps (profile 15, Fig. 5A) and beneath the transition to the Pannonian Basin (profiles 3 and 15, Figs. 4C, 5A) is marked by a shallow, strongly negative anomaly lid and, at depths between 150 and 400 km, by a strong, blob-like positive anomaly (5-6%) surrounded by a negative anomaly and unconnected to the Alpine-Carpathian foreland (profiles 2, 3, 12 in Figs. 4B, 4C, 6A). The pronounced E-W change in anomaly structure below the core of the Alps is best seen in the orogen-parallel profiles (profile 15, Fig. 5A), where the 150-200 km thick positive-negative velocity layering characteristic of the Central and Western Alps gives way in the Eastern Alps, more precisely beneath the western Tauern Window, to a negative anomaly extending down to about 130 km underlain by the deep (130-300 km) positive anomalies mentioned above. In the next chapter, we interpret this orogen-parallel change to represent a first-order difference in the structure and composition of the subducted and delaminated slabs beneath the Alps.

325   The transitional area between Eastern Alps and Western Carpathians (profile 5, Fig. 5B) and
326 the Pannonian Basin (profile 11, Fig. 6B) is characterized by widespread $-v_p$ anomalies and by the
327 almost complete absence of $+v_p$ anomalies above the 410 km discontinuity marking the top of the
328 Mantle Transition Zone. These $-v_p$ anomalies extend to the shallow mantle and directly underlie the
329 7.25 km/s Moho proxy marking the base of thinned orogenic crust. Weak $+v_p$ anomalies directly
330 below the Moho are restricted to small parts of the Pannonian Basin (profile 11 in Fig. 6B).
331 However, stronger $+v_p$ anomalies underlying the Moho are found beneath the Adriatic Sea (profiles
332 1, 2, 3 and 11, Figs. 4A-C, 6B), marking the still largely undeformed part of the plate of the same
333 name.
334
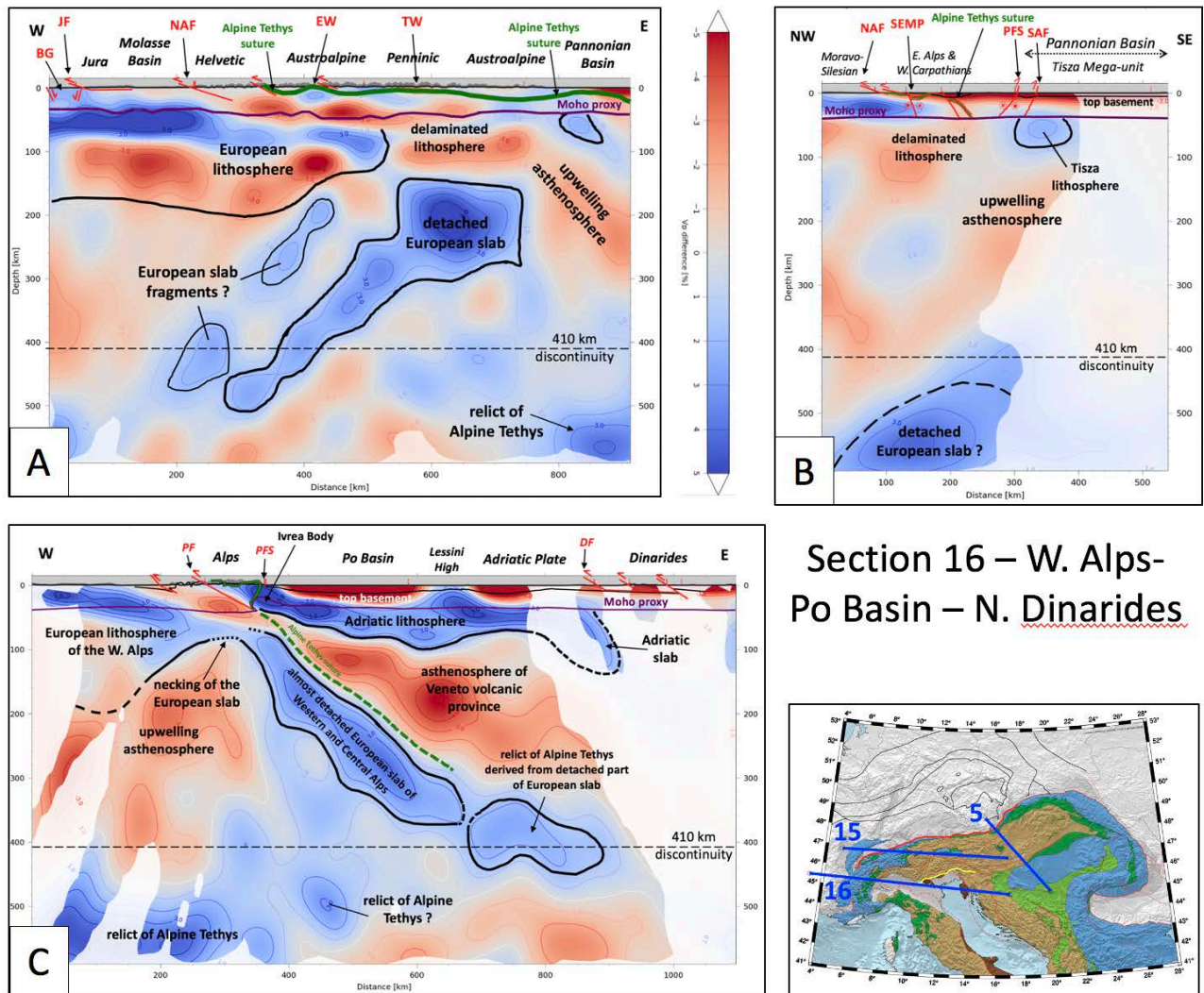
335
336 **Figure 5**: Cross sections of the Alps along traces 15, 5 and 16 shown in inset: (A) Orogen-parallel profile 15 from
337 the Central Alps across the Eastern Alps to the Pannonian Basin; note the decrease in thickness of the European
338 lithosphere before its delamination from the crust at and east of latitude 12°E crossing the area of the western
339 part of the Tauern Window (TW); (B) Profile 5 from the Variscan Belt in the northwest to the Pannonian Basin in
340 the southeast across the transitional area between Eastern Alps and Western Carpathians. The European
341 lithosphere has completely delaminated during Neogene stretching in the greater Pannonian area that formed a
342 backarc basin in the upper plate consisting of the ALCAPA and Tisza Mega-units during Carpathian rollback
343 subduction. See legend of Fig. 3 for further explanations; (C) Profile 16 from the Western Alps across the Po Basin
344 to the northern Dinarides (same as profile M1 in Paffrath et al. 2021b); note the apparent dip of the still-attached

European slab beneath the Western and Central Alps, as well as the trace of a slab of Adriatic lithosphere under the northern Dinarides.

Beneath the northern Dinarides (profile 11, Fig. 6B), no positive anomaly deeper than 100 km is observed. The resolution is poor in this area, but the interpretation is in line with previous teleseismic studies (e.g., Bijwaard & Spakmann, 2000; Wortel & Spakmann, 2000; Piromallo and Morelli, 2003; Spakman and Wortel, 2004; Serretti and Morelli, 2011; Koulakov et al., 2009). However, somewhat further to the north, beneath the northernmost Dinarides in Istria crossed by profile 16 (Fig. 5C), a generally northeast-dipping slab anomaly is fairly well resolved beneath the Dinaride front, reaching a depth of about 140 km. Note that profile 16 is the same as that presented as profile M1 in Paffrath et al. (2021b).
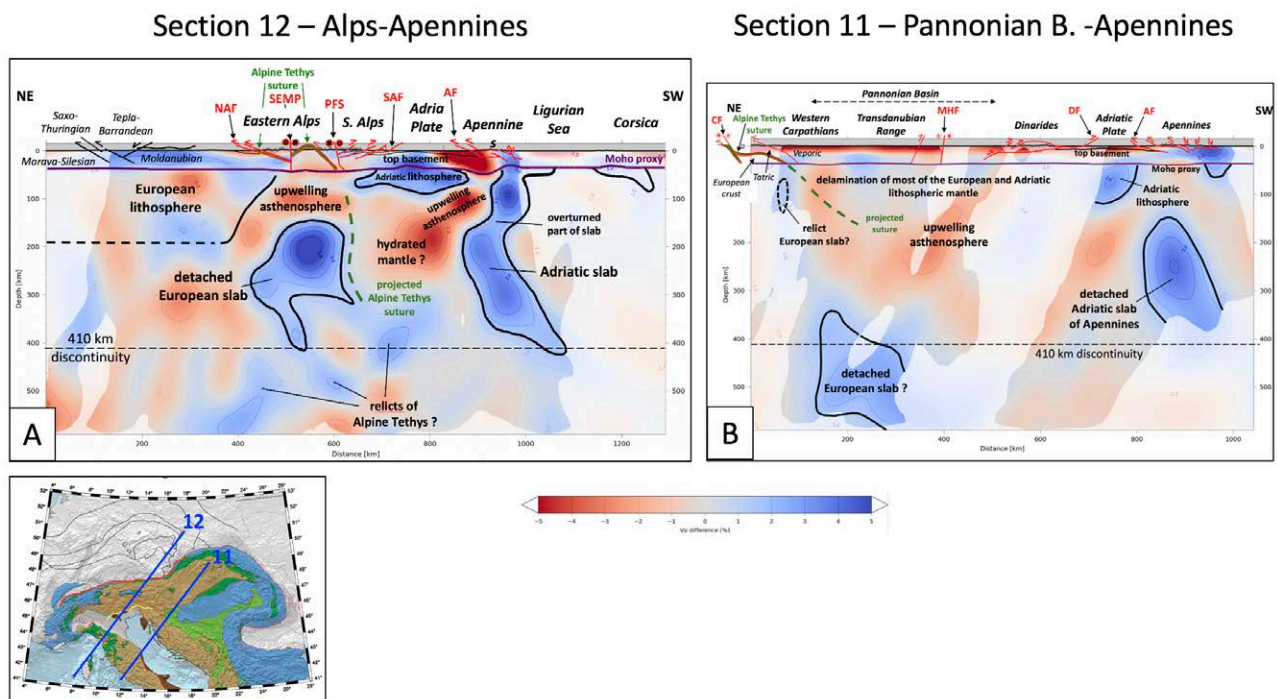
Figure 6: Profiles 12 and 11 along traces shown in Figs. 1 and 2 across the greater Alpine area, Adria and the Apennines: (A) Profile from the Variscan Belt across the Eastern Alps to the northern Apennines and the Ligurian Basin. The European slab beneath the Alps is detached, whereas the Adriatic slab beneath the Apennines hangs subvertically and is partly overturned (see text); (B) Profile from the Central Western Carpathians across Pannonian Basin, northern Dinarides, Adriatic plate, Central Apennines to the Tyrrhenian Sea. The European lithosphere is completely delaminated, the Adriatic slab beneath the Dinarides is almost absent and the Adriatic slab beneath the Apennines is detached from a remnant of the Adriatic lithosphere beneath the Adriatic Sea. See legend of Fig. 3 for further explanations. Alpine faults and related structures (labeled red): NAF - North Alpine Front, SAF – Southern Alps Front; PFS - Periadriatic Fault System, SEMP – Salzach-Ennstal-Mariazell-Puch Fault, MHF – Mid-Hungarian Fault Zone, CF – Carpathian Front, DF – Dinaric Front, AF – Apennine Front.

A large, subvertically dipping positive anomaly directly below the Northern Apennines in profile 12 (Fig. 6A) is only connected to the crust near the Ligurian Sea and disconnected from the flat-lying high V_p mantle below the undeformed part of the Adriatic Plate further to the NE. This Adria-derived slab dips down to the 410 km discontinuity. Further to the southeast beneath the Tuscan Apennines in profile 11 (Fig. 6B), this anomaly is completely disconnected from the orogenic crust and dips steeply to the SW in a depth interval of 100-350 km. In a profile parallel to the Apennines (profile 7, Fig. 3B), this positive anomaly is seen to lose its connection with the orogenic crust between profiles 12 and 11 in Figs. 6A and 6B. Unfortunately, the resolution drops off to the SW

377   beneath the Ligurian and Tyrrhenian Seas, but the faint anomalies in the former region suggest that
378   the Moho proxy is directly underlain by a negative anomaly.
379
380
381   4. **Choices in the interpretation of seismic structure**
382   The tomographic profiles in Figs. 3-6 depict relative velocities as percentages of deviation from a
383   mean velocity model for crust and mantle (Paffrath et al. 2021b). There are two main challenges in
384   interpreting the anomaly patterns down to a depth of around 600 km: (1) Distinguishing the effects
385   of the present thermal state of the rocks from composition and structural anisotropy on the
386   anomalies. This is difficult, if not impossible, in the absence of corroborative evidence from
387   independent approaches, e.g., heat flow, gravity, conductivity and/or other seismological methods;
388   (2) accounting for poor resolution of the tomographic images that often precludes a unique
389   determination of the geometry of the anomalies. This is especially true of anomalies at great depth
390   in the mantle, where vertical smearing blurs the images (Foulger et al., 2013).
391   Further headway in interpretation can be made by invoking geological criteria and what we
392   broadly call "the geodynamic context" in order to weigh the consistency, and therefore the
393   plausibility, of some interpretations over others. To illustrate this important point, we consider
394   profile B across the Central Alps in Fig. 3C, shown without interpretation in Fig. 7A and with two
395   contrasting interpretations in Figs. 7B and 7C. This profile is a good place to begin our interpretative
396   foray, because the geology (i.e., structure, kinematics, metamorphism, thermal and stratigraphic
397   ages) is well known along this classic section of the Alps (e.g., Schmid et al., 1996, 2004) and
398   previous active-source seismology provides tight constraints on the crustal structure down to the
399   Moho (Pfiffner and Hitz, 1997) and other sources in NFP-20 volume (Pfiffner et al. 1997, eds).
400   The uninterpreted profile B of Fig. 7A shows two main features:(1) the positive-negative
401   anomaly layering extending down to about 200 km observed in the Alpine foreland and extending
402   to well south of the Northern Alps Front down to 180 km depth, as described in the previous
403   section; and (2) domains of deep-seated positive anomalies labeled with question marks, one
404   dipping northward from the Southern Alps down to the 410 km discontinuity below the Alpine
405   foreland, a second minor one dipping southward below the Po Basin. In Fig. 7B, the positive-
406   negative anomaly layering is interpreted to make up a coherent kinematic entity that moved as a
407   unit with respect to the orogenic front and was subducted to the south beneath the Adriatic Plate.
408   The -V_p layer is interpreted to form the bottom half of the lithosphere, i.e., the non-convecting part
409   of the mantle. We point out that not all plates in the greater Alps area comprise such thick,
410   heterogeneous lithosphere. Indeed, as shown in the next section, the Adriatic Plate and the Adria-
411   derived slab beneath the Apennines comprise lithosphere in the standard sense of a seismically
412   "fast", more homogeneous kinematic entity.
413   The slab of thick lithosphere descending beneath the Northern Alpine front in Fig. 7B is
414   interpreted to be broken, with its fragment continuing down to the 410 km discontinuity beneath
415   the Po Basin. Weaker positive anomalies beneath the Alps in the 300-600 km depth interval may be
416   subducted and detached relics of the Alpine Tethyan Ocean. However, resolution is poor at these
417   depths, so our interpretation of such relics is speculative, as signified by question marks in the
418   figures.
419   In the interpreted profile B (Fig. 7B) other -V_p anomalies in the mantle occur immediately
420   beneath the Moho in the cores of the Alps and Apennines where the Moho lies at c. 50 km depth
421   and where the lower crust is also characterized by low V_p. Finally, a deep-seated -V_p anomaly is
422   found below the Adriatic lithosphere, between the detached part of the European slab and the
423   Northern Apennines slab derived from Adriatic lithosphere (Fig. 7B). In the former case, the -V_p

424 anomaly in the mantle immediately below the Moho is interpreted to manifest a depression of the
425 absolute velocities by the occurrence of hydrous, less-dense and therefore seismically slower
426 material in the subduction channel. In the case of the deep-seated -V_p anomaly labeled "upwelling
427 asthenosphere", the negative anomalies of up 5-6% could possibly be caused by still hot, upwelling
428 asthenosphere. However, as argued in section 6.3, this would need a ΔT of some 600-700°C
429 resulting in temperatures well above 1400°C. Following the suggestion by Giacomuzzi et al. (2011),
430 we envisage hydrated, possibly decarbonated mantle (Malusà et al. 2018, 2021) in a backarc
431 position behind the descending non-detached and detached parts of the European lithosphere
432 rather than still-existing, substantially elevated temperatures as a suitable explanation for the low
433 V_p in this area.

434
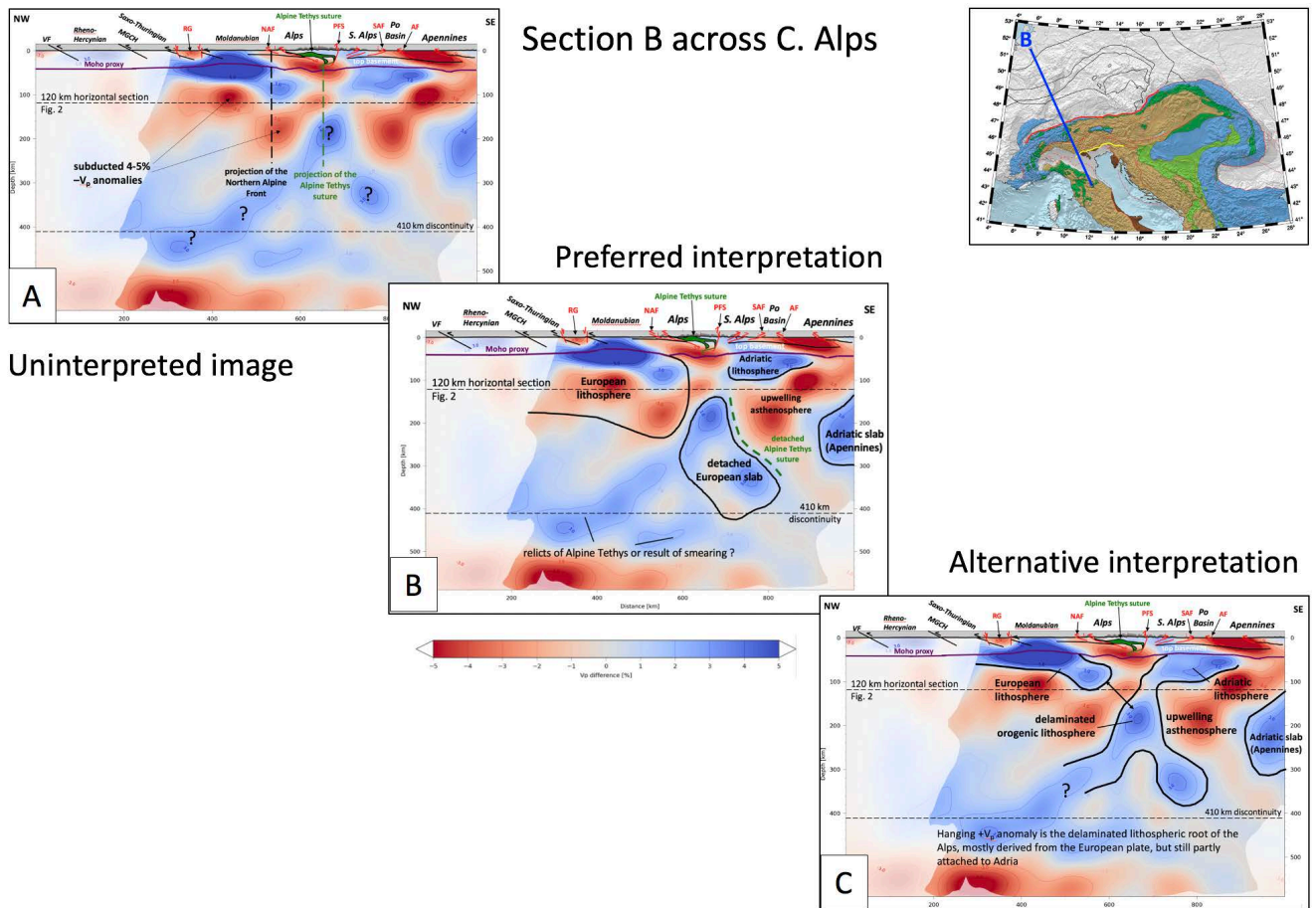
435
436 **Figure 7**: Raw image of vertical tomographic profile B across the Central Alps and two alternative interpretations:
437 (A) Raw image showing layered positive and negative V_p anomalies extending from the Variscan Belt to south of
438 the Northern Alpine Front (NAF, see also Fig. 2); (B) Preferred interpretation shown in Fig. 3C, indicating
439 coherence of layered positive and negative V_p anomalies that are interpreted as thick and old (Variscan or older?)
440 European lithosphere dipping to the south beneath the Alps. The European slab is detached. In contrast, the
441 Adriatic lithosphere beneath the Po Basin and Apennines is thin and underlain by a large negative anomaly
442 interpreted as upwelling asthenosphere; (C) Standard interpretation of lithosphere as comprising only positive V_p
443 anomalies, thought to be old, cold lithosphere. The long N-dipping positive V_p anomaly is interpreted as the
444 delaminated lithospheric root of the Alps, mostly derived from the European Plate, but still partly attached to the
445 Adriatic Plate (see text for discussion).

446

447   In the contrasting interpretation shown in Fig. 7C, all anomalies are considered primarily to
448 reflect temperature anomalies, such that positive anomalies at depths below the Moho are
449 interpreted as subducted lithosphere, whereas negative anomalies below the Moho are equated

450 with hot asthenosphere and are not part of a subducted plate. This is in line with the thermo-
451 rheological definition of a descending sheet of rigid and cold lithosphere. Thus, the base of the
452 positive anomaly extending from the European foreland to below the Alpine front would mark a
453 descending lithospheric plate only 80 km thick, whereas the long north-dipping, positive anomaly
454 domain in this profile could be interpreted as subducted Adriatic lithosphere connected to Adriatic
455 lithosphere beneath the Po Basin and the Adriatic Sea (Fig. 7C). If true, this would imply an
456 anomolously thin European continental lithosphere and necessitate hundreds of kilometers of
457 shortening in the Alps within predominantly S-facing folds and thrusts for which there is no
458 geological evidence. Most folding and thrusting in the Alps is N- to NW-vergent, as documented by
459 more than a century of detailed study. Within the Southern Alps where S-vergent thrusting is
460 indeed observed, only about ≤ 72 km of shortening was accommodated, mostly in Oligo-Miocene
461 time (Schönborn, 1992; Schmid et al., 1996; Rosenberg and Kissling, 2013). This effectively
462 precludes any scenario involving north-directed subduction of large amounts of Adriatic lithosphere
463 beneath the Alps. Moreover, the continuity of the NW-dipping +Vp anomaly in Fig. 7C may reflect
464 smearing, which is prevalent in profiles with this azimuthal orientation (see section 2 above).
465   This leaves Fig. 7B with its anomalously thick (180-200 km) subducting European lithosphere as
466 the preferred interpretation. The total length of subducted European slab according to the
467 interpretation in Fig. 7B is roughly 400 km, as measured between the Northern Alpine Front down
468 to the 410 km discontinuity (see also profile 6 in Appendix A1). This is consistent with the amount of
469 shortening in the Alps since European lithosphere entered the subduction zone in the Alps in
470 Eocene time (Schmid et al., 1997; Handy et al., 2010), lending further support to our interpretation.
471 We return to this point in section 6 below.
472
473

5. Regional tectonic interpretation

475 In interpreting the images in Figs. 3-6 and all the additional profiles in Appendix A, we marked
476 boundaries (thick black lines) around kinematically coherent images whose geometry is consistent
477 with available data on Moho depth and with the kinematic history of tectonic units exposed at the
478 surface. Dashed solid black lines delimit very poorly defined or even putative boundaries. The base
479 of the European foreland lithosphere in the Central Alps is well defined and taken to be the base of
480 the -V_p layer at about 180 km depth, as discussed in the previous section (profiles 1, 4, 6, 9, 15 and B
481 in Appendix A). In other profiles, especially in the Eastern Alps where the base of the lithosphere is
482 poorly defined, we placed the lower boundary at approximately the same 180-200 km depth to
483 avoid abrupt along-strike variations in lithospheric thickness beneath foreland crust with the same
484 Variscan and pre-Variscan history. Thus, some boundaries are drawn across seismically fast and
485 slow domains, highlighting the difficulty of using solely seismological criteria to define the LAB
486 (Artemieva, 2011). In Figs. 8 and 9, we include two horizontal depth slices at 240 km and 90 km,
487 respectively, to show the main structures outlined by velocity anomalies in map view.
488
489 5.1 Alps
490 European lithosphere of Variscan and/or pre-Variscan origin originating in the Alpine foreland is
491 evident in all cross sections of the Central Alps (Figs. 3, 4), though its base in the Eastern Alps is
492 undefined (e.g., profile 2 in Fig. 4B). Beneath the Central Alps and westernmost Eastern Alps, this
493 lithosphere dips to the S to become the thick, subducted European slab (profiles B and 1 in Figs. 3C,
494 4A), whereas in the Western Alps (profiles 8 and 7 in Figs. 3A, B) and in the Eastern Alps east of 12°E
495 (profiles 2, 3 and 12 in Figs. 4B, C, 6A), the European slab is completely detached from its foreland.
496 Only in the transitional area between Western and Central Alps is the slab still tenuously connected

to the European lithosphere of the Alpine foreland (profile 16, Fig. 5C). The moderate dip and inordinate length of the slab beneath the entire E-W extent of the Po Basin in this particular profile reflect the fact that this W-E running profile obliquely slices the European slab at a high angle to the SE dip of Alpine subduction in the Western and Central Alps. Moreover, the E-dipping positive anomaly seen in Fig. 5C comprises different pieces, with the positive anomaly at the eastern end (below the Adriatic plate east of the Lessini Mountains, at a depth of around 350-450 km) originating from a south-dipping slab fragment below the Eastern Alps depicted in Fig. 4A. This easternmost part of the positive anomaly in profile 16 of Fig. 5C also slices minor, discontinuous relics of Alpine Tethys south of the main slab in the Eastern Alps (see lower right-hand side of N-S trending profile 2 in Fig. 4B).

In the Western Alps, detachment of the European slab (Figs. 3A, 3B) was previously noted by Lippitsch et al. (2003) and interpreted as a subhorizontal tear that is currently propagating from SW to NE towards the still-attached part of the slab in the western Central Alps (Kissling et al., 2006). The detachment of this part of the slab (profile A in Appendix A), possibly combined with unloading due to glacial erosion and melting (Champagnac et al., 2007; Mey et al., 2016), have been deemed responsible for rapid Plio-Pleistocene exhumation and surface uplift of the Western Alps (Fox et al., 2015, 2016) which have the highest peaks (up to 5000 m) and greatest relief (3000 m) of the entire Alpine chain.

In the Eastern Alps, the detached European slab hangs subvertically to steeply N-dipping in a depth interval ranging from 150 to 350-400 km. We note that the pronounced along-strike change in orogenic mantle structure between nearby profiles 1 and 2 (Figs. 4A and 4B) does not coincide with the Austroalpine-Penninic boundary marking the Alpine Tethys suture between the Central and Eastern Alps at the surface. This along-strike change is best seen by comparing the mantle structure in an orogen-parallel profile with the location of the suture in the tectonic map (profile 15 in Fig. 5A) and its projected trace in the horizontal depth slice at a depth of 90 km (Fig. 9). Rather, it coincides with the northward projection of the Giudicarie Belt (marked GB in Fig. 1), a post-collisional fault of latest Oligocene to Miocene age (Pomella et al., 2012) which sinistrally offsets the eastern and southern parts of the Alpine orogenic edifice, including the Periadriatic Fault System (Verwater et al., 2021). The northward projection of the Giudicarie Belt, which lies in the Tauern Window in map view, coincides with the westernmost point of eastward, orogen-parallel extrusion of the Alpine and Western Carpathian lithosphere in latest Oligocene to Miocene time (e.g. Scharf et al., 2013; Schmid et al., 2013; Favaro et al., 2017). This allochthonous block is referred to in the literature as the ALCAPA mega-unit. The orogenic Moho beneath this block shallows dramatically to the east (e.g., Grad et al., 2009; Kind et al., 2021), reaching a depth of some 20 km beneath the Pannonian Basin (profiles 15 and 5 in Figs. 5A, B). The occurrence of negative V_p anomalies and reduced gravity anomalies (Zahorec et al., 2021) immediately below this shallow orogenic Moho in the Eastern Alps (e.g., profile 12, Fig. 6A, highlighted low V_p area in Fig. 9) strongly suggests that the entire lithospheric mantle reaching from the Tauern Window of the Eastern Alps to their transition with the western Carpathians (profile 5 in Fig. 5B) has been delaminated.

5.2 Pannonian Basin

The negative V_p anomaly of the Eastern Alps continues further to the NE to beneath the Vienna Basin and the Central Western Carpathians, as seen in the 90 km and 120 km depth slices (Figs. 2, 8). This is the area overlying slab remnants that have descended into the Mantle Transition Zone (e.g., profile 5 in Fig. 5B). The Central Carpathians host a province of 17-14 Ma post-collisional sub-alkaline magmatism (Seghedi and Downes, 2011; Seghedi et al., 2013) related to Miocene extension of the Pannonian domain, including the Western Carpathians. Given the fact that this magmatism

544 ended some 14 Ma ago, it is uncertain if the low V_p anomaly in the Western Carpathians is solely
545 related to a persistent positive thermal anomaly. In this context, it is relevant to note that the area
546 of the Tisza mega-unit south of the Mid-Hungarian Shear Zone (MHZ in Fig. 1) and characterized by
547 high heat flux (Horvath et al., 2015, their Fig. 12) does not exhibit such a negative V_p anomaly. This
548 indicates that present-day heat production does not everywhere correlate with negative
549 seismological anomalies.
550   Relics of delaminated and detached European lithosphere can be detected at and below the
551 410 discontinuity beneath the Pannonian Basin (profiles 5 and 11 in Figs. 5B, 6B) as previously
552 discovered in the passive array swath experiment of Dando et al. (2011). As mentioned in discussing
553 Fig. 7, the 400 km down-dip length of the slab segments is broadly consistent with estimates of
554 shortening since the European slab entered the subduction zone after the closure of Alpine Tethys
555 at around 40 Ma (e.g., Schmid et al., 1996; Handy et al., 2010; Kurz et al., 2008). This suggests that
556 the detached slab remnants comprise mostly European lithosphere (Mitterbauer et al., 2011;
557 Rosenberg et al., 2018; Kästle et al., 2020).
558
559 5.3 Adriatic Plate
560 The Adriatic Plate is 100-120 km thick as defined by the lower limit of the horizontal $+V_p$ anomalies
561 beneath the Adriatic Sea. We label this as Adriatic lithosphere and regard it as Adriatic lithosphere
562 in a kinematic sense (e.g., profiles 1, 2, 3 and 12 in Figs. 4, 6A). This is less than half the thickness of
563 the European lithosphere. It is generally accepted that in the Alps the former Adriatic Plate formed
564 the upper plate during convergence, whereas in the Dinarides and Apennines, Adria is the
565 subducting plate. The Adriatic slab in the Apennines possibly has a simpler velocity structure than
566 the European slab in the Alps, comprising thinner and compositionally more homogeneous
567 lithosphere with only $+V_p$ anomalies (Fig. 6). In contrast to the European foreland (Franke, 2020),
568 most of the former Adriatic Plate was not affected by high-grade metamorphism and never
569 experienced the closure of various Paleozoic oceans. Instead, it has been interpreted as the
570 southern, Gondwana-derived foreland of the Variscan belt (Molli et al., 2020).
571   The Adriatic lithosphere is underlain by a pronounced low-velocity mantle in depth interval
572 of 150-350 km (profiles B and 3 in Figs. 3C, 4C right hand side; profile 12 in Fig. 6; profiles B, 3, 12,
573 11 in Appendix A). This thick low-velocity zone coincides at the surface in the eastern Po Basin and
574 northern Adriatic Sea with the Veneto volcanic province (Figs. 1, 8), which comprises mostly
575 primitive basalts diluted by a depleted asthenospheric mantle component (Macera et al., 2003). Its
576 age range between Late Paleocene to Late Oligocene (Becculava et al., 2007) spans the transitional
577 time from subduction to collision in the Alps (Handy et al., 2010 and refs therein). It is thus tempting
578 to attribute this magmatism to the combined effects of heat and fluid advection behind the
579 originally S-dipping European slab in the Alps (Macera et al., 2008). The release of water and
580 incompatible elements from deeply buried sediments along the slab interface may have caused
581 hydration of the overlying mantle, giving rise to an overall decrease in seismic velocity, as proposed
582 by Giacomuzzi et al. (2011) to explain the negative anomaly layer beneath the Adriatic Plate.
583
584 5.4 Apennines
585 Switches in the polarity of subduction are manifested at the surface by changes in thrust vergence
586 and location of the orogenic fronts at the Alps-Apennines and Alps-Dinarides transitions (Fig. 1). The
587 mantle structure at the Alps-Apennines transition is simpler than the complex surface fault
588 structure due to switching subduction polarity (Molli et al., 2010; Schmid et al., 2017) would
589 suggest. There, the European and Adriatic slabs are easily distinguished in profiles 8 and 7 (Fig. 3A,
590 B). In the horizontal slice at 240 km depth in Fig. 8, the two slabs cannot be distinguished at the

591 resolution of the horizontal depth slice because they are very close to each other (see Figs. 3A, B).
592 However, the horizontal slice at 90 km (Fig. 9) shows them separated by the downward projection
593 of the Alpine Tethys suture. Note that the European slab beneath the Western and Central Alps was
594 subducted to the SE below the Adriatic Plate prior to 35 Ma, ultimately leading to the Alpine Tethys
595 suture depicted in Fig. 9. Adria-Europe suturing occurred before the Apennines formed in latest
596 Oligocene to Miocene and Pliocene time. When considering profiles 8 and 7 in Fig. 3A, as well as
597 profiles 12 and 11 in Figs. 6A and 6B in the following discussion, it is important to note that the
598 Adriatic slab beneath the northern Apennines originally dipped to the SW when it was still attached
599 to the then-still undeformed western part of the Adriatic Plate (Facenna et al. 2004, Schmid et al.
600 2017). Apenninic orogenesis involved E-directed rollback of this former Adriatic Plate that currently
601 makes up the slab below the Northern Apennines.
602   In profile 12 (Fig. 6A) across the northern Apennines, the upper 200 km of the Adriatic slab
603 anomaly dip to the NE and are hence overturned, as pointed out in section 3. This slab is detached
604 from the Adriatic lithosphere and located in the NE foreland of the Apennines. Somewhat more to
605 the south in profile 11 (Fig. 6B) across the central (Tuscan) Apennines, the Adriatic slab is normally
606 inclined, i.e., dips to the SW, and completely detached from the orogenic wedge of the Apennines.
607 In profile 7 (Fig. 3B) running parallel to the strike of the Apennines slab, a subhorizontal tear is
608 clearly visible beneath the Tuscan Apennines at a depth of 80-100 km. We speculate that once the
609 Apennines stopped advancing in Plio-Pleistocene time (e.g., Molli et al., 2010), the heavy Northern
610 Apennines slab steepened. The subhorizontal tear visible in Fig. 3B appears to have propagated
611 from SE to NW, i.e., in a direction of decreasing orogen-normal shortening in the Apennines and
612 towards the pole for Neogene counterclockwise rotation of the Corsica-Sardinia block with respect
613 to Europe (Speranza et al., 2002), also affecting the Apenninic orogen (Maffione et al., 2008). Partial
614 tearing allowed the detached part of the slab in the SE to retreat and sink under its own weight,
615 while the smaller, still-partly attached segment in the NW became vertical and locally overturned
616 (profile 12 in Fig. 6A). The maximum depth (8-9 km) of Plio-Pleistocene fill in the northern Apenninic
617 foreland or "Po" Basin (Bigi et al., 1989) and the deepest Moho beneath the northern Apennines
618 (50-60 km, Spada et al., 2013) are both attributed to the downward pull of this still partially
619 attached slab segment depicted in profile 12 of Fig. 6A (Picotti and Pazzaglia, 2008).
620   The horizontal depth slice at 90 km in Fig. 9 shows the area traversed by profiles 12 and 11
621 discussed above that is characterized by low V_p and interpreted to outline lithospheric delamination
622 during slab detachment. These areas extend from NW to SE along the front of the NE-facing
623 Apennines nappe stack. This indicates that the Adriatic slab below the Apennines has detached
624 from the little-deformed Adriatic Plate in the Adriatic Sea almost all along the strike of the Northern
625 and Central Apennines. Note that this area of delamination is slightly NE of the outline of the
626 detached and subvertical Adriatic slab shown in the horizontal depth slice at 240 km depth (Fig. 8).
627
628 5.5 Dinarides
629 Our data only cover the area of the northern Dinarides and the Dinarides-Alps transition area in
630 Slovenia (Stipčević et al., 2011, 2020). Collisional shortening after the closure of the Neotethyan
631 oceanic tract in the northern Dinarides started earlier than in the Alps; major collisional shortening
632 lasted from Late Cretaceous to Oligocene time, with only very minor shortening in the Miocene
633 (e.g., Schmid et al., 2008). In the Alps, collisional shortening after the closure of Alpine Tethys
634 started later, namely in the late Eocene and lasted until Pliocene times. The transition between the
635 Alps and the Dinarides is marked at the surface by the Southern Alpine Front that thrusted the
636 Southern Alps southward over older NW-SE striking Dinaric thrusts (Fig. 1) in the late Miocene.
637 South-directed thrusting in this transition area, combined with dextral strike slip reactivating Dinaric

638 structures, is still seismically active (e.g., Kastelic et al., 2008; see yellow line marking the presently
639 active plate boundary in the Alps in Fig. 1).
640   An east- to northeast-dipping positive V_p anomaly is partly imaged beneath the Dinarides in
641 profile 16 (Fig. 5C), but is lacking in profile 11 (Fig. 6B) which crosses the frontal Dinarides to the
642 south. Unfortunately, the resolution in this latter profile is very poor. A slab gap in the
643 northernmost Dinarides has been recorded by global tomography (Bijwaard and Spakman, 2000;
644 Piromallo and Morelli, 2003), possibly due to the previous inability of imaging a slab of only ≤ 140
645 km length in this area. Ustaszewski et al. (2008), Schefer et al. (2011) and Horvath et al. (2015)
646 invoked asthenospheric upwelling at the SE limit of the Pannonian basin associated with the
647 breakoff of part of the NE-dipping Adriatic slab. This is thought to have permitted asthenosphere to
648 flow from beneath the Adriatic Plate to below the extending Pannonian Basin in the upper plate of
649 the retreating Carpathian subduction (Jolivet et al., 2009; Handy et al., 2015; Horvath et al., 2015;
650 Kiraly et al., 2018).
651
652 5.6 Summary of the tectonic interpretation
653 We summarize by combining all the profiles in Appendix A as a basis for the interpretation of
654 horizontal depth slices (Figs. 8, 9). The 240 km depth slice in Fig. 8 maximizes the number of slabs
655 intersected and exhibits various degrees of attachment of the slabs to their orogenic edifice and
656 their forelands. The horizontal depth slice of Fig. 9 at 90 km visualizes areas of negative V_p in the
657 uppermost mantle.
658
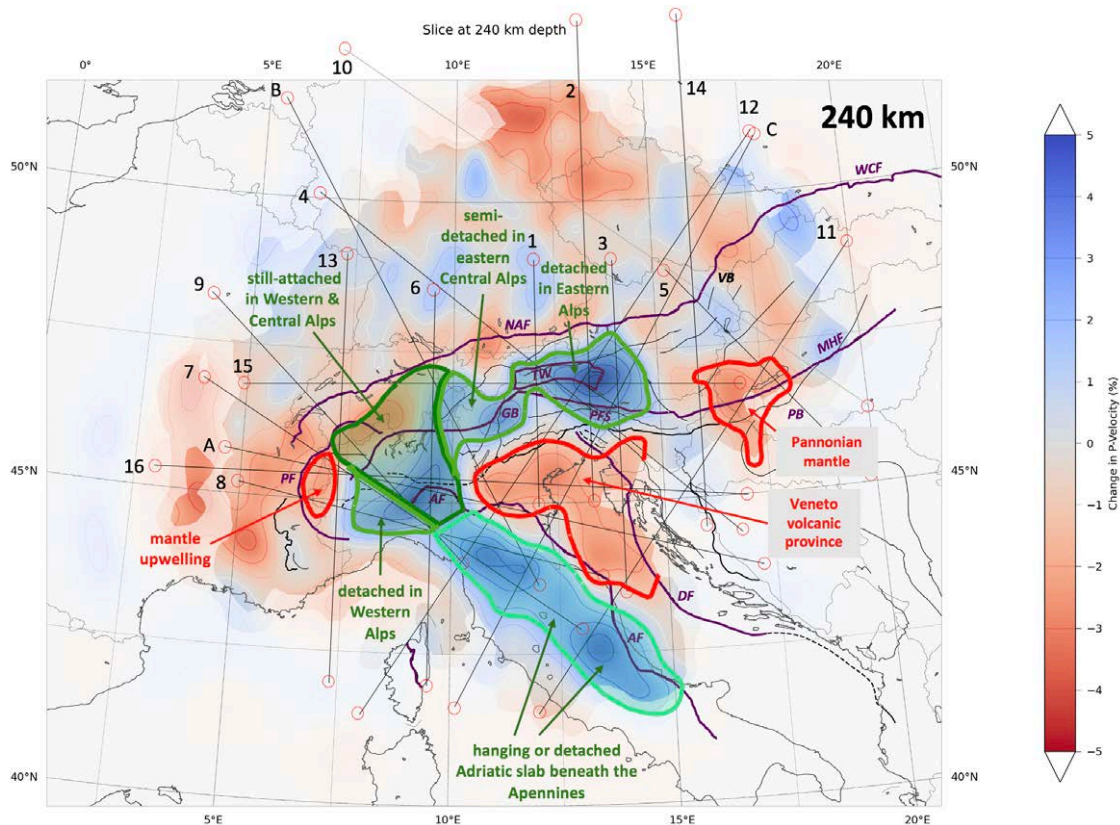
659
660 **Figure 8**: Horizontal V_p tomographic slice at 240 km. Blue and red areas represent fast and slow teleseismic p-
661 wave anomalies, respectively. Isolines indicate deviation in % of P-wave velocities from the mantle model in
662 Paffrath et al. (2021b). Green lines are boundaries of slabs at their intersection with the horizontal plane of the
663 depth slice. The slab boundaries were obtained by projecting the interpreted slab outlines marked with black lines
664 in the 19 profiles in Appendix A (traces shown as thin black lines) into the plane of the depth slice. Shades of green
665 denote various degrees of attachment of the European slab to the European lithosphere in the Alpine foreland

666 (see interpreted profiles and text). Red lines outline domains of mantle upwelling. Thick black lines are major
667 Alpine faults: NAF - North Alpine Front, PFS - Periadriatic Fault System, GB – Giudicarie Belt, PF – Penninic Front,
668 TW – Tauern Window, VB – Vienna Basin, PB – Pannonian Basin, MHF – Mid-Hungarian Fault Zone, AF – Apennines
669 Front, DF – Dinarides Front.
670
671
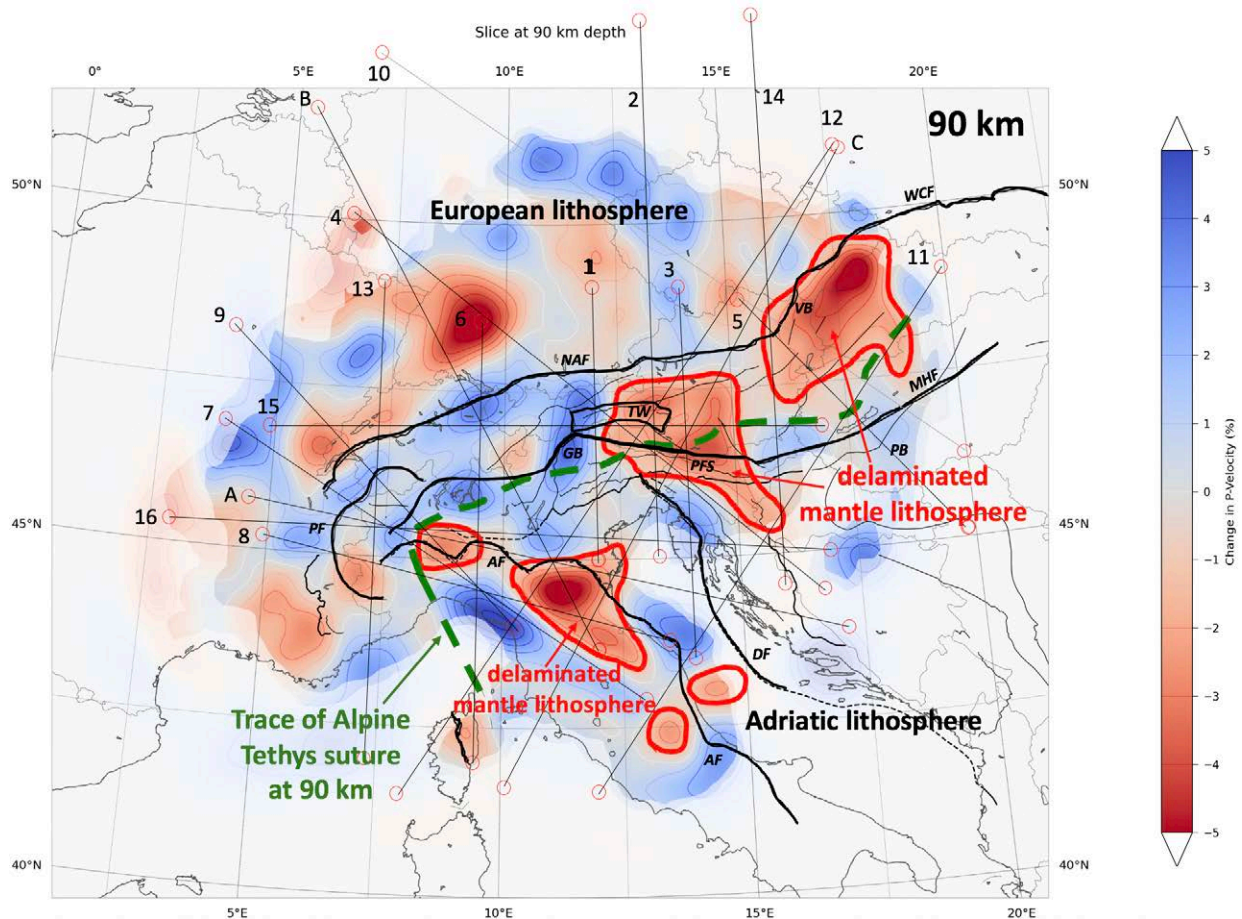
672
673 **Figure 9**: Horizontal V_p tomographic slice at 90 km depth. Blue and red areas represent fast and slow teleseismic
674 p-wave anomalies, respectively. Isolines indicate deviation in % of P-wave velocities from the mantle model in
675 Paffrath et al. (2021b). Thick dashed green line is the projection of the suture zone of Alpine Tethys down to 90
676 km based on interpretation of the profiles. This green line marks the southern boundary of the European Plate
677 with the Adriatic Plate and the lithosphere of the Tisza megaunit beneath the Pannonian Basin. Note the variable
678 P-wave velocities within the European lithosphere at this depth due to pre-Alpine tectogenesis. Areas outlined in
679 red indicate areas with low V_p located within the Alpine-age orogens where shallow asthenosphere replaced
680 delaminated mantle lithosphere after slab detachment in the Alps, Western Carpathians and the Apennines
681 occurred.
682
683   Figure 8 shows that in the Alps, slab attachment is only complete in the Central and northern
684 Western Alps between 7° and 10°E. This is corroborated by surface-wave tomography (Kaestle et al.
685 2018, their Fig. 12) indicating continuous positive velocity anomalies down to depths below 180 km
686 in the Central Alps. Detachment is complete in the southernmost Western Alps and modest in the
687 eastern Central Alps between 10° and 12°. It is complete in in the Eastern Alps east of about 12°E
688 where we observe the detached Eastern Alps slab (Fig. 8) dipping to the NE (e.g., Lippitsch et al.,
689 2003; see Figs. 4B, 4C and 6A). No significant positive V_p anomaly is seen at 240 km depth in the
690 easternmost Eastern Alps and the Western Carpathians east of 15°E, where the relicts of former
691 slabs reside below the 410 km discontinuity (see Fig. 5). Where detachment is complete, the slabs

692   have been supplanted by upwelling asthenosphere, as is seen by three areas of negative V_p
693   anomalies outlined in the depth slice for 90 km (Fig. 9) in the southern Western Alps, the Veneto
694   volcanic province and the Pannonian basin. In the Apennines, the Adriatic slab is locally hanging, but
695   mostly completely detached from its overlying orogenic root and foreland. There too, upwelling
696   asthenosphere has locally replaced the descending slab in the frontal, i.e., NE parts of the orogen,
697   eliminating the former connection of the slab with the remaining undeformed part of the Adriatic
698   Plate in the Adriatic Sea.
699   Figure 9 also features a dashed green line marking the location of the Alpine Tethys suture zone
700   projected from the crustal down to 90 km, separating the European lithosphere from the Adriatic
701   lithosphere. We emphasize that the downward projection of this suture in the profiles (dashed
702   green lines) is hypothetical in the sense that mapping it involved tracing the suture through
703   domains that were extensively modified during delamination and mantle upwelling. The severe
704   bending of the putative trace of this suture zone at the Alps-Apennines transition reflects
705   counterclockwise rotation of the Corsica-Sardinia block and the Ligurian Alps in Miocene time
706   (Schmid et al., 2017 and references therein). Likewise, bending of the projected suture north of the
707   Mid-Hungarian fault zone is due to the counterclockwise rotation of the Western Carpathians, also
708   in Neogene time (Márton et al., 2015).
709
710

711 **6. Discussion**

712

713 6.1 Subduction polarity – was there a switch in the Alps?
714   The polarity of subduction in the Alps, particularly at its junction with the northern Dinarides, has
715   been a bone of contention ever since the publication of P-wave tomographic images showing high
716   velocity anomaly some 200 km long dipping some 50° to the NE beneath the Eastern Alps (Babuska
717   et al. 1990) and connected with the upper mantle of the undeformed Adriatic Plate according to
718   Lippitsch et al. (2003). The Eastern Alps slab was thought to be separated from the SE-dipping
719   European slab anomaly in the Central and Western Alps by a decrease in strength of the positive
720   anomaly, interpreted by these authors as a slab gap in map view. The attribution of the Eastern Alps
721   slab to the Adriatic Plate by Lippitsch et al. (2003) was challenged by Mitterbauer et al. (2011),
722   whose teleseismic model showed a steeper (75° or more) and longer Eastern Alps slab reaching
723   down to the 410 km discontinuity. The Eastern Alps slab was thought to have been Adriatic
724   lithosphere that had been laterally wedged from the Dinarides (Lippitsch et al., 2003) or subducted
725   beneath the Eastern Alps in Neogene time (Schmid et al., 2004; Kissling et al., 2006; Handy et al.,
726   2015). Although N-directed subduction was inconsistent with north-vergent nappe stacking along
727   strike of the entire Alpine chain, these authors postulated a late-stage switch in subduction polarity
728   in Miocene times, i.e., after nappe stacking. Another possible problem with a Miocene switch in
729   subduction polarity is that the easternmost part of the slab anomaly imaged by Lippitsch et al.
730   (2003) is significantly longer (200 km) than the estimated amount of south-directed shortening in
731   the eastern Southern Alps, which amounts to ≥50 km (Schönborn, 1999; Nussbaum, 2000). One way
732   to explain the excess slab length was also to take into account some 85 km of Miocene N-S
733   shortening accommodated in the Eastern Alps and some 55 km Miocene shortening taken up at the
734   front of the northernmost Dinarides (Ustaszewski et al., 2008, their fig. 6). Another way was to
735   assume that the eastern part of the slab is partly of European origin (Handy et al., 2015). Indeed,
736   recent models based on pre-AlpArray seismological data have combined ambient noise and P-wave
737   tomography to propose that Eastern Alps slab is actually a composite of predominantly European
738   lithosphere and a subordinate amount of Adriatic lithosphere (Kästle et al., 2020).

Our new results clearly show that there is only one slab below the Alps, rather than the two proposed by adherents of a switch in subduction polarity. A switch in the polarity of subduction beneath the Alps can thus be ruled out based on our new data. The notion of only one continuous European slab beneath the Alps was previously advanced by Mitterbauer et al. (2011), with the added observation that this slab is overturned and acquires a northward dip in the Eastern Alps, as also noted in our profiles (Fig. 4). A comparison of profiles across the Eastern Alps between the model of Lippitsch et al. (2003) in Fig. 10A and this work (Fig. 10B) demonstrates the poor fit of the models and highlights why mantle delamination and slab detachment rather than a change in subduction polarity are the most recent processes to leave their imprint in the Eastern Alps. The most striking difference, apart from the length of the slab, is that the detached European slab according to our model has no connection to the Adriatic lithosphere from which it is separated by low-velocity upper mantle (Fig. 10B).
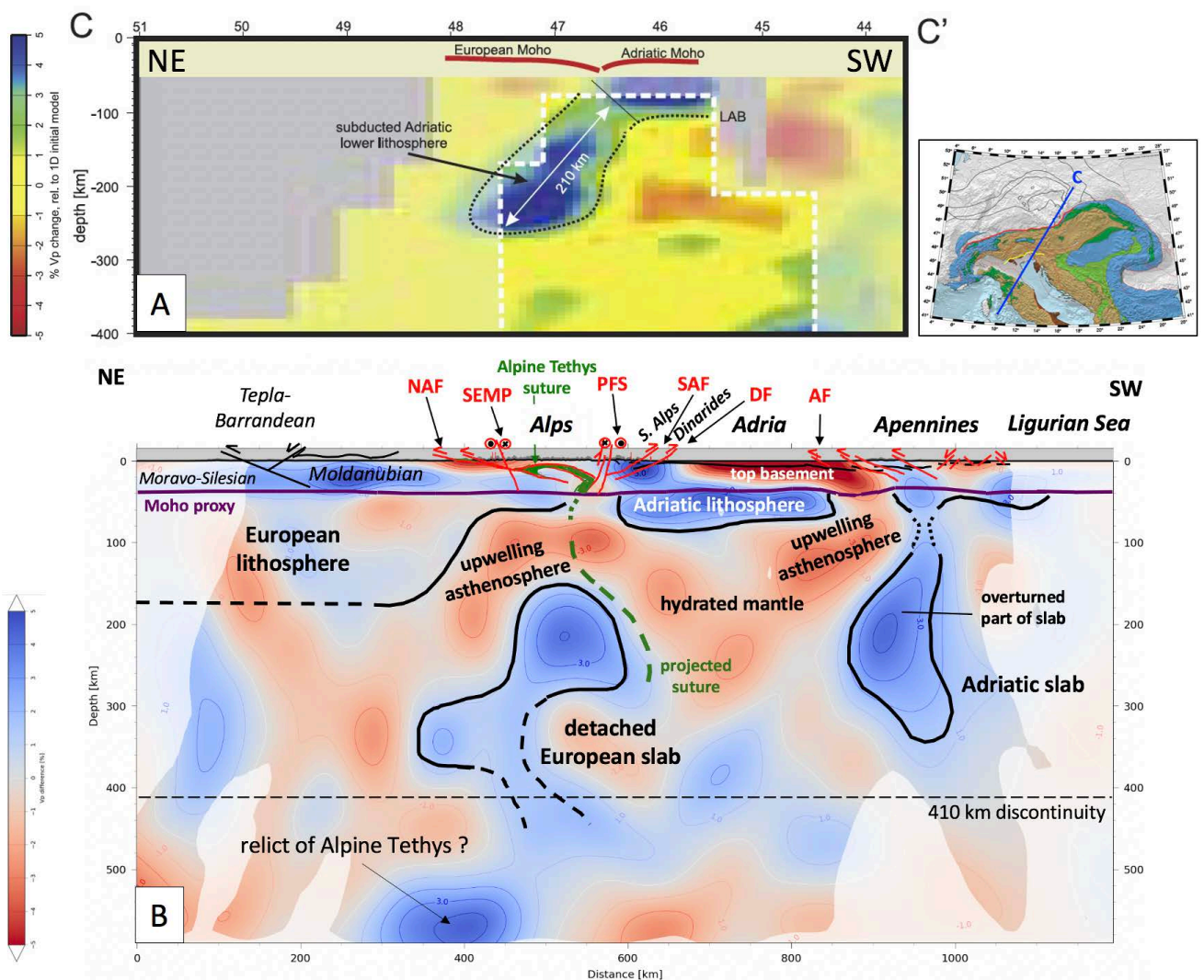
Figure 10: Two tomographic profiles along the trace of profile C (given in inset map) on the same scale: (A) Lippitsch et al. 2003; (B) this work. Yellow line in (B) is the outline of the slab anomaly in (A). The profiles show moderate agreement regarding slab detachment beneath the Eastern Alps, but disagreement regarding the dip and length of the slab anomaly. Our preferred model in (B) provides evidence for delamination of most of the underpinnings of Adria and Europe beneath the Alps, Adria and Apennines. A direct connection of the NE-dipping slab beneath the Eastern Alps to the Adriatic lithosphere shown in (A) becomes untenable in light of the new data presented in (B).

760

761   The length of the slab measured in profiles varies along strike between 220 and ≥ 500 km,
762 with even the latter estimates regarded as minima given that in some profiles the positive
763 anomalies continue below the 410 km discontinuity into the Mantle Transition Zone (e.g., profile 8
764 in Fig. 3A and profiles 6, 8, A and C in Appendix A). These lengths are not a reliable measure of the
765 amount of subducted lithosphere, because the slabs appear to be highly deformed and, anyway,
766 resolution decreases at such depths (Foulger, 2013). Nevertheless, the range of lengths overlaps
767 with palinspastic estimates of the total width of the Alpine Tethyan domain and its continental
768 margins in the Alps subducted between 84 and 35 Ma as measured in a NNW-SSE direction parallel
769 to Adria-Europe convergence (350-400 km, Le Breton et al., 2021; van Hinsbergen et al., 2020; 500
770 km, Handy et al., 2010). An interesting implication of this overall consistency between subducted
771 and seismically imaged lithosphere is that potentially more of the Alpine subduction is preserved in
772 the mantle than hitherto believed. Based on earlier teleseismic tomography, Handy et al. (2010)
773 estimated a deficit between subducted and imaged lithosphere of between 10 and 30%, depending
774 on the contour intervals of positive P-wave anomalies used in their areal assessments of positive
775 anomalies.
776   The steep northward dip of the part of the European slab beneath the Eastern Alps must
777 have been acquired after southward subduction of the European lithosphere stopped in this part of
778 the Alps. The youngest exhumed high-pressure rocks that are testimony to an exhumed subduction
779 zone in this part of the Alps are found in the central Tauern Window (Gross et al., 2000) and the age
780 of subduction-related metamorphism is estimated to be around 35-45 Ma (Kurz et al., 2008;
781 Ratschbacher et al., 2004 and refs. therein). A younger age range for this metamorphism was
782 proposed (32-35 Ma, allanite U-Pb, Smye et al. 2011; Lu-Hf, Nagel et al., 2013), but these are
783 inconsistent with evidence for substantial exhumation of high-pressure units before the intrusion of
784 the Periadriatic plutons and the onset of movements along the Periadriatic Fault System
785 (Rosenberg, 2004). The 35-45 Ma age range for HP metamorphism certainly pre-dates indentation
786 of the eastern Southern Alps along the Giudicarie Belt starting at around 23 Ma (Scharf et al., 2013).
787 Hence, roll back and steepening of the European slab, followed by slab detachment and rotation of
788 the detached Eastern Alps slab into a steeply N-dipping orientation most likely occurred sometime
789 within the 39-23 Ma time interval, most likely at around 23 Ma according to geological evidence
790 (e.g., Scharf et al., 2013). The mechanisms of such rotation and verticalization during opening of the
791 Pannonian backarc behind the European slab subducting beneath the Eastern Carpathians are
792 unclear. The slab might have been twisted while still attached to a descending slab relict beneath
793 the Pannonian Basin (profile 5 in Fig. 5B; Dando et al., 2011). However, we favor reorientation of
794 the slab by asthenospheric flow during or after northward Adriatic indentation and slab detachment
795 in Neogene time (e.g., Ratschbacher et al., 1991; Favaro et al., 2017). The arcuate convex-
796 northward pattern of fast SKS directions beneath the Eastern Alps are suggestive of east-directed
797 asthenospheric flow (e.g., Qorbani et al., 2015) and would be consistent with both of these
798 interpretations.
799

800 6.2 Slab attachment and detachment
801 An intact slab dipping down to a depth of 300 km and beyond is only observed beneath the Western
802 to Central (Swiss-Italian) Alps between latitudes 7°E and 10°E (see area marked as un-detached in
803 Fig. 8; profiles 6 and 9 in Appendix A. Interestingly, Singer et al. (2014) noticed that lower crustal
804 seismicity in the European lithosphere is restricted to this same range of latitudes. They proposed
805 that this deep crustal seismicity is driven by stresses transferred to the foreland from the still-
806 attached segment of the European slab, which they argue is steepening as it retreats toward the

807 foreland. Kissling and Schlunegger (2018; their fig. 5c) present a schematic 3-D diagram of this
808 remaining undetached European slab, argueing that such slab retreat during attachment is
809 responsible for the striking isostatic disequilibrium between the low surface topography and the
810 thick crustal root (some 50 km, e.g., Spada et al. 2013) beneath this segment of the Alps.
811   Complete delamination during the advanced stages of detachment of the European
812 lithosphere occurred in the Eastern Alps and resulted in a broad zone of low-velocity material
813 interpreted to be upwelling mantle (Fig. 9), typically at a depth between 70 and 130 km (e.g., profile
814 15 in Fig. 5A) east of 12°E (i.e., east of the western Tauern Window, Fig. 1). East of 15°E, no
815 substantial remnants of the European slab are found above the 410 km discontinuity (Fig. 8 and
816 profiles 5, 11, 10 in Appendix A). This conforms with the findings of Dando et al. (2011) and
817 indicates that roll back subduction in the Carpathians followed by detachment of the European slab
818 played a fundamental role in forming the greater Pannonian area (Horvath et al., 2006; Matenco
819 and Radivojević, 2012). West of the Tauern window, between 12° and about 9.5°E traversed by
820 profile B (Fig. 3C), detachment is only moderate. A third area in the Alps where substantial
821 detachment occurs is the southern part of the Western Alps (profiles 8 in Fig. 3A, and A in Appendix
822 A) that is transitional to the northern Apennines. Such detachment was first noticed by Lippitsch et
823 al (2003; their profile A-A'), but recently refuted by Zhao et al. (2016). There, the detached
824 European slab of the Alps slab resides beneath the westernmost Apennines at a depth of 240 km,
825 while upwelling mantle occupies the area beneath the Western Alps at this same depth (Fig. 8).
826   The completely detached slab beneath most of the Northern Apennines (except for the
827 westernmost parts) hangs subvertically (profiles 11 and 12 in Fig. 6; profile C in Appendix A),
828 confirming the findings of Giacomuzzi et al. (2011, 2012) from teleseismic tomography, but at odds
829 with the interpretation of still-attached continental slabs without oceanic precursors in Sun et al.
830 (2019). A clear boundary between the European slab under the westernmost Apennines and the
831 delaminated Adriatic mantle lithosphere of the Northern Apennines slab cannot be resolved in the
832 horizontal depth slices, but is evident in profiles (e.g., Fig. 3A), where we interpret the boundary
833 between the two slabs to coincide with the Alpine Tethys suture.
834
835 6.3 Nature of low velocity domains in the greater Alpine area
836 In the text and profiles above, we interpret low V_p areas within the circum-Adriatic area as resulting
837 from upwelling mantle material (Pannonian Basin, Eastern Alps) and hydration effects (Veneto
838 Basin), whereas negative V_p areas in the lower part of the European lithosphere reflect inherited
839 Variscan or pre-Variscan structural anistropy and/or compositional differences rather than
840 enhanced temperature (section 4).
841   Insight into the nature of the European lithosphere comes from the striking coincidence of
842 its lower layer of large -V_p anomaly (Figs. 2, 7) with NE-SW oriented SKS directions and 1-2s delay
843 times reported for this area in the literature (Barruol et al. 2011) and AlpArray studies (Link and
844 Rümpker, pers. comm.). Given a relation of 100 km thickness for every second of delay time, one
845 obtains a thickness of 100-200 km for the anisotropic layer, which matches the observed thickness
846 of the -V_p layer. A well-known effect of azimuthal anisotropy is to retard near-vertical-incident body
847 waves (Hammond, 2014; Munzerová et al., 2018), thus providing a possible explanation for the
848 anomalous -V_p layer. Taken together, this suggests that the -V_p layer in the lower European
849 lithosphere is structurally anisotropic and may have accommodated viscous flow. This is contrary to
850 previous interpretations in which the anisotropy was attributed to arc-parallel asthenospheric flow
851 around the European slab (Barruol et al., 2011). The NE-SW orientation of SKS directions below the
852 Central Alps is inconsistent with the SE-subduction direction of European lithosphere, leaving a
853 Variscan or pre-Variscan age for lower lithospheric flow as the most likely alternative.

854   We consider a thermal anomaly unlikely to have caused the large $-V_p$ anomaly in the
855 European lithosphere because the ΔT-values corresponding to the observed 5-6% $-V_p$ would be
856 unrealistically high (300-600°C using the ΔV_p-T relations of Goes et al., 2000; Cammarano et al.,
857 2003; Perry et al., 2006) for old, inactive mantle lithosphere in the down-going plate of a collisional
858 orogen. Variscan crust in the foreland of the Alps underwent amphibolite- to locally granulite-facies
859 regional metamorphism some 340-360 Ma ago, followed by calc-alkaline magmatism and thermal
860 overprinting at 320-260 Ma (e.g., Matte 1986; Franke, 2000 and refs. therein). This Late
861 Carboniferous to Early Permian magmatic event is at least 200 Ma older than the onset of collision
862 in the Alps at 40-32 Ma (e.g., Handy et al., 2010 and refs. therein). Though it has been argued that
863 compositional differences can stabilize vertical and horizontal thermal gradients (Jordan 1975,
864 1981), thus contributing to the longevity of the observed seismic heterogeneity, there is no known
865 mechanism to maintain such a pronounced thermal anomaly for such a long time.
866   Regarding the Adriatic Plate, the question remains if the younger, low V_p patches attributed
867 to Miocene asthenospheric upwelling following lirthospheric delamination (Fig. 9) still represent
868 volumes of substantially elevated temperatures today. In view of the fact that water content in
869 addition to temperature influences seismic wave velocities in the mantle (Karato and Jung, 1998;
870 Shito et al., 2006), we propose that at least in the case of the Veneto volcanic province (Fig. 8)
871 temperature is unlikely to be the dominant factor, especially given that present-day heat flow in the
872 Adriatic region is low (Giacomuzzi et al., 2011).
873
874 6.4 _Timing of slab detachment and its consequences_
875 A rough estimate of the time since slab detachment in the Eastern Alps can be obtained from the
876 average sink rate of slabs around the world (12 mm/a, van der Meer et al., 2010, 2018). The rate is
877 derived from a compilation of teleseismically imaged slabs of known lengths and ages that are still
878 attached to their lower plate lithospheres, mostly in Circum-Pacific convergent zones. When applied
879 to the Eastern Alps, this approach yields minimum values of the time since detachment because
880 delamination of the European lithosphere is inferred to have preceded slab detachment (Figs. 4 and
881 6). They range from 10 to 25 Mas, respectively, beneath the Eastern Alps and the Pannonian Basin.
882 The 10-25 Ma time range since slab detachment encompasses the period of orogen-parallel
883 extension and rapid exhumation and lateral escape in the Tauern Window -(23-11 Ma, e.g., Scharf et
884 al., 2013) and overlaps with the duration of extension in the Pannonian Basin (21-15 Ma, Horvath et
885 al., 2015 and references therein). This supports our suggestion that lithospheric delamination, slab
886 detachment and asthenospheric upwelling were instrumental in triggering decoupling that enabled
887 Neogene orogen-parallel lateral extrusion of the ALCAPA tectonic megaunit (upper plate crustal
888 edifice of Alps and Carpathians) towards the Pannonian Basin. This raises questions about the depth
889 of detachment at the base of the ALCAPA megaunit during its lateral extrusion and the nature of the
890 Moho beneath the Pannonian Basin. Horvath et al. (2015) proposed that during lateral extrusion the
891 extending crust of the ALCAPA megaunit could directly overlay the hot asthenosphere of the
892 Carpathian embayment and that since then, most of the Pannonian Basin cooled, allowing a new
893 mantle lithosphere to grow. If correct, this would imply that the Moho imaged beneath the
894 Pannonian basin is of Miocene or younger age.
895   An intriguing aspect of Adriatic indentation and Alpine slab detachment is their potential
896 effects on the fore- and hinterland basins of the Alps. The 25-10 Ma time window for slab
897 detachment brackets the time when thrusting in the eastern Molasse basin stopped advancing (21-
898 22 Ma) and changed from in-sequence to out-of-sequence (wedge-top) mode (Hinsch, 2013). It also
899 includes the time when the basin rapidly filled with terrigeneous components at 19-18 Ma (Grunert
900 et al., 2013), leading to a shift in the paleo-drainage direction from eastward to northwestward

(Kuhlemann and Kempf, 2002). Subsequent uplift and erosion of the entire Molasse Basin at 10 to 5 Ma (Cederbom et al., 2011) was greater in the east (0.3-0.5 km) than the west (0.5-1.5 km, Baran et al., 2014). These first-order orogen-parallel variations in foreland basin fill and erosion may be related to the degree of slab attachment, with full attachment in the Central Alps lengthening the flexural response of the foreland to slab loading, whereas complete slab detachment and delamination in the east after 25-20 Ma (Handy et al., 2015) favored a very rapid decrease in basin depth (Genser et al., 2007). This period at 23 Ma coincided with the aforementioned onset of rapid exhumation in the Tauern Window (Fügenschuh et al., 1997) and eastward escape of the Eastern Alps into the Pannonian Basin in the upper plate of the retreating Carpathians (Ratschbacher et al., 1991; Scharf et al., 2013).

Finally, a rather vexing consequence of the calculations above is that the 25-10 Ma time window for slab detachment is younger than the 34-28 Ma age range of the Periadriatic calc-alkaline intrusive suite along the Periadriatic Fault (e.g., Rosenberg, 2004), which has been attributed to slab breakoff (von Blankenburg and Davies, 1995). We note that Oligo-Miocene calc-alkaline intrusives occur all along the Periadriatic Fault, extending from the Western Alps to the Mid-Hungarian Fault Zone in the Pannonian Basin (Fig. 1). This broad lateral extent (7.5-19°E, Fig. 1) encompasses the narrow corridor of slab attachment between 7-10°E in the Central Alps (Fig. 8), suggesting that the detached slab segments observed in this study may have had little, if anything, to do with Periadriatic magmatism. Thus, either our estimates of detachment times above are based on questionable assumptions and the time since detachment exceeded 25 Ma or there was an older late Oligocene breakoff event involving an originally longer slab than presently imaged. A further possibility is that the calc-alkaline magmatism with a lithospheric mantle component reflects deep-seated processes other than slab breakoff.

7. Conclusions

The images presented here resolve some long-standing debates while compelling us to reassess the role of plates and their structure in mountain-building. Figure 11 is a graphic attempt to visualize the complex 3-D geometry of mantle structure in the area covered by AlpArray. This figure is a composite view of the Alps seen from the SE, i.e., from a vantage point above the Dinarides, with the Adriatic Plate removed to reveal the slabs. The slabs and foreland structures were constructed from the interpreted outlines in the 19 profiles in Appendix A.
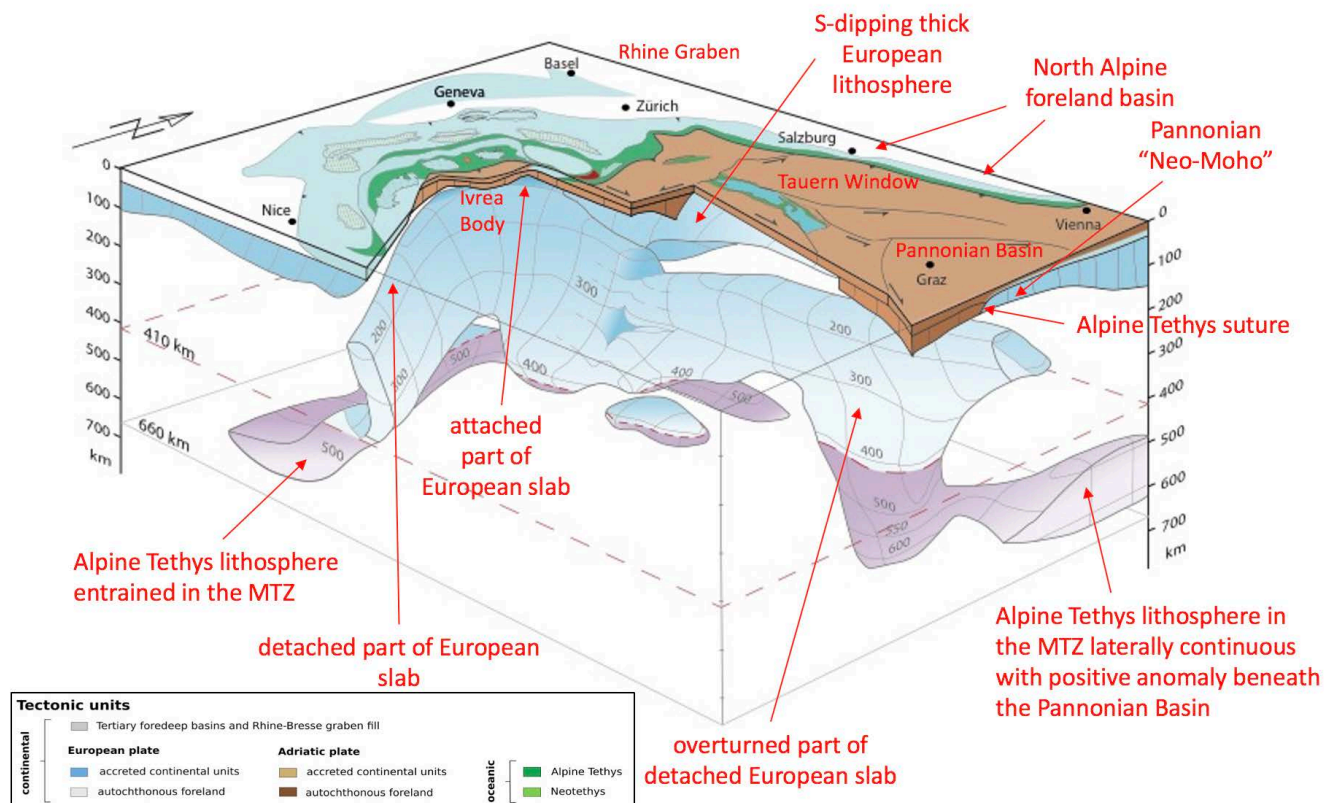
Figure 11: 3D-diagram of the slab beneath the Alps as viewed from the southeast. Slab geometry based on projections of all vertical tomographic profiles in Appendix B and horizontal sections from the model of Paffrath et al (2021b). Tectonic map of the surface is simplified from maps of Schmid et al. (2004) and Schmid et al. (2008).

A prime outcome of this study is that the European and Adriatic Plates involved in Alpine collision have first-order differences in seismic structure: the down-going European lithosphere is thick (c. 180 km) and marked by laterally continuous positive and negative P-wave anomalies. These are believed to be inherited Variscan or pre-Variscan anisotropic and compositional differences. In the Central (Swiss-Italian Alps), they descend as part of a coherent slab from the Alpine foreland to beneath the Northern Alpine Front. In contrast, the Adriatic Plate is thinner (100-120 km) and has a poorly defined base at the lower boundary of $+V_p$ anomalies. The underlying negative anomaly in the depth interval of 120-270 km is attributable partly to compositional effects (e.g., mantle hydration due to upwelling fluids from the Alpine slab) and partly to upwelling asthenosphere in the aftermath of delamination and slab detachment in the Alps and Apennines.

This fundamental difference in the structure of the lower and upper plates may be responsible for two of the most striking features of the Alps compared to other Alpine-Mediterranean orogens, namely the rugged, high altitude Alpine topography and the disproportionately large amount of accreted, deeply subducted and exhumed lower-plate units exposed in the deeply eroded core of the Alps (Fig. 11). Thick lithosphere is expected to be relatively stiff and buoyant upon entering collision, favoring tectonic underplating of accreted and subducted tectonic units as subduction proceeds. By comparison, "normal" lithosphere, as found in the Adriatic Plate and its slab beneath the Apennines, is expected to sink more easily under its own weight, favoring roll-back subduction, the development of low topography and upper plate extension with only limited exhumation of subducted units.

Another new outcome of this study is the extent of delamination and detachment of slabs in both the Alps and the Apennines. Detachment is complete in the southwesternmost Alps, and on a

much larger scale, in the Eastern Alps (Fig. 11) and Western Carpathians. There, relicts of European lithosphere hang at various depths, with depth increasing towards the east and even reaching the MTZ beneath the Pannonian Basin. Large-scale upwelling of asthenosphere was the response of the mantle to delamination of the European lithosphere and downward motion of detached slabs since at least 25 Ma. The asthenosphere below delaminated lithosphere occupies very shallow depths, in some cases immediately below the Moho marking the base of thinned Alpine orogenic crust, which was stretched in Neogene time during lateral orogenic escape and upper-plate extension forming the Pannonian Basin.

In this study, we claim to have resolved the debate over the polarity of Alpine subduction beneath the Eastern Alps in favor of the model of a single European slab that originally subducted to the south. The presently steep, northward dip of the now-fragmented and deformed Eastern Alps slab segment (Fig. 11) which gave rise to the alternative view of Adriatic subduction in the first place, is clearly a secondary feature acquired during or after slab detachment.

A lesson learned in collating and interpreting this extraordinary data set has been that, after initially acquiring and processing seismological data, methodological development and tectonic interpretation must go hand-in-hand if they are to yield meaningful, testable models. Figure 11 is an initial model of tectonic boundaries based on an assessment of geophysical data in a plate kinematic context. The next step is obviously to parameterize this model in order to compare it with independent sources of data and determine its thermo-mechanical characteristics.

Appendices

985

Profiles used in interpretations

987
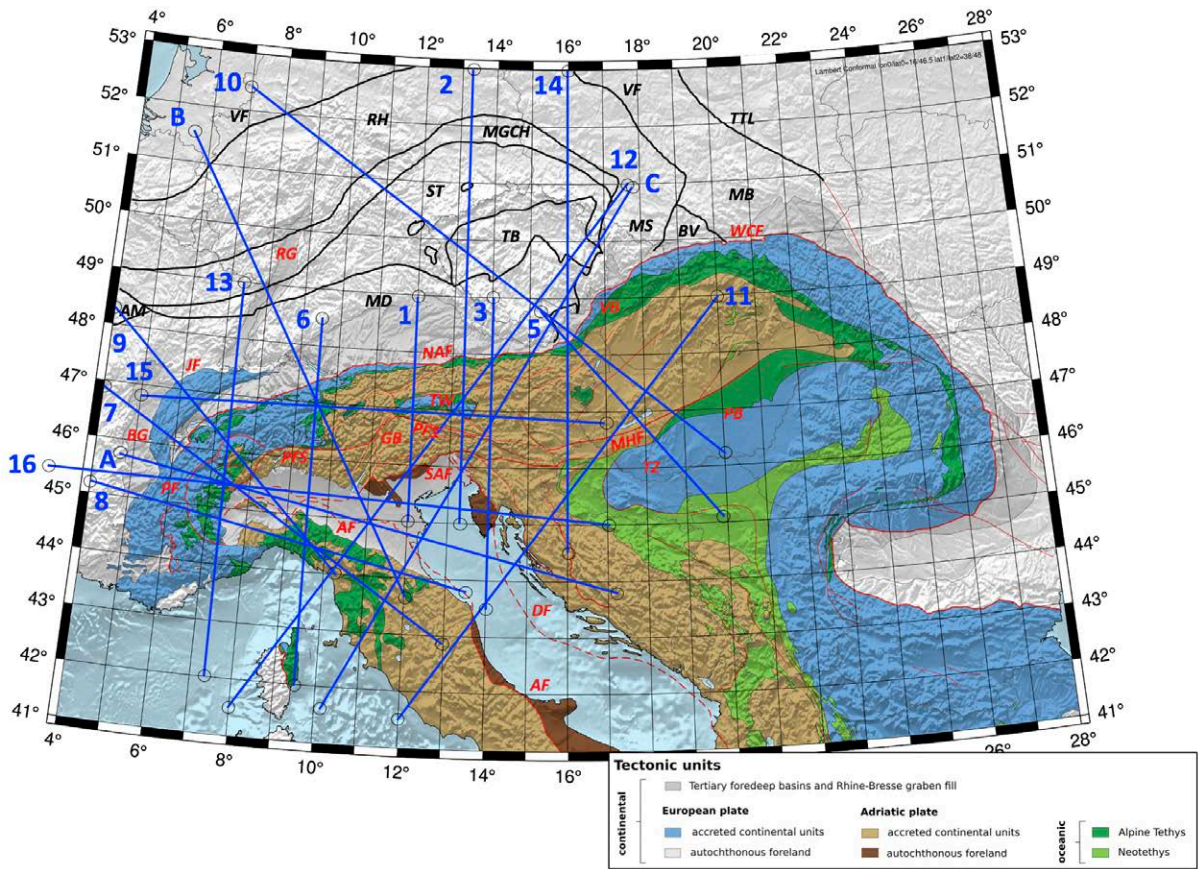
988
989   Fig. A0   Tectonic map with traces of all tomographic profiles used in this study
990
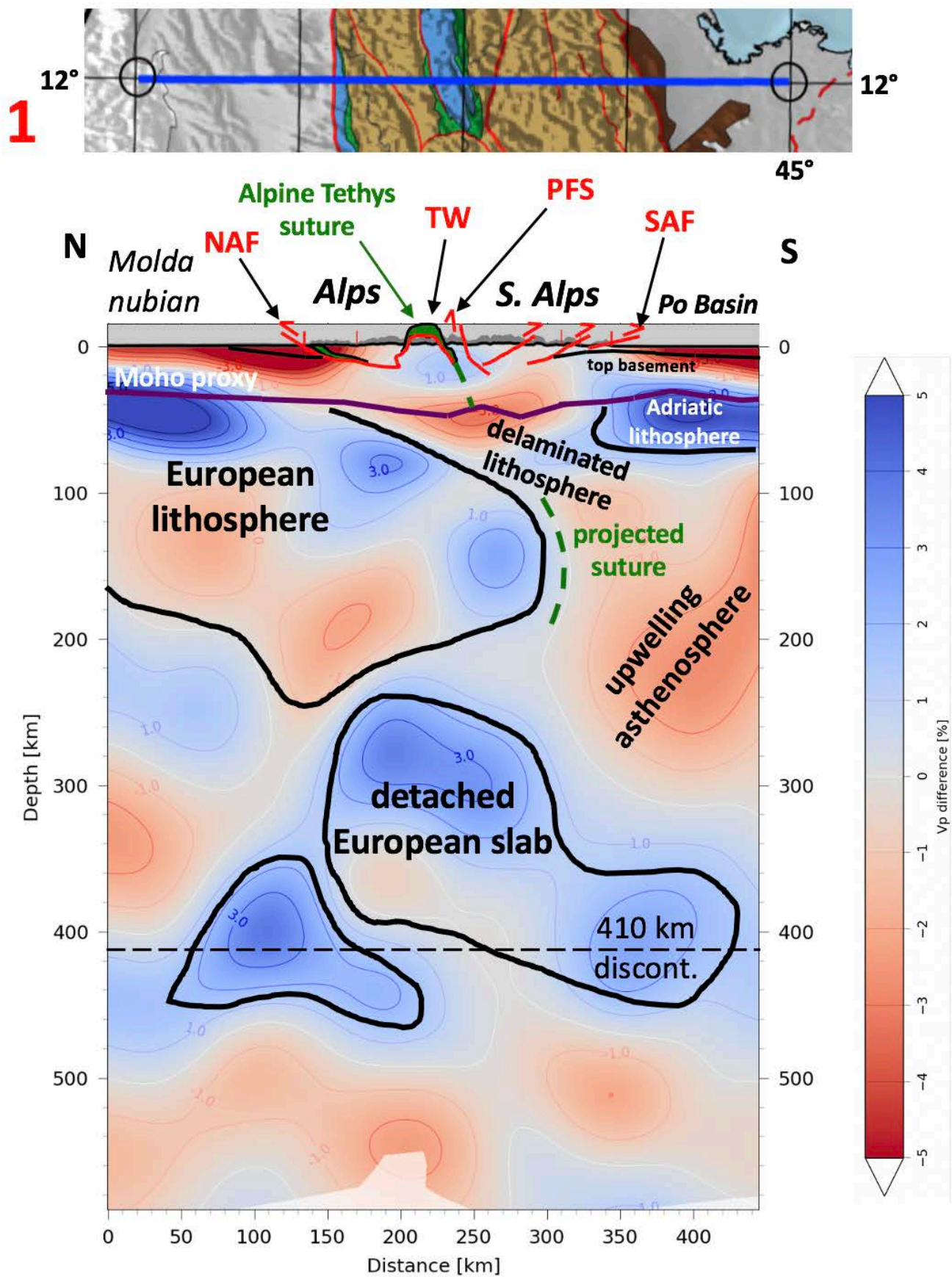
991
992   Fig. A1   Profile 1

993
994   Fig. A2   Profile 2

995

996   Fig. A3   Profile 3

NW NAF SEMP Alpine Tethys suture PFS SAF **SE**

Moravo-Silesian *E. Alps & W. Carpathians* *Pannonian Basin* *Tisza Mega-unit*

top basement

Moho proxy

delaminated lithosphere

Tisza lithosphere

upwelling asthenosphere

410 km discontinuity

detached European slab ?

Depth [km]

Distance [km]

997

998
999   Fig. A4   Profile 4
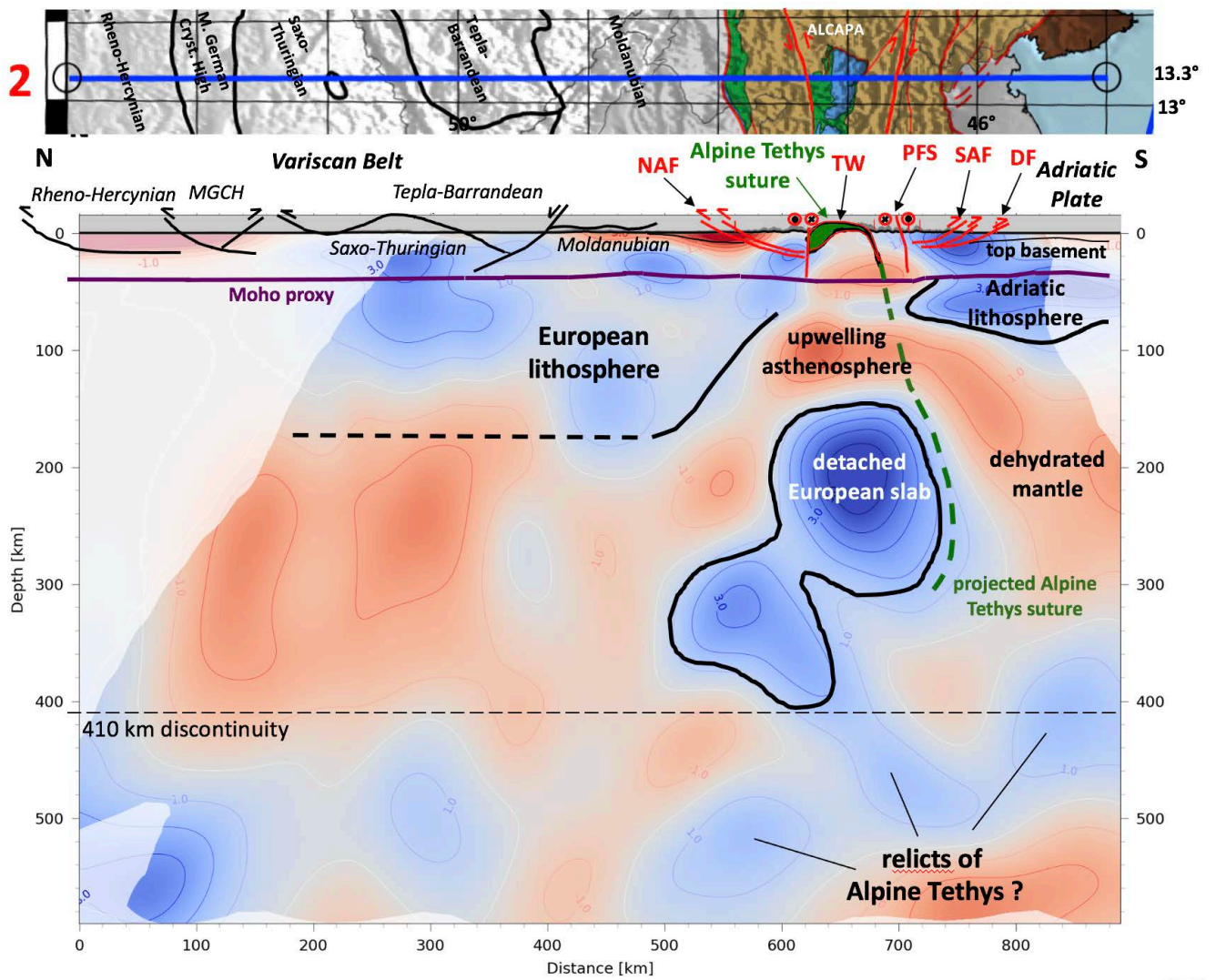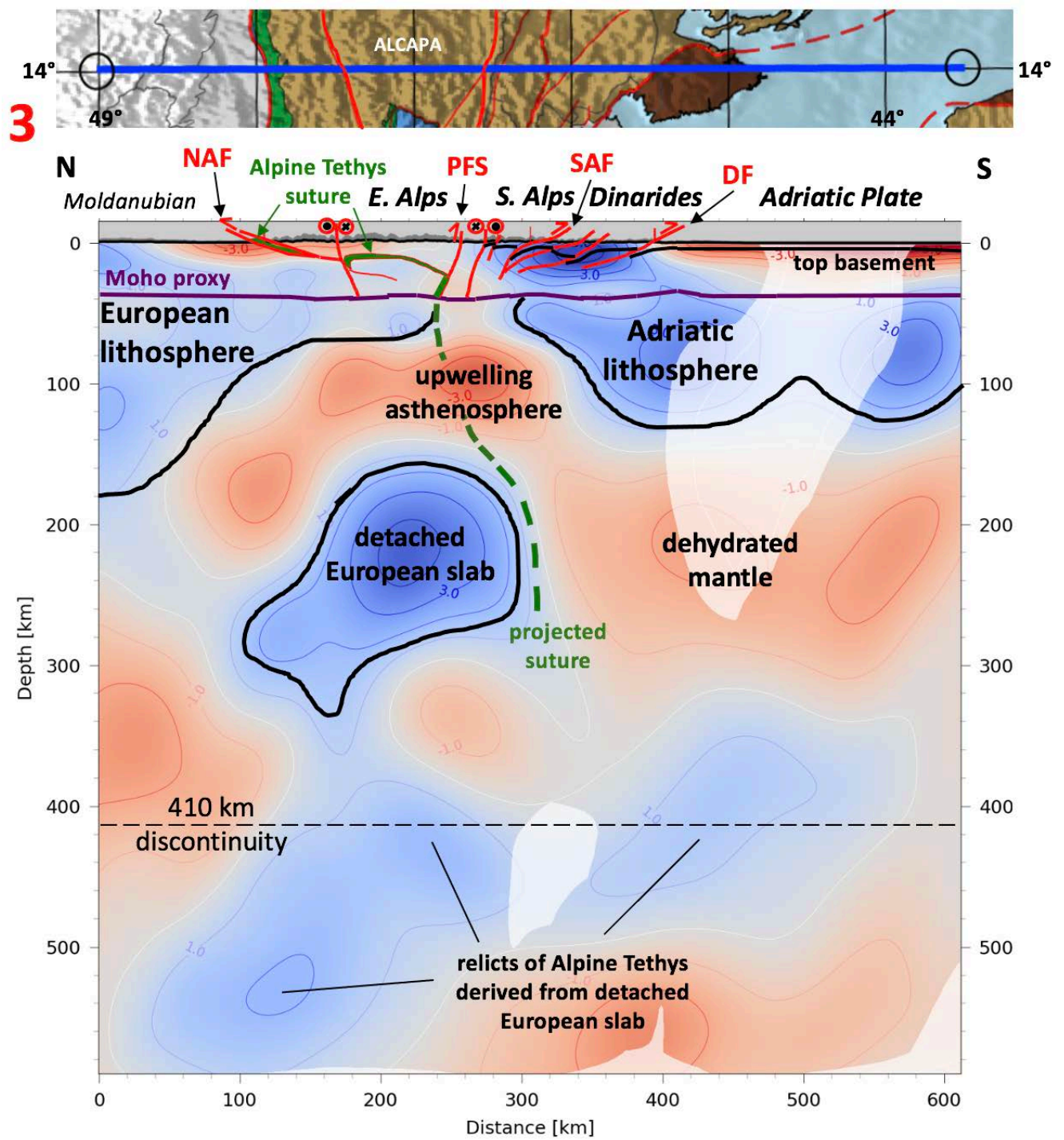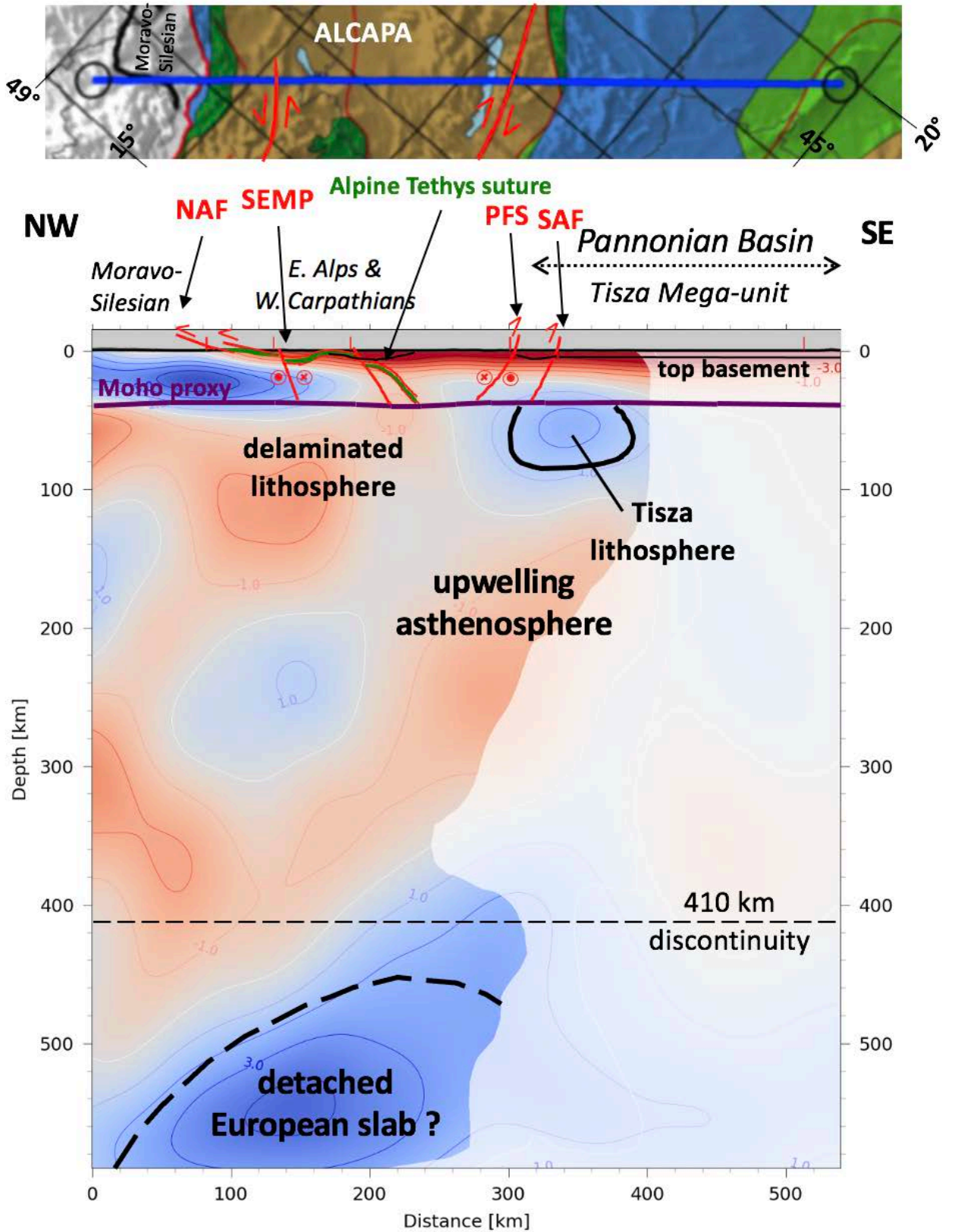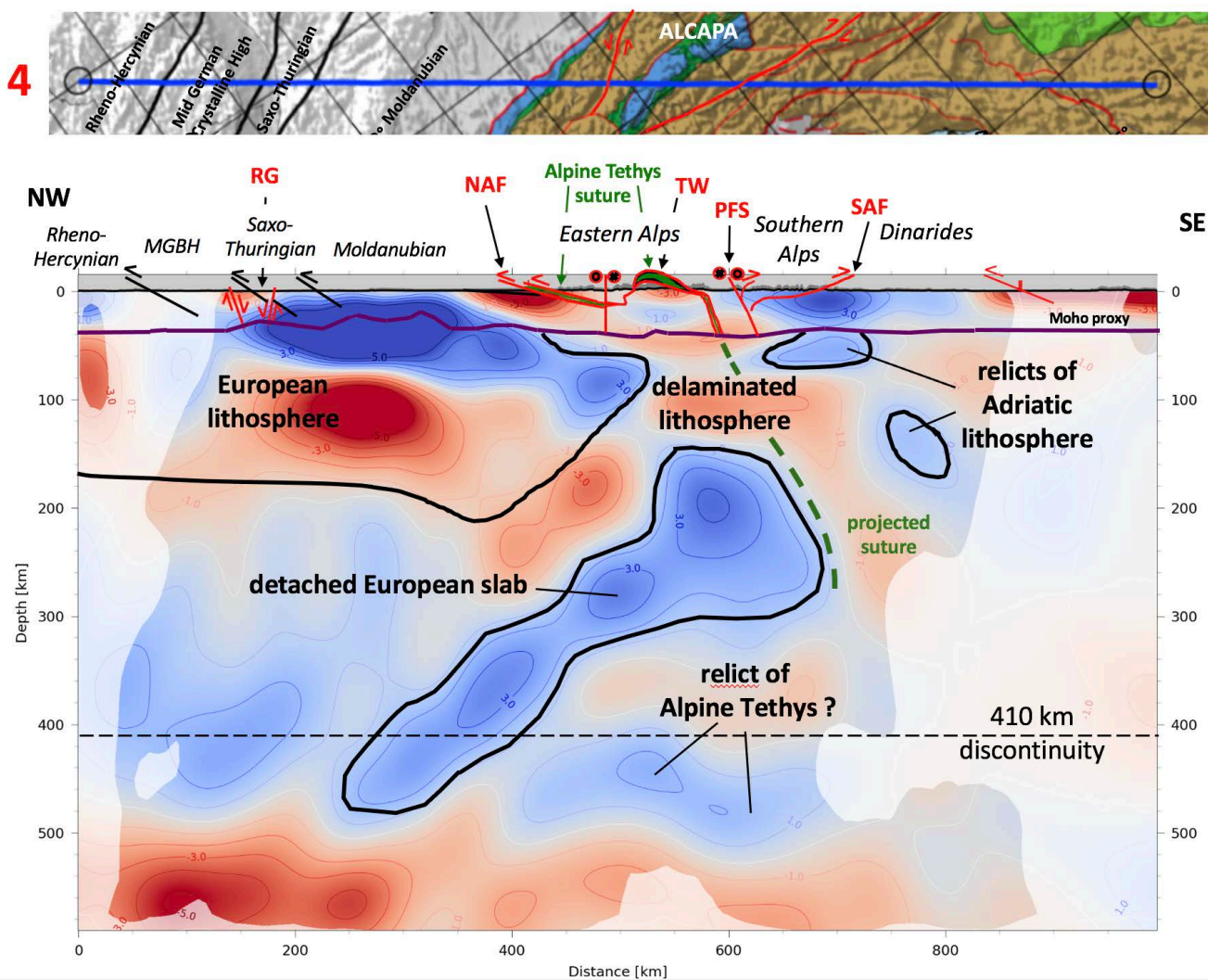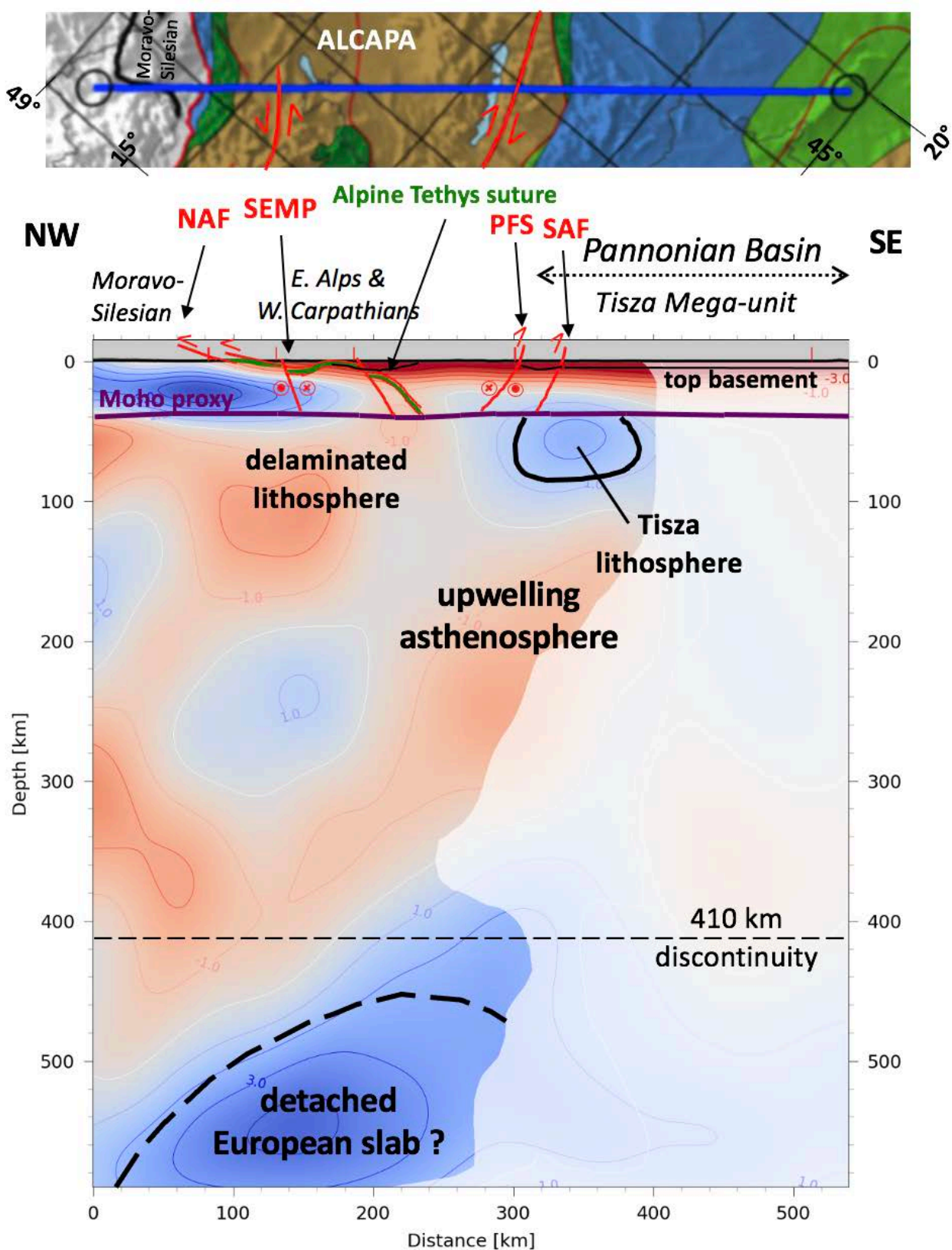
1000
1001   Fig. A5   Profile 5
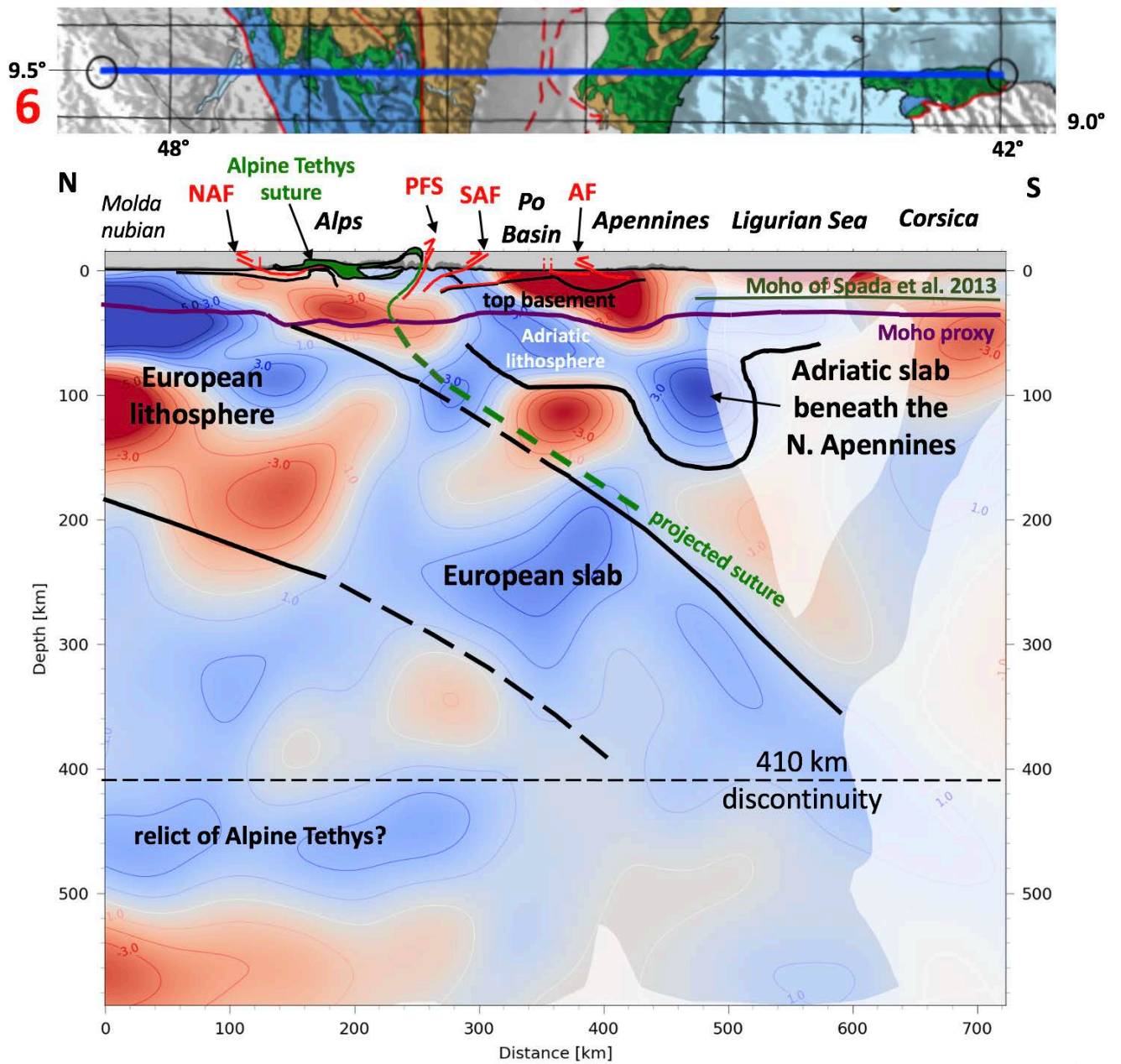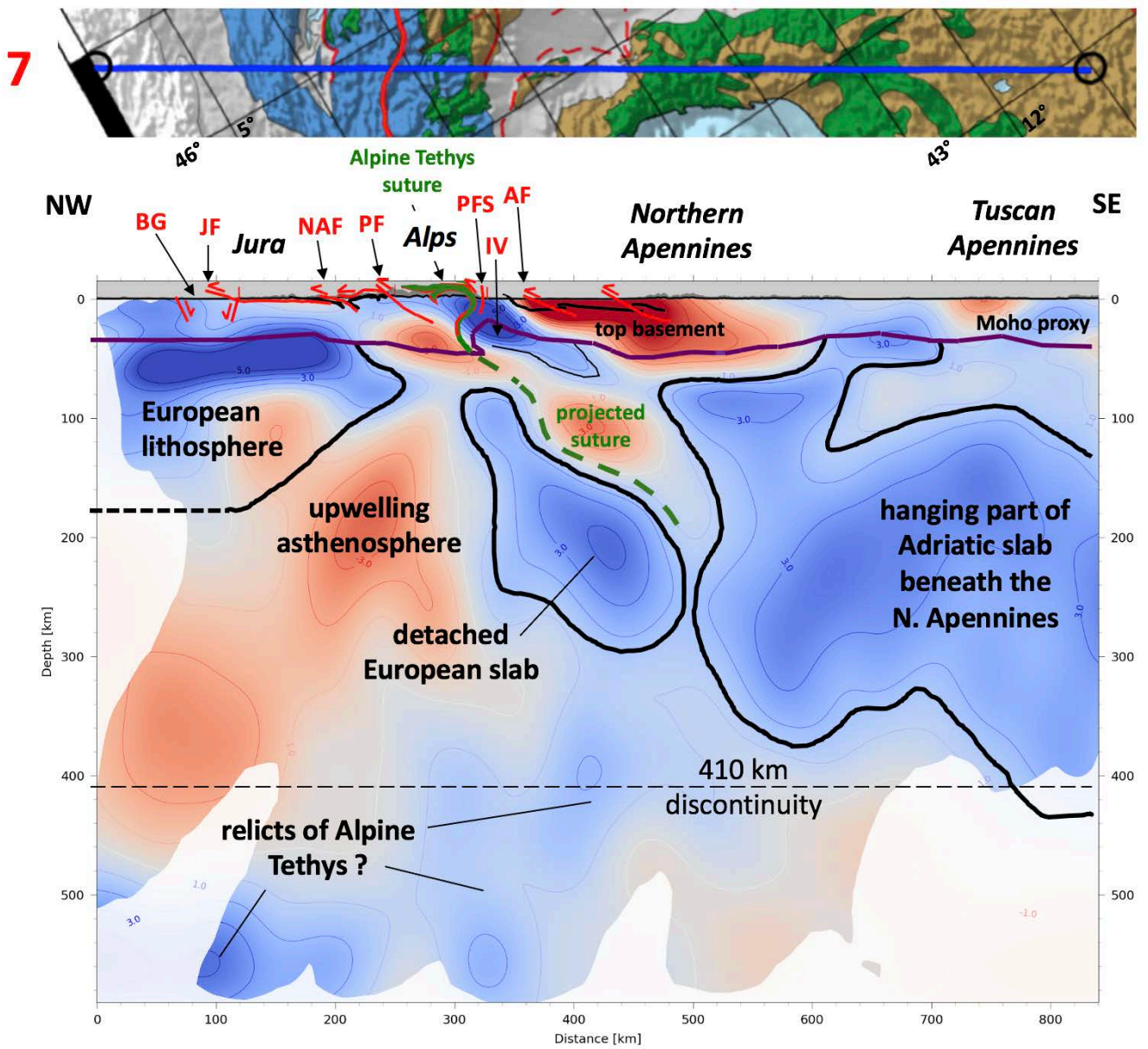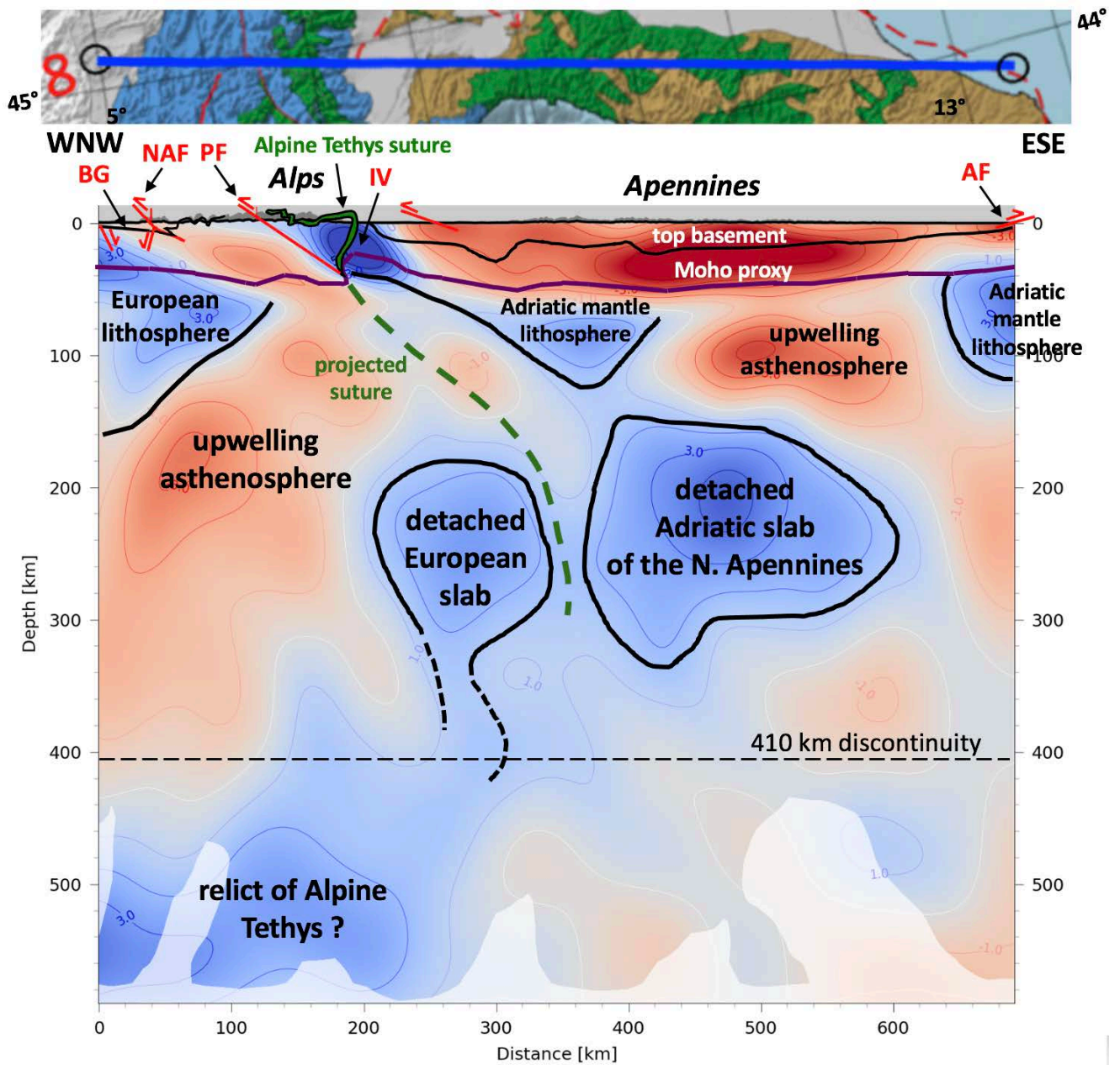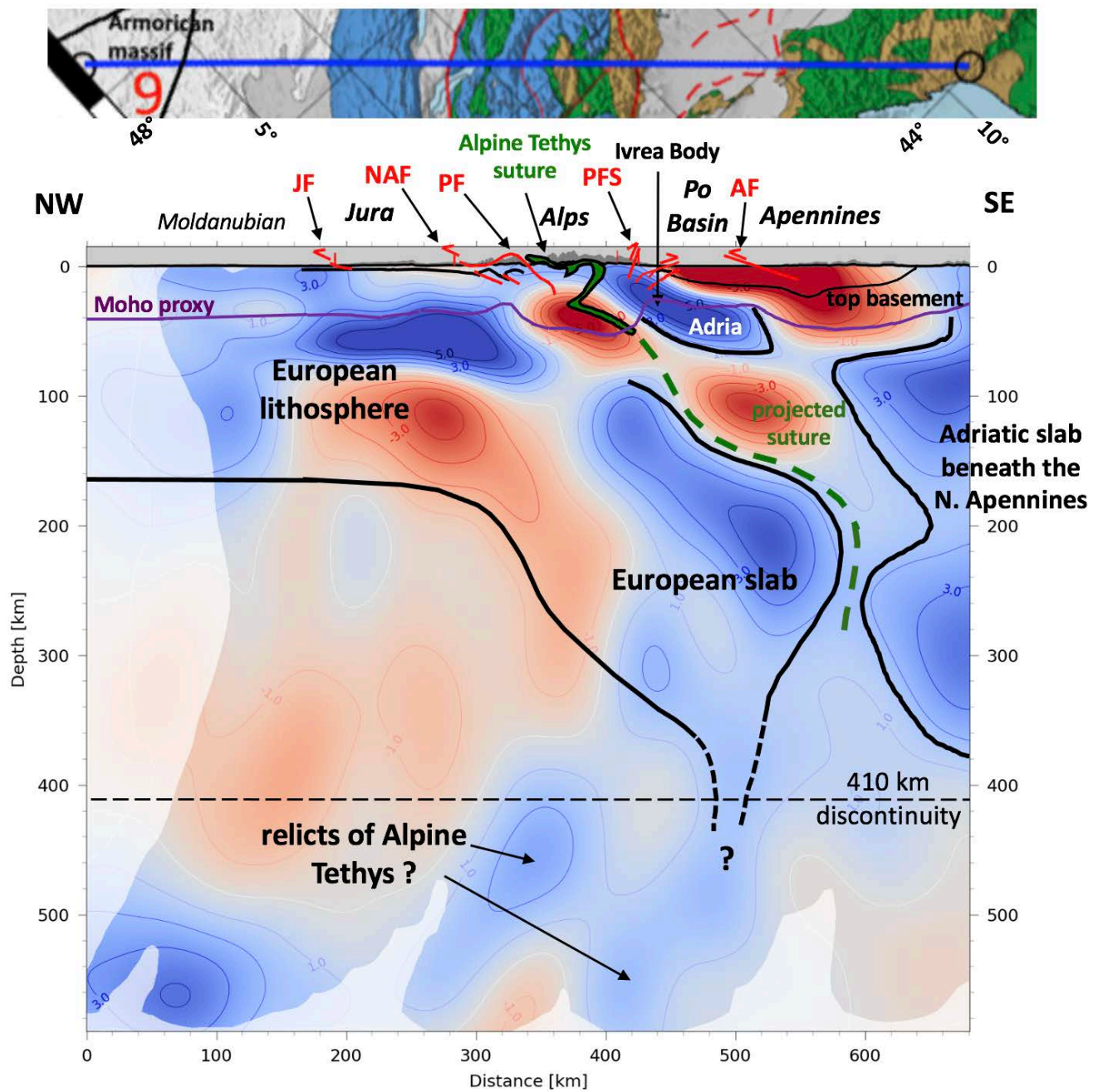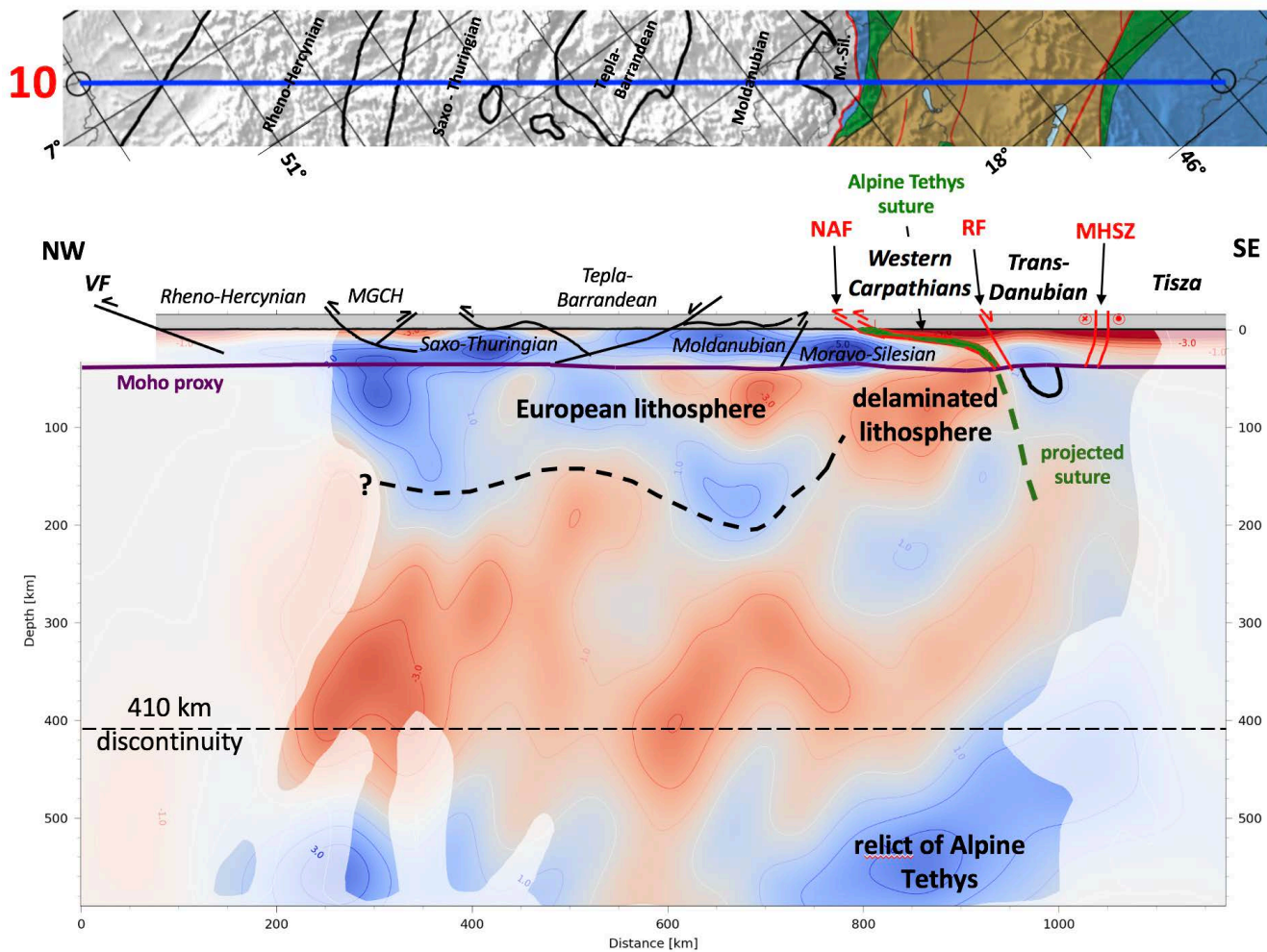
1002
1003   Fig. A6   Profile 6

1004
1005   Fig. A7   Profile 7

1006
1007   Fig. A8   Profile 8

1008
1009 Fig. A9   Profile 9

1010
1011   Fig. A10   Profile 10

1012
1013   Fig. A11   Profile 11

1014
1015   Fig. A12   Profile 12
1016

1017
1018   Fig. A13   Profile 13
1019

1020
1021   Fig. A14   Profile 14
1022

1023
1024   Fig. A15   Profile 15
1025
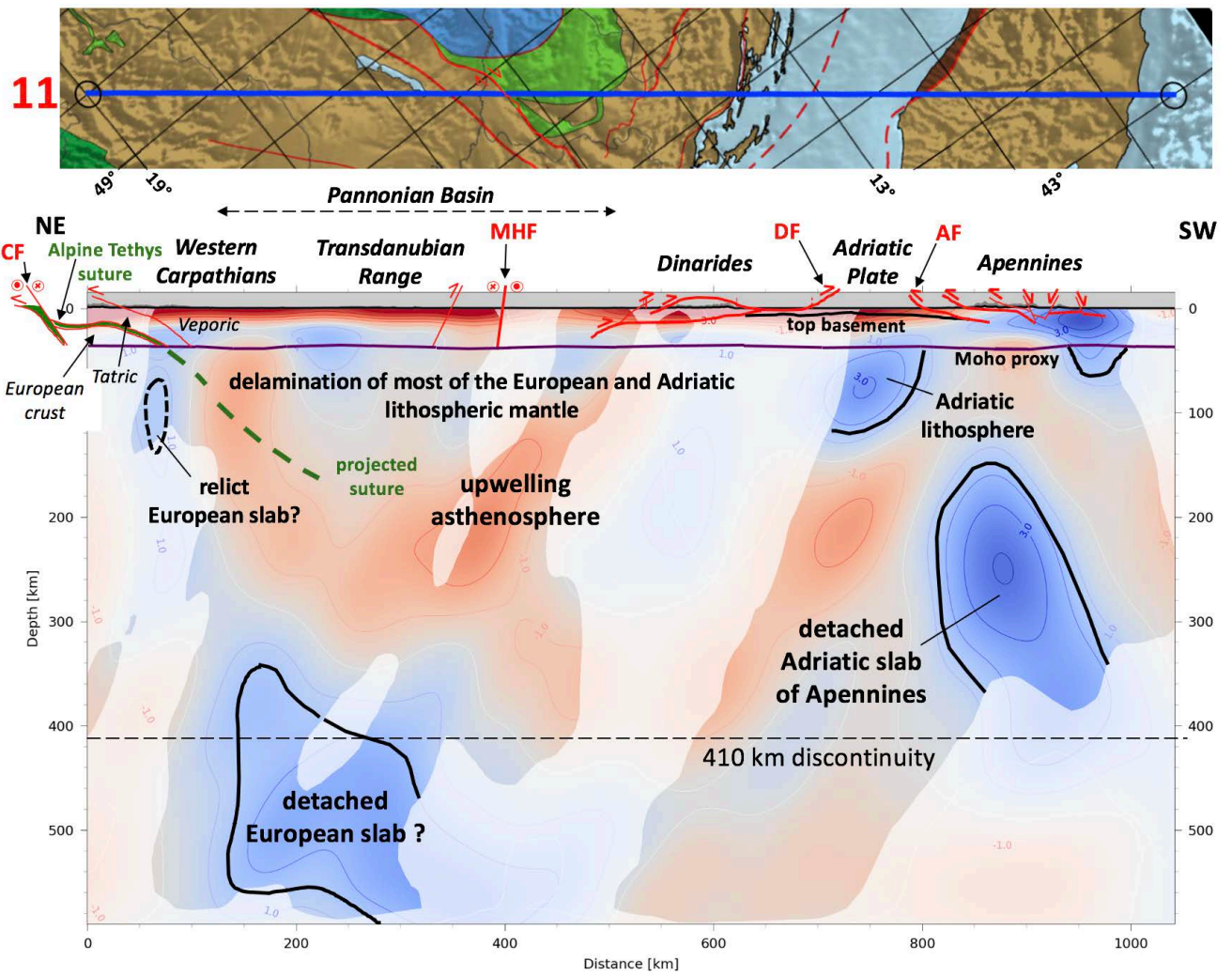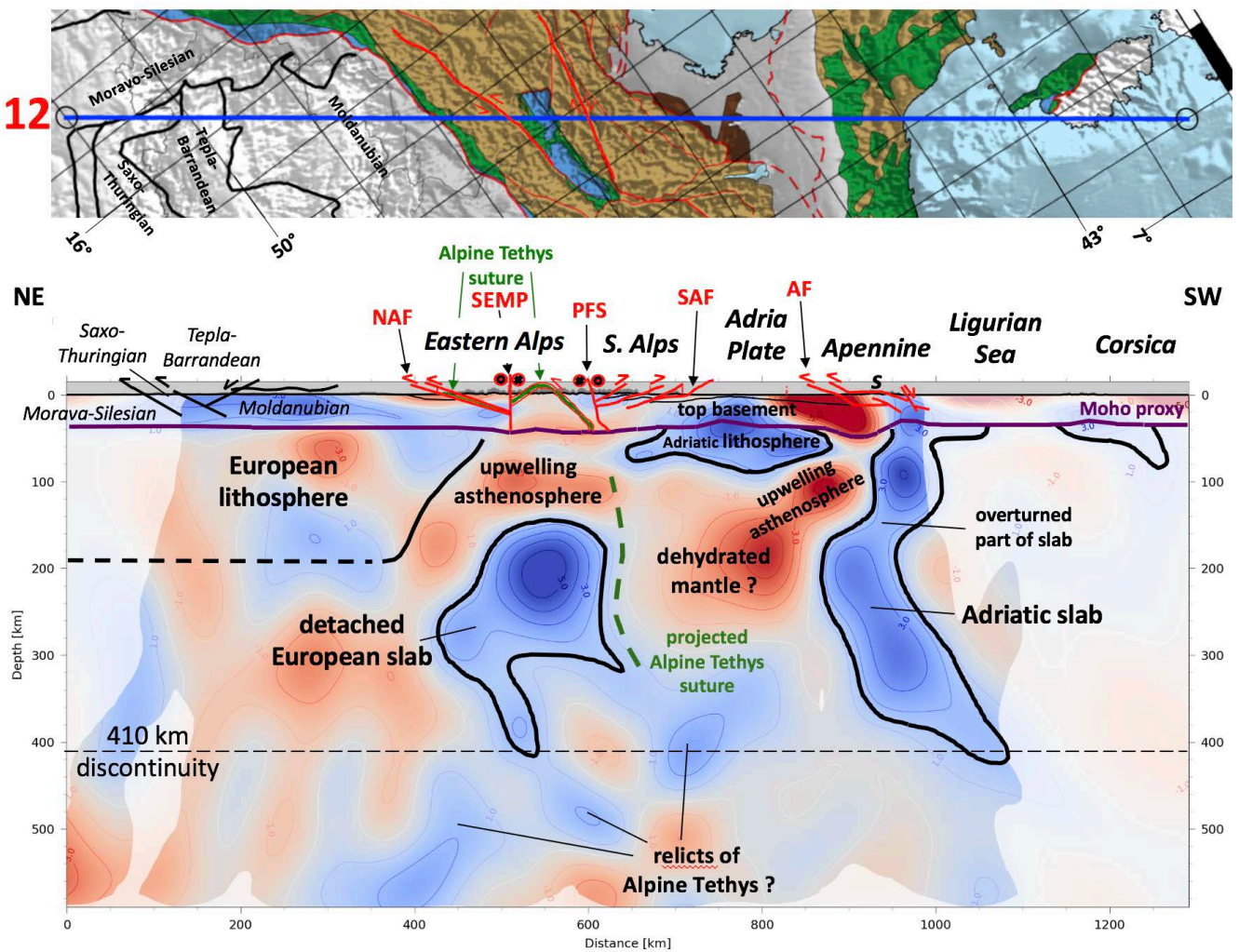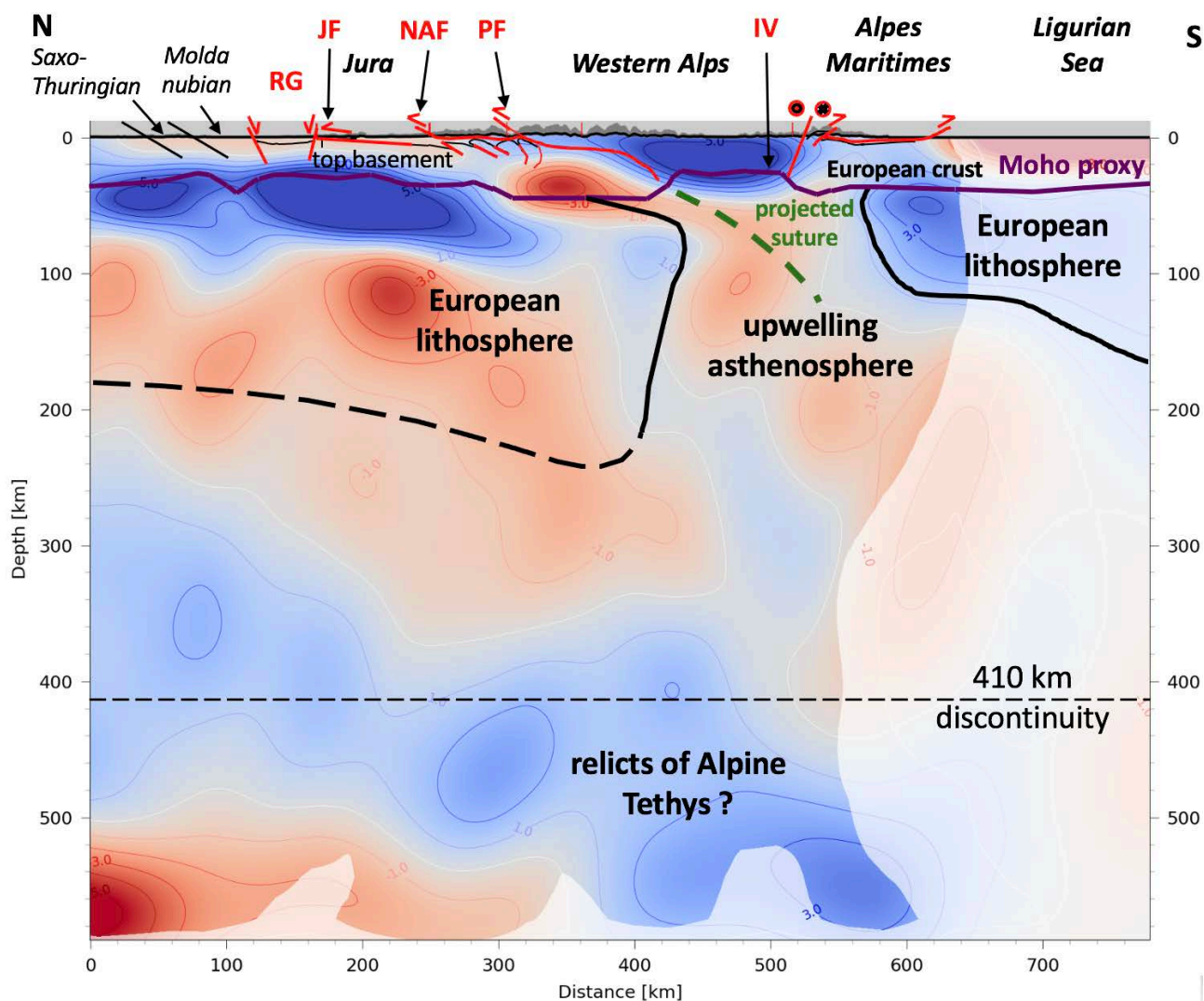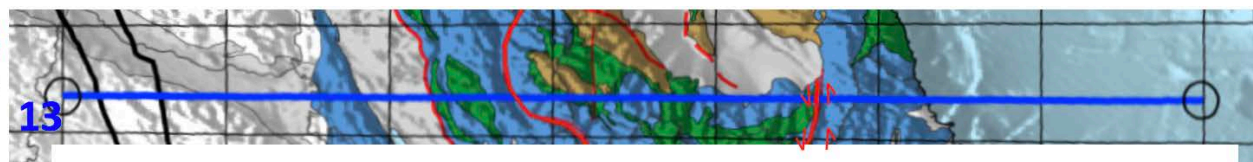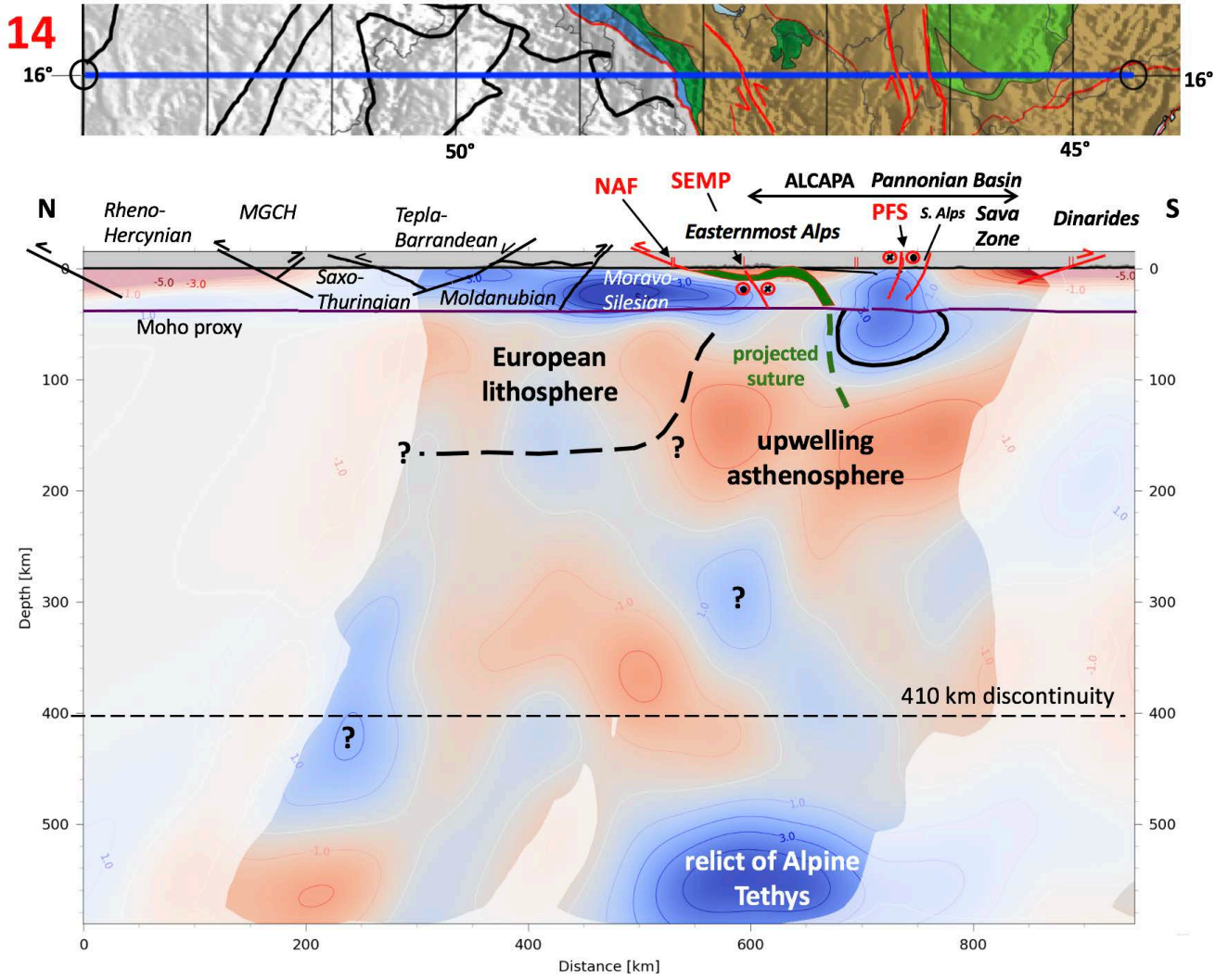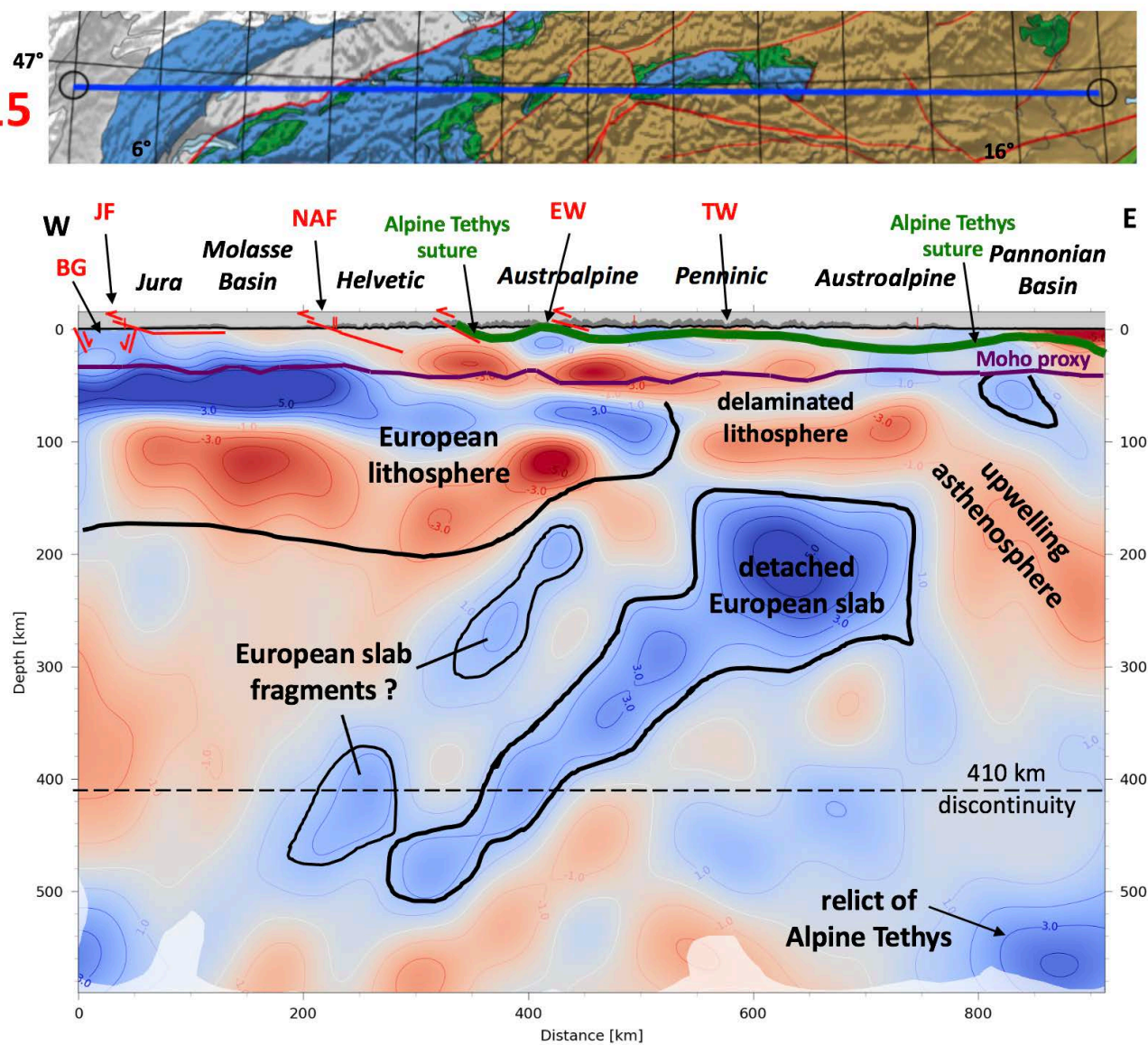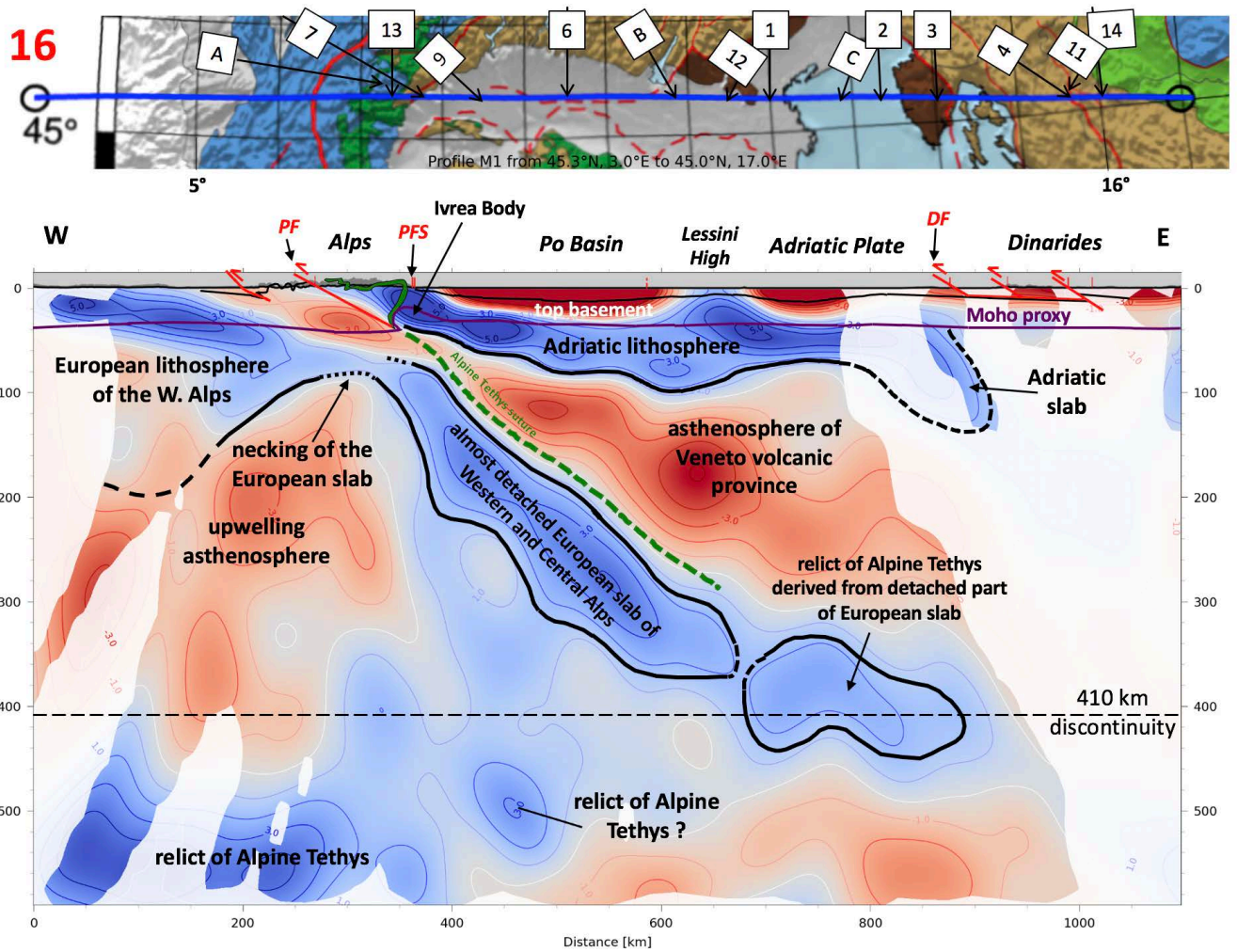
1026
1027   Fig. A16   Profile 16. Numbered labels at top indicate intersecting profiles.
1028

1029
1030   Fig. A17   Profile A
1031

1032
1033   Fig. A18   Profile B
1034

1035
1036   Fig. A19   Profile C
1037
1038

1039
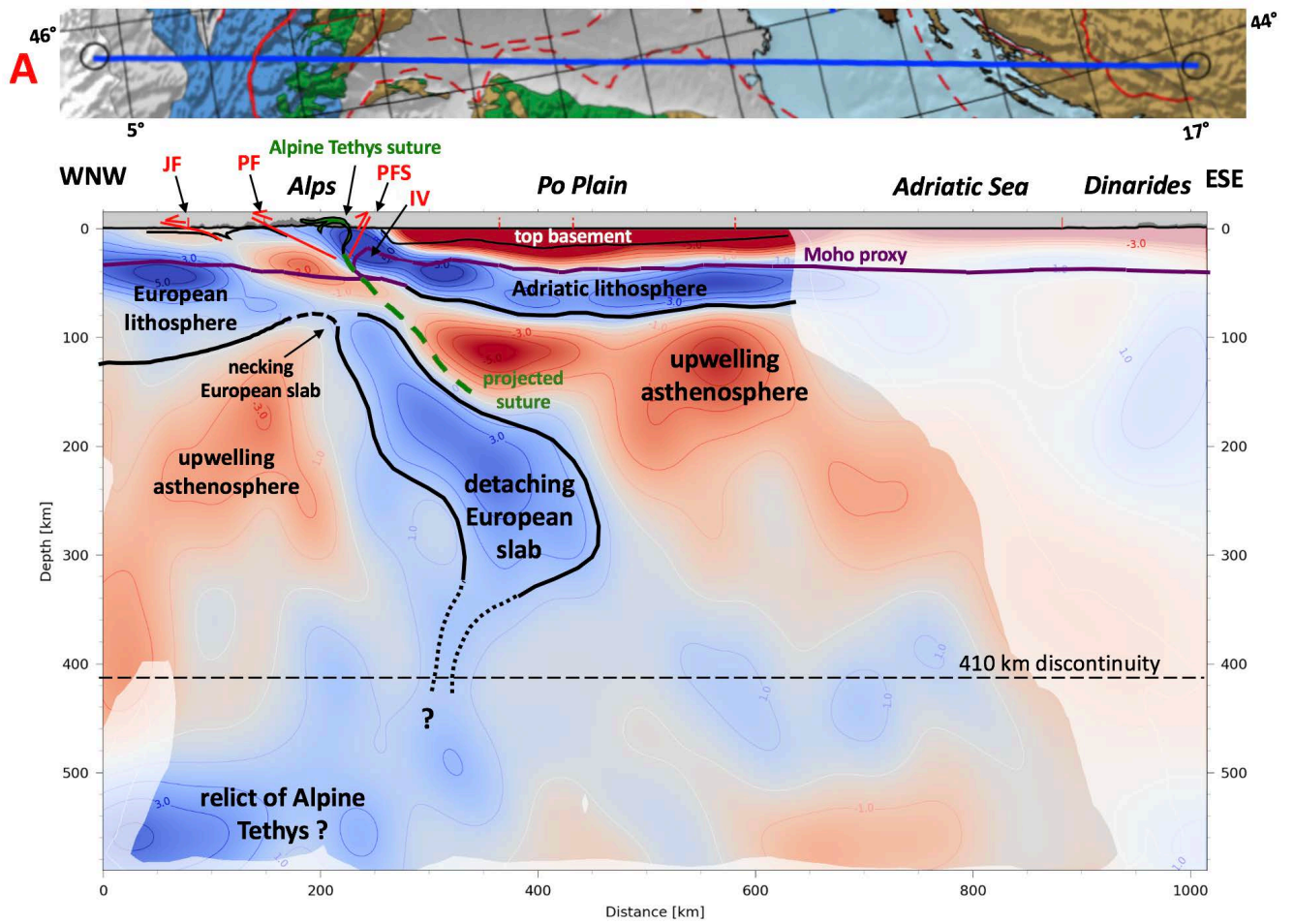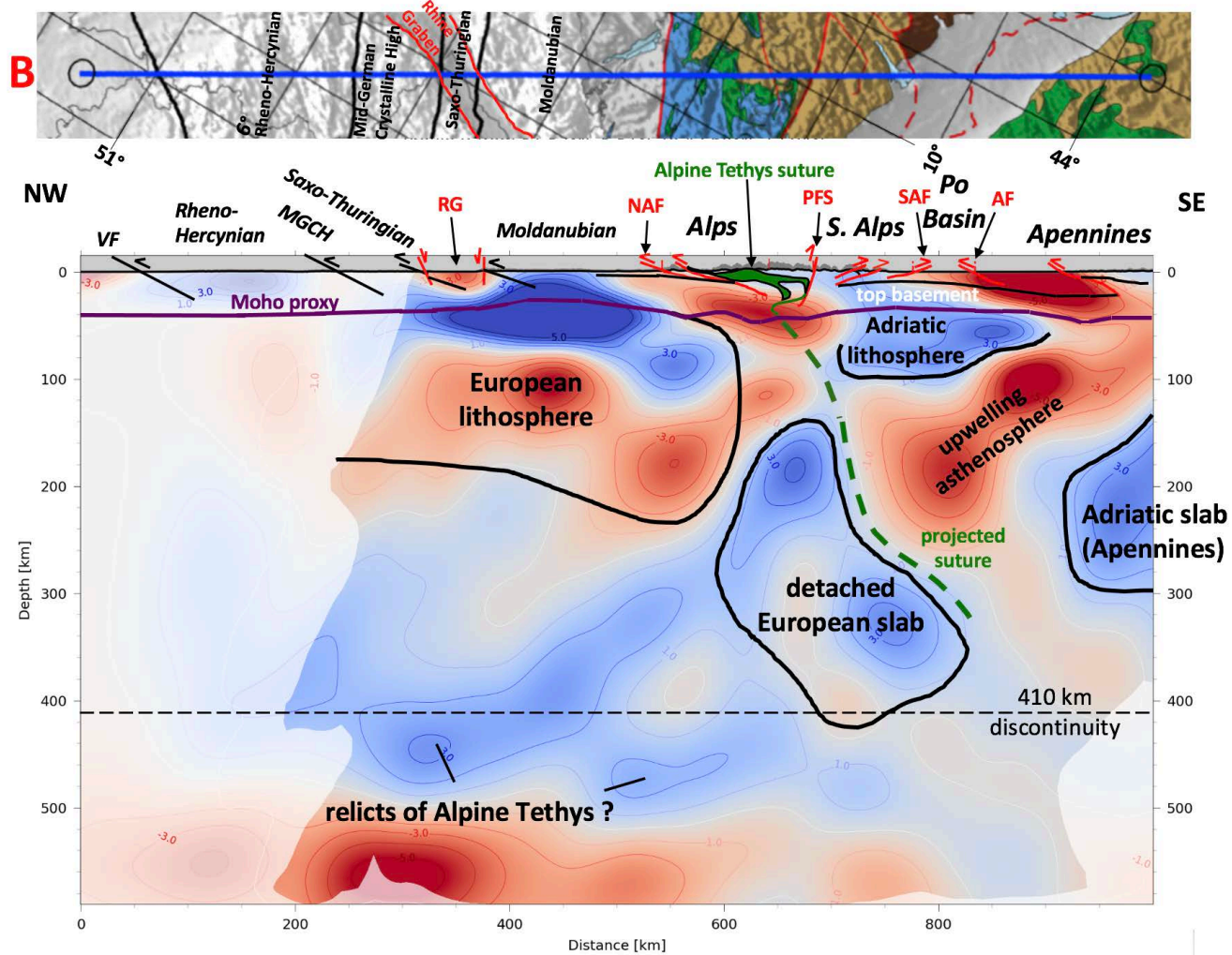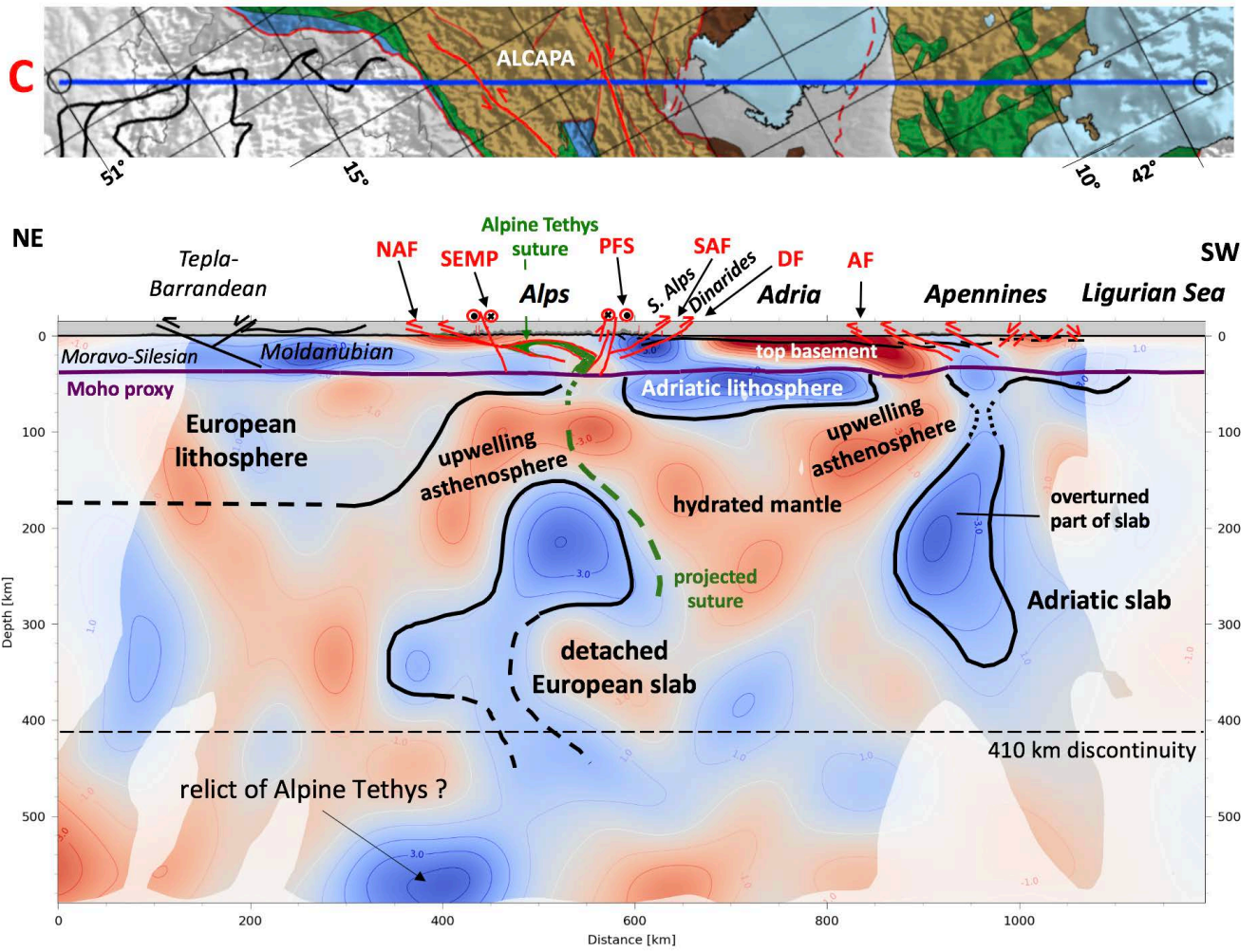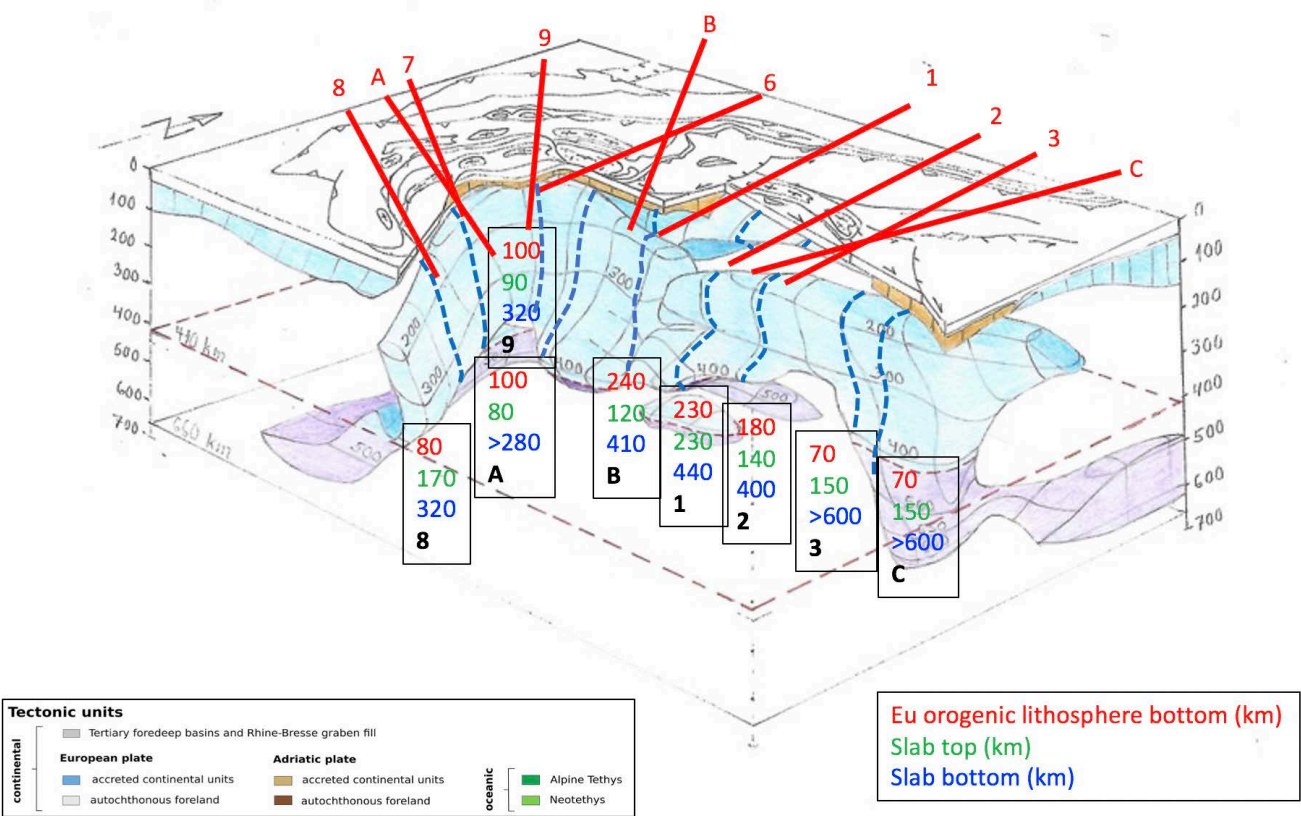
1040
1041
1042   Fig. B1   3D block diagram with depths to slab tops and bottoms
1043
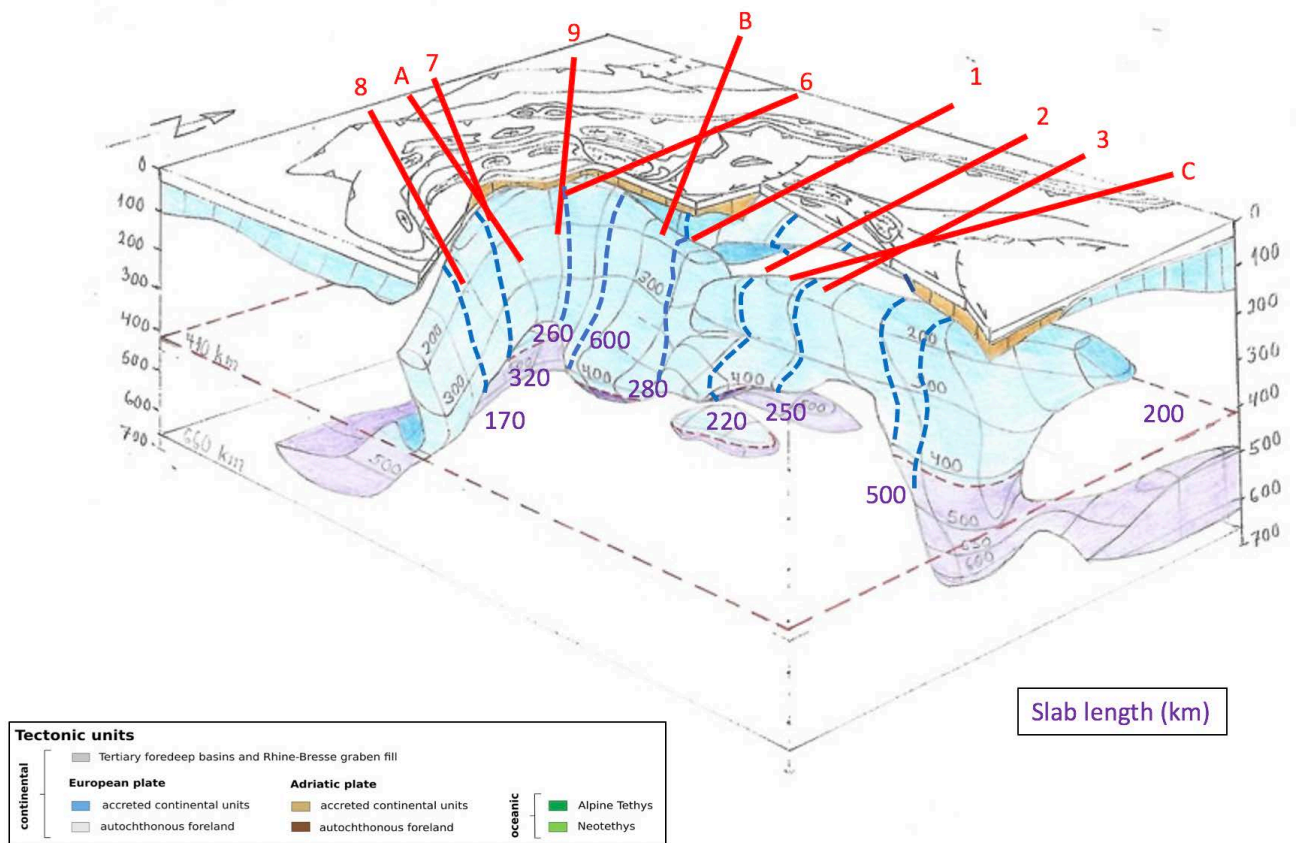
Fig. B2   3D block diagram with slab lengths

Team List

1. Mark R. Handy - Institut für Geologische Wissenschaften, Freie Universität Berlin, Malteserstr. 74-100, 12249 Berlin, Germany; Institut für Geologie, ETH-Zürich, Sonneggstr. 5, 8092 Zürich
2. Stefan M. Schmid - Institut für Geophysik, ETH-Zürich, Sonneggstr. 5, 8092 Zürich
3. Marcel Paffrath - Institut für Geologie, Mineralogie, Geophysik, Ruhr-Universität Bochum, 44780 Bochum, Germany
4. Wolfgang Friederich - Institut für Geologie, Mineralogie, Geophysik, Ruhr-Universität Bochum, 44780 Bochum, Germany
5. AlpArray Working Group: http://www.alparray.ethz.ch/en/seismic_network/backbone/data-policy-and-citation/.

Author contributions

Mark Handy and Stefan Schmid interpreted the tomographic profiles and slices that were provided in raw form by Marcel Paffrath. The latter co-author and Wolfgang Friederich provided the methods that generated the tomographic sections. Mark Handy conceived of and prepared the manuscript with contributions from all co-authors.

Competing interests – Mark Handy is a member of the editorial board of this special issue

Disclaimer - none

Special Issue Statement – this manuscript has been submitted for inclusion in the special issue „New insights on the tectonic evolution of the Alps and the adjacent orogens"

Acknowledgements

We acknowledge the generous funding of the German Science Foundation. (DFG) in the form of Special Priority Program 2017 "Mountain-Building in Four-Dimensions (4D-MB). This is an arm of the European "AlpArray" project, which involved the following subprojects: Ha-2403/22-1, Ha-2403/23-1, Ha-2403/24-1 and FR 1146/12-1. We thank our colleagues in AlpArray for discussions on various topics, some who were only marginally related to this paper, but all of whom provided a stimulating research background for the ideas presented here: Tobias Diehl, György Hetényi, the late Frank Horvath, Rainer Kind, Edi Kissling, Eline Le Breton, Frederick Link, Thomas Meier, Jan Pleuger, Georg Rümpker, Wim Spakman, Frederik Tilmann, Claudia Piromallo, Anne Bernhardt, Vincent Verwater, Philip Groß, Julian Hülscher. A complete list of members of the AlpArray Working Group can be found here: http://www.alparray.ethz.ch/en/seismic_network/backbone/data-policy-and-citation/.

1090 **References**
1091

1092 Agard, P., and Handy, M.R.: Ocean subduction dynamics in the Alps, in: Shedding Light on the
1093   European Alps, McCarthy, A. and Müntener, O., Guest Editors, Elements 17, 1, 2021.
1094

1095 Argand, E.: Des Alpes et de l'Afrique: Bulletin de la Société Vaudoise des Sciences Naturelles, 55,
1096   233–236, 1924.
1097

1098 Artemieva, I.: The Lithosphere: An Interdisciplinary Approach, Cambridge University Press
1099   Monograph, 794 pp., ISBN 9780521843966, 2011.
1100

1101 Babuska, V., Plomerova, J., and Granet, M.: The deep lithosphere in the Alps: a model inferred from P
1102   residuals, Tectonophysics, 176, 137-165, https://doi.org/10.1016/0040-1951(90)90263-8, 1990.
1103

1104 Baran, R., Friedrich, A. M., and Schlunegger, F.: The late Miocene to Holocene erosion pattern of the
1105   Alpine foreland basin reflects Eurasian slab unloading beneath the western Alps rather than
1106   global climate change, Lithosphere, 6/2, 124–131, doi: 10.1130/L307.1, 2014.
1107

1108 Beccaluva, L., Bianchini, G., Bonadiman, C., Coltorti, M., Milani, L., Salvini, L., Siena, F., and Tassinari,
1109   R.: Intraplate lithospheric and sublithospheric components in the Adriatic domain: Nephelinite
1110   to tholeiite magma generation in the Paleogene Veneto volcanic province, southern Alps,
1111   Geological Society of America Special Paper, 418, 131–152, doi:10.1130/2007.2418(07), 2007.
1112

1113 Behm, M., Brückl, E., Chwatal, W., and Thybo, H.: Application of stacking and inversion techniques
1114   to three-dimensional wide-angle reflection and refraction data of the Eastern Alps, Geophys. J.
1115   Int. 170, 275–298, doi.org/10.1111/j.1365-246X.2007.03393.x, 2007
1116

1117 Bigi, G., Castellarin, A., Catalano, R., Coli, M., Cosentino, D., Dal Piaz, G.V., Lentini, F., Parotto, M.,
1118   Patacca, E., Praturlon, A., Salvini, F., Sartori, R., Scandone, P., and Vai, G.: Synthetic structural
1119   kinematic map of Italy, Sheets 1 and 2, C.N.R., Progetto Finalizzato Geodinamica, SELCA Firenze,
1120   1989.
1121

1122 Bijwaard, H., and Spakman, W.: Non-linear global P-wave tomography by iterated linearized
1123   inversion, Geophys. J. Int., 141,71–82, doi.org/10.1046/j.1365-246X.2000.00053.x, 2000.
1124

1125 Brenker, F.E., and Brey, G.P.: Reconstruction of the exhumation path of the Alpe Arami garnet-
1126   peridotite from depths exceeding 160 km. J. metamorphic Geol., 15, 581-592,
1127   doi/abs/10.1111/j.1525-1314.1997.tb00637.x, 1997.
1128

1129 Brückl, E., Bleibinhaus, F., Gosar, A., et al.: Crustal structure due to collisional and escape tectonics
1130   in the Eastern Alps region based on profiles Alp01 and Alp02 from the ALP 2002 seismic
1131   experiment. J. Geophys. Res. 112, B06308, doi:10.1029/2006JB004687, 2007.
1132

1133 Cammarano, F., Goes, S., Vacher, P., and Giardini, D.: Inferring upper-mantle temperatures from
1134   seismic velocities, Physics of the Earth and Planetary Interiors, 138, 197–222,
1135   doi:10.1016/S0031-9201(03)00156-0, 2003.
1136

1137 Cassano, E., Anelli, L., Fichera, R., and Cappelli, V: Pianura Padana: Interpretazione integrate di dati
1138   Geofisici e geologici, 73° Congresso Società Geologica Italiana, Roma, AGIP, 27 pp, 1986.
1139

1140 Champagnac, J.D., Molnar, P., Anderson, R.S., Sue, C., and Delacou, B.: Quaternary erosion-induced
1141   isostatic rebound in the western Alps, Geology, 35; 195-198, doi: 10.1130/G23053A.1, 2007.

1142 Chopin, C.: Coesite and pure pyrope in high-grade blueschists of the Western Alps: a first record and
1143   some consequences, Contr. Mineral. and Petrol. 86, 107–118,
1144   https://doi.org/10.1007/BF00381838, 1984.

1145 Cederbom C.E., van der Beek, P., Schlunegger, F., Sinclair, H.D., and Oncken, O.: Rapid extensive
1146   erosion of the North Alpine foreland basin at 5-4 Ma, Basin Research, 23, 528–550, doi:
1147   10.1111/j.1365-2117.2011.00501.x, 2011.

1148 Dando B.D.E., Stuart, G.W., Houseman, G.A., Hegedüs, E., Brückl. E., and Radovanovic, S.:
1149   Teleseismic tomography of the mantle in the Carpathian–Pannonian region of central Europe.
1150   Geophys. J. Int., 186, 11–31, doi: 10.1111/j.1365246X.2011.04998.x, 2011.
1151

1152 Diehl, T., Husen, S., Kissling, E., and Deichmann, N.: High-resolution 3-D P-wave model of the Alpine
1153   crust, Geophys. J. Int., 179, 1133–1147, doi: 10.1111/j.1365246X.2009.04331.x, 2009.
1154

1155 Faccenna, C., Piromallo, C., Crespo-Blanc, A., Jolivet, L., and Rossetti, F.: Lateral slab deformation and
1156   the origin of the western Mediterranean arcs, Tectonics, 23, TC1012,
1157   doi:10.1029/2002TC001488, 2004.
1158

1159 Favaro S., Handy, M.R., Scharf, A., and Schuster, R.: Changing patterns of exhumation and
1160   denudation in front of an advancing crustal indenter, Tauern Window (Eastern Alps), Tectonics,
1161   36, 1053-1071, doi: 10.1002/2016TC004448, 2017.
1162

1163 Foulger, G. R., Panza, G. F., Artemieva, I. M., Bastow, I. D., Cammarano, F., Evans, J. R., Hamilton, W.
1164   B., Julian, B. R., Lustrino, M., Thybo, H., and Yanovskaya, T. B.: Caveats on tomographic images,
1165   Terra Nova, 25, 259-281, doi: 10.1111/ter.12041, 2013.
1166

1167 Fox, M., Herman, F., Kissling E., and Willet, S.D.: Rapid exhumation in the Western Alps driven by
1168   slab detachment and glacial erosion, Geology, doi:10.1130/G36411.1, 2015.
1169

1170 Fox, M., Herman F., Willett, S.D., and Schmid, S.M.: The exhumation history of the European Alps
1171   inferred from linear inversion of thermochronometric data: American Journal of Science, 316,
1172   505-541, doi: 10.2475/06.2016.01, 2016.
1173

1174 Franke, W.: The Mid-European segment of the Variscides: tectonostratigraphic units, terrane
1175   boundaries and plate tectonics evolution, Geological Society, London, Special Publications, 179,
1176   35-61, https://doi.org/10.1144/GSL, 2000.
1177

1178 Franke, W., Cock, L.R.M., and Torsvik, T.H.: The Palaeozoic Variscan oceans revisited. Gondwana
1179   Research, 48, 257-284, http://dx.doi.org/10.1016/j.gr.2017.03.005, 2017.
1180

1181 Fügenschuh, B., Seward, D., and Mancktelow, N.S.: Exhumation in a convergent orogen: the western
1182   Tauern Window. Terra Nova, 9, 213–217, doi: 10.1111/j.1365-3121.1997.tb00015.x, 1997
1183
1184 Geissler, W.H., Sodoudi, F., and Kind, R.: Thickness of the central and eastern European lithosphere
1185   as seen by S receiver functions: Geophysical Journal International, 181, 604–634, doi:
1186   10.1111/j.1365-246X.2010.04548.x, 2010.
1187
1188 Genser, J., Cloetingh, S. A, L., and Neubauer, F.: Late orogenic rebound and oblique Alpine
1189   convergence: New constraints from subsidence analysis of the Austrian Molasse basin, Global
1190   and Planetary Change, 58, 1–4, 214–223, doi: 10.1016/j.gloplacha.2007.03.010, 2007.
1191
1192 Giacomuzzi, G., Chiarabba, C., and De Gori, P.: Linking the Alps and Apennines subduction systems:
1193   New constraints revealed by high-resolution teleseismic tomography. Earth and Planetary
1194   Science Letters, 301, 531–543, doi:10.1016/j.epsl.2010.11.033, 2011.
1195
1196 Giacomuzzi, G., Civalleri, M., DeGori, P., and Chiarabba, C.: A 3D Vs model of the upper mantle
1197   beneath Italy: Insight on the geodynamics of central Mediterranean, Earth and Planetary
1198   Science Letters, 335-336, 105-120, doi.org/10.1016/j.epsl.2012.05.004, 2012.
1199
1200 Goes, S., Govers, R., and Vacher, P.: Shallow mantle temperatures under Europe from P and S wave
1201   tomography: Journal of Geophysical Research 105/B5, 11153-11169,
1202   doi.org/10.1029/1999JB900300, 2000.
1203
1204 Grad, M., Tiira, T., and ESC Working Group: The Moho depth map of the European Plate. Geophys. J.
1205   Int. 176, 279–292, doi: 10.1111/j.1365-246X.2008.03919.x, 2009.
1206
1207 Grenerczy, G., Sella, G., Stein, S., Kenyeres, A.: Tectonic implications of the GPS velocity field in the
1208   northern Adriatic region, Geophysical Research Letters, 32, doi:10.1029/2005GL022947, 2005.
1209
1210 Gross, P., Handy, M. R., John, T., Pestal, G., and Pleuger, J.: Crustal-scale sheath folding at HP
1211   conditions in an exhumed Alpine subduction zone (Tauern Window, Eastern Alps), Tectonics,
1212   39, doi.org/10.1029/2019TC005942, 2020.
1213
1214 Grunert, P., Hinsch, R., Sachsenhofer, R. F., Bechtel, A., Ćorić, S., Harzhauser, M., Piller, W.E., and
1215   Sperl, H.: Early Burdigalian infill of the Puchkirchen Trough (North Alpine Foreland Basin,
1216   Central Paratethys): Facies development and sequence stratigraphy. Marine and Petroleum
1217   Geology, 39/1, 164–186, doi: 10.1016/j.marpetgeo.2012.08.009, 2013.
1218
1219 Hammond, J. O. S.: Constraining melt geometries beneath the Afar Depression, Ethiopia from
1220   teleseismic receiver functions: The anisotropic H-κ stacking technique, Geochem. Geophys.
1221   Geosyst., 15, 1316–1332, doi:10.1002/2013GC005186, 2014
1222
1223 Handy, M. R., Schmid, S. M., Bousquet, R., Kissling, E., and Bernoulli, D.: Reconciling plate-tectonic
1224   reconstructions with the geological-geophysical record of spreading and subduction in the Alps,
1225   Earth Science Reviews, 102, 121-158, doi:10.1016/j.earscirev.2010.06.002, 2010.
1226

1227 Handy, M. R., Ustaszewski, K., and Kissling, E.: Reconstructing the Alps–Carpathians–Dinarides as a
1228   key to understanding switches in subduction polarity, slab gaps and surface motion, Int. J. Earth
1229   Sci. (Geol. Rundsch.), 104,1–26 doi, 10.1007/s00531-014-1060-3, 2015.

1231 Hetényi, G. Molinari, I., Clinton, J., Bokelmann, G., Bondár, I., Crawford, W.C., Dessa, J.X., Doubre, C.,
1232   Friederich, W., Fuchs, F., Giardini, D., Gráczer, Z., Handy, M.R., Herak, M., Jia, Y., Kissling, E.,
1233   Kopp, H., Korn, M., Margheriti, L., Meier, T., Mucciarelli, M., Paul, A., Pesaresi, D., Piromallo, C.,
1234   Plenefisch, Th., Plomerová, J., Ritter, J., Rümpker, G., Šipka, V., Spallarossa, D., Thomas, Ch.,
1235   Tilmann, F., Wassermann, J., Weber, M., Wéber, Z., Wesztergom, V., Živčić, M., and AlpArray
1236   Seismic Network Team , AlpArray OBS Cruise Crew, AlpArray Working Group: The AlpArray
1237   Seismic Network: A large-scale European experiment to image the Alpine orogen. Surveys in
1238   Geophysics, 39, 1009-1033, doi.org/10.1007/s10712-018-9472-4, 2018.

1240 Hinsch, R.: Laterally varying structure and kinematics of the Molasse fold and thrust belt of the
1241   Central Eastern Alps: Implications for exploration, AAPG Bulletin, 97, 10, 1805–1831.
1242   doi:10.1306/04081312129, 2013.

1244 Horváth, F., Bada, G., Szafian, P., Tari, G., Adam, A. and Cloetingh, S.: Formation and deformation of
1245   the Pannonian Basin: constraints from observational data. In: Gee, D. G. & Stephenson, R. A.
1246   (eds), European Lithosphere Dynamics, Geological Society London Memoirs, 32, 191–206,
1247   doi.org/10.1144/GSL.MEM.2006.032.01.11, 2006.

1249 Horváth, F., Musitz, B., Balázs, A., Végh, A., Uhrin, A., Nádor, A., Koroknai, B., Pap, N., Tóth, T., and
1250   Wórum, G.: Evolution of the Pannonian basin and its geothermal resources. Geothermics, 53,
1251   328–352, doi.org/10.1016/j.geothermics.2014.07.009, 2015.

1253 Jolivet, L., Faccenna, C., and Piromallo, C.: From mantle to crust: Stretching the Mediterranean,
1254   Earth and Planetary Science Letters, 285, 1–2, 198-209.
1255   https://doi.org/10.1016/j.epsl.2009.06.017, 2009.

1257 Jones, A., G., Plomerova, J., Korja, T., Sodoudi, F., and Spakman, W.: Europe from the bottom up: A
1258   statistical examination of the central and northern European lithosphere–asthenosphere
1259   boundary from comparing seismological and electromagnetic observations, Lithos, 120, 14-29,
1260   doi:10.1016/j.lithos.2010.07.013, 2010.

1262 Jordan, T.H.: The Continental Tectosphere, Reviews of Geophysics and Space Physics, 13/3,
1263   doi.org/10.1029/RG013i003p00001, 1975.

1265 Jordan, T.H.: Continents as a chemical boundary layer, Phil. Trans. R. Soc. Lond., A 301, 359-373,
1266   1981.

1268 Karato, S., and Jung, H.: Water, partial melting and the origin of the seismic low velocity and high
1269   attenuation zone in the upper mantle, Earth and Planetary Science Letters, 157, 193–207, 1998.

1271 Karousová, H., Babuška, V., and Plomerová, J.: Upper-mantle structure beneath the southern
1272   Bohemian Massif and its surroundings imaged by high-resolution tomography, Geophys. J. Int.,
1273   194, 1203–1215, https://doi.org/10.1093/gji/ggt159, 2013.

1274

1275 Kastelic, V., Vrabec, M., Cunningham, D., and Gosar, A.: Neo-Alpine structural evolution and
1276   present-day tectonic activity of the eastern Southern Alps: The case of the Ravne Fault, NW
1277   Slovenia, Journal of Structural Geology, 30, 963-975, doi:10.1016/j.jsg.2008.03.009, 2008.

1278

1279 Kästle, E.D., Rosenberg, C., Boschi, L., Bellahsen, N., Meier, T., El-Sharkawy, A.: Slab break-offs in
1280   the Alpine subduction zone. Int. J. Earth Sci. (Geol Rundsch), 109, 587–603,
1281   https://doi.org/10.1007/s00531-020-01821-z, 2020.

1282

1283 Kind, R., Schmid, S. M., Yuan, X, Heit, B., Meier, T., and the AlpArray and AlpArray-SWATH-D
1284   Working Groups: Moho and uppermost mantle structure in the greater Alpine area from S-to-P
1285   converted waves, Solid Earth, this volume, 2021.

1286

1287 Király, Á., Faccenna, C., and Funiciello, F: Subduction zones interaction around the Adria microplate
1288   and the origin of the Apenninic arc: Tectonics, 37, 3941–3953,
1289   https://doi.org/10.1029/2018TC00521, 2018.

1290

1291 Kissling, E., and Schlunegger, F.: Rollback orogeny model for the evolution of the Swiss Alps,
1292   Tectonics, 37, doi.org/10.1002/2017TC004762, 2018.

1293

1294 Kissling, E., Schmid, S. M., Lippitsch, R., Ansorge, J., and Fügenschuh, B.: Lithosphere structure and
1295   tectonic evolution of the Alpine arc: new evidence from high-resolution teleseismic
1296   tomography, Geological Society of London Memoirs, 32, 129-145,
1297   doi.org/10.1144/GSL.MEM.2006.032.01.08, 2006.

1298

1299 Koulakov, I., Kaban, M., Tesauro, M., and Cloetingh, S.: P-and S-velocity anomalies in the upper
1300   mantle beneath Europe from tomographic inversion of ISC data, Geophys. J. Int., 179, 345–366,
1301   doi: 10.1111/j.1365-246X.2009.04279.x, 2009.

1302

1303 Kuhlemann, J., and Kempf, O.: Post-Eocene evolution of the North Alpine Foreland Basin and its
1304   response to Alpine tectonics, Sedimentary Geology, 152, 45–78, doi.org/10.1016/S0037-
1305   0738(01)00285-8, 2002.

1306

1307 Kurz, W., Handler, R., and Bertoldi, C.: Tracing the exhumation of the Eclogite Zone (Tauern
1308   Window, Eastern Alps) by 40Ar/39Ar dating of white mica in eclogites, Swiss J. Geosci. 101,
1309   Supplement 1, S191–S206, 10.1007/s00015-008-1281-1, 2008.

1310

1311 Le Breton, E., Brune, S., Ustaszewski, K., Zahirovic, S., Seton, M., and Müller, R. D.: Kinematics and
1312   extent of the Piemont-Liguria Basin – implications for subduction processes in the Alps, Solid
1313   Earth, https://doi.org/10.5194/se-2020-161, 2021.

1314

1315 Lippitsch, R., Kissling, E., and Ansorge, J.: Upper mantle structure beneath the Alpine orogen from
1316   high-resolution teleseismic tomography, J. Geophys. Res., 108(B8), 2376,
1317   doi:10.1029/2002JB002016, 2003.

1318

1319 Lyu, C., Pedersen, H.A., Paul, A., Zhao, L., Solarino, S., and CIFALPS Working Group: Shear wave
1320 velocities in the upper mantle of theWestern Alps: new constraints using array analysis of
1321 seismic surface waves. Geophys. J. Int. (2017) 210, 321–331, 2017. doi: 10.1093/gji/ggx166.
1322

1323 Macera, P., Gasperini, D., Piromallo, C., Blichert-Toft, J., Bosch, D., Del Moro, A., and Martin, S.:
1324 Geodynamic implications of deep mantle upwelling in the source of Tertiary volcanics from the
1325 Veneto region (South-Eastern Alps), Journal of Geodynamics, 36, 563–590,
1326 doi:10.1016/j.jog.2003.08.004, 2003.
1327

1328 Macera, P., Gasperini, D., Ranalli, G., and Mahatsente, R.: Slab detachment and mantle plume
1329 upwelling in subduction zones: an example from the Italian South-Eastern Alps, Journal of
1330 Geodynamics, 45, 32–48, doi:10.1016/j.jog.2007.03.004, 2008.
1331

1332 Maffione, M., Speranza, F., Faccenna, C., Cascella, A., Vignaroli, G., and Sagnotti, L.: A synchronous
1333 Alpine and Corsica-Sardinia rotation: Journal of Geophysical Research, 113, B03104,
1334 doi:10.1029/2007JB005214, 2008.
1335

1336 Malusà, M. G., Frezzotti, M. L., Ferrando, S., Brandmayr, E., Romanelli, F., and Panza, G. F.: Active
1337 carbon sequestration in the Alpine mantle wedge and implications for long-term climate trends.
1338 Scientific Reports, 8(1), 1–8, 2018.
1339

1340 Malusà, M. G., Guillot, S., Zhao, L., Paul, A., Solarino, S., Dumont, T., Schwartz, S., Aubert, C.,
1341 Baccheschi, P., Eva, E., Lu, Y., Lyu, C., Pondrelli, S., Salimbeni, S., Sun, W. and Yuan, H.: The deep
1342 structure of the Alps based on the CIFALPS seismic experiment: A synthesis. Geochemistry,
1343 Geophysics, Geosystems, 22, e2020GC009466. https://doi.org/10.1029/2020GC0094662021

1344 Márton, E., Grabowski, J., Tokarski, A.K., and Túnyi, I.: Palaeomagnetic results from the fold and
1345 thrust belt of the Western Carpathians: an overview, Geological Society, London, Special
1346 Publications, 425, 7-36, https://doi.org/10.1144/SP425.1, 2015.

1347 **Matenco, L., and Radivojević, D.: On the formation and evolution of the Pannonian Basin:**
1348 **Constraints derived from the structure of the junction area between the Carpathians and**
1349 **Dinarides, Tectonics, 31, TC6007, doi:10.1029/2012TC003206, 2012.**

1350 Matte, P.: Tectonics and plate tectonics model for the Variscan belt of Europe. Tectonophysics, 126,
1351 2–4, 15, 329-332, 335-344, 347-374. https://doi.org/10.1016/0040-1951(86)90237-4. 1986.
1352

1353 Mazur, S., Aleksandrowski, P., Gągała, Ł., Krzywiec, P., Żaba, J., Gaidzik, K., and Sikora, R.: Late
1354 Palaeozoic strike-slip tectonics versus oroclinal bending at the SW outskirts of Baltica: case of
1355 the Variscan belt's eastern end in Poland, International Journal of Earth Sciences, 109, 1133-
1356 1160, doi:10.1007/s00531-019-01814-7, 2020.
1357

1358 Mey, J., Scherler, D., Wickert, A. D., Egholm, D. L., Tesauro, M., Schildgen, T. F., and Strecker M. R.:
1359 Glacial isostatic uplift of the European Alps, Nature Communications, 7: 13382,
1360 doi:10.1038/ncomms13382, 2016.
1361

1362 Mitchell, B.J.: Anelastic structure and evolution of the continental crust and upper mantle from
1363   seismic surface wave attenuation, Reviews of Geophysics, 33, 441-462,
1364   https://doi.org/10.1029/95RG02074

1366 Mitterbauer, U., Behm, M., Brückl, E., Lippitsch, R., Guterch, A., Keller, G. R., Koslovskaya, E.,
1367   Rumpfhuber, E. M., and Šumanovac, F.: Shape and origin of the East-Alpine slab constrained by
1368   the ALPASS teleseismic model, Tectonophysics 510, 195–206, doi:10.1016/j.tecto.2011.07.001,
1369   2011.

1371 Molli, G., Crispini, L., Mosca, P., Piana, P., and Federico, L.: Geology of the Western Alps-Northern
1372   Apennine junction area: a regional review. Journal of the Virtual Explorer, 36/9, 1-49,
1373   doi:10.3809/jvirtex.2010.00215, 2010.

1375 Molli, G., Brogi, A., Caggianelli, A., Capezzuoli, E., Liotta, D., Spina, A., and Zibra, I.: Late Palaeozoic
1376   tectonics in Central Mediterranean: a reappraisal, Swiss Journal of Geosciences, 113,
1377   doi.org/10.1186/s00015-020-00375-1, 2020.

1379 Munzerová, H., Plomerová, J., and Kissling, E.: Novel anisotropic teleseismic body-wave tomography
1380   code AniTomo to illuminate heterogeneous anisotropic upper mantle: Part I —Theory and
1381   inversion tuning with realistic synthetic data. Geophys. J. Int. (2018) 215, 524–545, doi:
1382   10.1093/gji/ggy296, 2018.

1384 Nagel, T. J., Herwartz, D., Rexroth, S., Münker, C., Froitzheim, N., and Kurz, W.: Lu-Hf dating,
1385   petrography, and tectonic implications of the youngest Alpine eclogites (Tauern Window,
1386   Austria), Lithos, 170, 179–190, https://doi.org/10.1016/j.lithos.2013.02.008, 2013.

1388 Nussbaum, C.: Neogene tectonics and thermal maturity of sediments of the easternmost Southern
1389   Alps (Friuli are, Italy), unpublished PhD thesis Université de Neuchâtel, Switzerland, 2000.

1391 Paffrath, M. H., Friederich, W., and AlpArray & AlpArray-SWATH D Working Groups: Teleseismic P-
1392   waves at the AlpArray seismic network: Wave fronts, absolute traveltimes and traveltime
1393   residuals, Solid Earth, https://doi.org/10.5194/se-2020-189, this volume, 2021a.

1395 Paffrath, M. H., Friederich, W., Schmid, S.M., Handy, M.R. and AlpArray & AlpArray-SWATH D
1396   Working Groups: Teleseismic traveltime tomography of the greater Alpine region. Solid Earth,
1397   this volume, 2021b.

1399 Perry, H. K. C., Jaupart, C., Mareschal, J.-C., and Shapiro, N. M.: Upper mantle velocity-temperature
1400   conversion and composition determined from seismic refraction and heat flow, J. Geophys.
1401   Res., 111, B07301, doi:10.1029/2005JB003921, 2006.

1403 Pfiffner, O.A., Lehner, P., Heitzmann, P., Mueller, St., and Steck, A. (Eds.) : Deep Structure of the
1404   Swiss Alps: Results of NRP 20: Birkhäuser et al., Basel, 460pp., ISBN 3-7643 5254 X, 1997.

1406 Pfiffner, O. A., and Hitz, L.: Geologic interpretation of the seismic profiles in the Eastern Traverse
1407   (lines E1 – E3, E7-E9): eastern Alps, Chapter 9 in Pfiffner et al. (Eds.) Deep Structure of the Alps:
1408   Results of NRP 20, Birkhäuser et al., Basel, 73-100, 1997.

1409

1410 Picotti, V., and Pazzaglia, F. J.: A new active tectonic model for the construction of the Northern
1411   Apennines mountain front near Bologna (Italy), J. Geophys. Res., 113, B08412,
1412   doi:10.1029/2007JB005307, 2008.

1413

1414 Piromallo, C., and Morelli, A.: P wave tomography of the mantle under the Alpine-Mediterranean
1415   area. J. Geophys. Res., 108(B2), 2065, doi:10.1029/2002JB001757, 2003.

1416

1417 Pomella, H., Klötzli, U., Scholger, R., Stipp, M., and Fügenschuh, B.: The Northern Giudicarie and the
1418   Meran-Mauls fault (Alps, Northern Italy) in the light of new paleomagnetic and
1419   geochronological data from boudinaged Eo-Oligocene tonalites, Int. J. Earth Sci., 100, 1827–
1420   1850, doi:10.1007/s00531-010-0612-4, 2011.

1421

1422 Pomella H, Stipp M, and Fügenschuh, B.: Thermochronological record of thrusting and strike-slip
1423   faulting along the Giudicarie fault system (Alps, Northern Italy). Tectonophysics, 79:118–130,
1424   2012.

1425

1426 Qorbani, E., Bianchi, I., and Bokelmann, G.: Slab detachment under the Eastern Alps seen by seismic
1427   anisotropy, Earth and Planetary Science Letters, 409, 96-108,
1428   doi.org/10.1016/j.epsl.2014.10.049, 2015.

1429

1430 Ratschbacher, L., Frisch, W., Linzer, H.-G., and Merle, O.: Lateral extrusion in the Eastern Alps, part
1431   2: Structural analysis. Tectonics, 10(2), 257–271 https://doi.org/10.1029/90TC0 2623, 1991.

1432

1433 Ratschbacher, L., Dingeldey, C., Miller, C., Hacker, B. R., and McWilliams, M. O.: Formation,
1434   subduction, and exhumation of Penninic oceanic crust in the Eastern Alps: Time constraints
1435   from 40 Ar/39 Ar geochronology, Tectonophysics, 394(3), 155–170,
1436   https://doi.org/10.1016/j.tecto.2004.08.003, 2004.

1437

1438 Rawlinson, N., and Sambridge, M.: The Fast Marching Method: An Effective Tool for Tomographic
1439   Imaging and Tracking Multiple Phases in Complex Layered Media, Exploration Geophysics, 36:4,
1440   341-350, doi:10.1071/EG05341, 2005.

1441

1442 Rawlinson, N., Reading, A. M., and Kennett, B. L. N.: Lithospheric structure of Tasmania from a novel
1443   form of teleseismic tomography, J. Geophys. Res., 111, B02301, doi:10.1029/2005JB003803,
1444   2006.

1445

1446 Rosenberg, C. L.: Shear zones and magma ascent: A model based on a review of the Tertiary
1447   magmatism in the Alps, Tectonics, 23, TC3002, doi:10.1029/2003TC001526, 2004.

1448

1449 Rosenberg, C.L., and Kissling, E.: Three-dimensional insight into Central-Alpine collision: Lower plate
1450   or upper-plate indentation?, Geology, 41/12, 1219–122, doi:10.1130/G34584.1, 2013.

1451

1452 Rosenberg, C. L., Schneider, S., Scharf, A., Bertrand, A., Hammerschmidt, K., Rabaute, A., and Brun,
1453   J.-P.: Relating collisional kinematics to exhumation processes in the Eastern Alps, Earth-Science
1454   Reviews, 176, 311–344, doi.org/10.1016/j.earscirev.2017.10.013, 2018.

1455

1456 Scharf, A., Handy, M.R., Favaro, S., Schmid, S.M., and Bertrand, A.: Modes of orogen-parallel
1457   stretching and extensional exhumation in response to microplate indentation and roll-back
1458   subduction (Tauern Window, Eastern Alps), International Journal of Earth Sciences, 102, 1627-
1459   1654, doi.10.1007/s00531-013-0894-4, 2013.

1461 Schefer, S., Cvetković, V., Fügenschuh, B., Kounov, A., Ovtcharova, M., Schaltegger, U., Schmid, S.
1462   M.: Cenozoic granitoids in the Dinarides of southern Serbia: age of intrusion, isotope
1463   geochemistry, exhumation history and significance for the geodynamic evolution of the Balkan
1464   Peninsula, Int. J. Earth Sci. 100, 1181-1206, https://doi.org/10.1007/s00531-010-0599-x, 2011.

1466 Schertl, H.-P., Schreyer, W., and Chopin, C.: The pyrope-coesite rocks and their country rocks at
1467   Parigi, Dora Maira Massif, Western Alps: detailed petrography, mineral chemistry and PT-path
1468   Contrib. Mineral. Petrol. 108, 1-21, 1991

1470 Schmid, S. M., Pfiffner, O. A., Froitzheim, N., Schönborn, G., and Kissling, E.: Geophysical-geological
1471   transect and tectonic evolution of the Swiss-Italian Alps, Tectonics, 15, 1036-1064,
1472   doi.10.1029/96TC00433, 1996.

1474 Schmid, S. M., Fügenschuh, B., Kissling, E., and Schuster, R.: Tectonic map and overall architecture of
1475   the Alpine orogen. Eclogae geologicae Helvetiae 97, 93-117, doi.org/10.1007/s00015-004-1113-
1476   x, 2004.

1478 Schmid, S. M., Bernoulli, D., Fügenschuh, B., Matenco, L., Schefer, S., Schuster, R., Tischler, M., and
1479   Ustaszewski, K.: The Alpine-Carpathian-Dinaridic orogenic system: correlation and evolution of
1480   tectonic units. Swiss Journal of Geosciences, 101, 139-183, doi:10.1007/s00015-008-1247-3,
1481   2008.

1483 Schmid, S. M., Scharf, A., Handy, M. R., and Rosenberg, C. L.: The Tauern Window (Eastern Alps,
1484   Austria): a new tectonic map, with cross-sections and a tectonometamorphic synthesis. Swiss
1485   Journal of Geosciences, 106, 1-32, doi. 10.1007/s00015-013-0123-y, 2013.

1487 Schmid, S. M., Kissling, E., Diehl, T., van Hinsbergen D. J. J., and Molli, G.: Ivrea mantle wedge, arc of
1488   the Western Alps, and kinematic evolution of the Alps–Apennines orogenic system, Swiss
1489   Journal of Geosciences, 110, 581-612, doi.10.1007/s00015-016-0237-0, 2017.

1491 Schönborn, G.: Alpine tectonics and kinematic models of the central Southern Alps, Mem. Sci. Geol.
1492   Padova, 44, 229–393, 1992.

1494 Schönborn, G.: Balancing cross sections with kinematic constraints: The Dolomites (northern Italy),
1495   Tectonics 18, 527–545, doi.org/10.1029/1998TC900018, 1999.

1497 Schulmann, K., Lexa, O., Vojtech J., Lardeaux, J. M., and Edel, J. B.: Anatomy of a diffuse cryptic
1498   suture zone: An example from the Bohemian Massif, European Variscides, Geology, 42, 275–
1499   278, doi:10.1130/G35290.1, 2014.

1501 Seghedi, I., and Downes, H.: Geochemistry and tectonic development of Cenozoic magmatism in the
1502   Carpathian–Pannonian region, Gondwana Research, 20, 655-672, doi:10.1016/j.gr.2011.06.009,

2011.

Seghedi, I., Ersoy, Y.E., and Helvacı, C.: Miocene–Quaternary volcanism and geodynamic evolution in the Pannonian Basin and the Menderes Massif: A comparative study, Lithos 180–181, 25–42, doi.org/10.1016/j.lithos.2013.08.017, 2013.

Serpelloni, E., Vannucci, G., Anderlini, L., and Bennett, R. A.: Kinematics, seismotectonics and seismic potential of the eastern sector of the European Alps from GPS and seismic deformation data, Tectonophysics 688, 157–181, dx.doi.org/10.1016/j.tecto.2016.09.026, 2016.

Serretti, P., and & Morelli, A.: Seismic rays and traveltime tomography of strongly heterogeneous mantle structure: application to the Central Mediterranean, Geophys. J. Int., 187, 1708–1724, doi: 10.1111/j.1365-246X.2011.05242.x, 2011.

Shito, A., Karato, S., Matsukage, K., N., and Nishihara Y.: Towards Mapping the Three-Dimensional Distribution of Water in the Upper Mantle from Velocity and Attenuation Tomography, Geophysical Monograph, 168, 225-236, DOI: 10.1029/168GM17, 2006.

Singer, J., Diehl, T., Husen, S., Kissling, E., and Duretz, T.: Alpine lithosphere slab rollback causing lower crustal seismicity in northern foreland, Earth and Planetary Science Letters, 397, 42–56, doi.org/10.1016/j.epsl.2014.04.002, 2014.

Smye, A. J., Bickle, M. J., Holland, T. J. B., Parrish, R. R., and Condon, D. J.: Rapid formation and exhumation of the youngest Alpine eclogites: A thermal conundrum to Barrovian metamorphism, Earth and Planetary Science Letters, 306(3–4), 193–204, https://doi. org/10.1016/j.epsl.2011.03.037, 2011.

Spada, M., Bianchi, I., Kissling, E., Piana Agostinetti, N., and Wiemer, S.: Combining controlled-source seismology and receiver function information to derive 3-D Moho topography for Italy, Geophys. J. Int., 194, 1050–1068, doi: 10.1093/gji/ggt148, 2013.

Spakman, W., and Wortel, M.J.R.: Tomographic View on Western Mediterranean Geodynamics, in: The TRANSMED Atlas, The Mediterranean Region from Crust to Mantle, edited by: Cavazza, W. et al., Springer, Berlin, Heidelberg, 31-52, https://doi.org/10.1007/978-3-642-18919-7_2, 2004.

Speranza, F., Villa, I.M., Sagnotti, L., Florindo, F., Cosentino, D., Cipollari, P., and Mattei, M.: Age of the Corsica–Sardinia rotation and Liguro–Provençal Basin spreading: new paleomagnetic and Ar/Ar evidence, Tectonophysics, 231-251, https://doi.org/10.1016/S0040-1951(02)00031-8, 2002.

Stipčević, J., Tkalčić, H., Herak, M., Markušić, S., and Herak, D.: Crustal and uppermost mantle structure beneath the External Dinarides, Croatia, determined from teleseismic receiver functions, Geophysical Journal International, 185(3), 1103–1119. doi:10.1111/j.1365-246x.2011.05004.x, 2011.

1548 Stipčević, J., Herak, M., Molinari, I., Dasović, I., Tkalčić, H., & Gosar, A.: Crustal thickness beneath the
1549   Dinarides and surrounding areas from receiver functions, Tectonics, 37,
1550   doi.org/10.1029/2019TC005872, 2020.
1551
1552 Sun, W., Zhao, L, Malusà, M.G., Guillot, S., Fu, L.-Y.: 3-D Pn tomography reveals continental
1553   subduction at the boundaries of the Adriatic microplate in the absence of a precursor oceanic
1554   slab. Earth and Planetary Science Letters 510, 131–141, 2019.
1555   https://doi.org/10.1016/j.epsl.2019.01.012
1556
1557 Tesauro, M., Kaban, M. K., and Cloetingh, S. A. P. L.: EuCRUST-07: A new reference model for the
1558   European crust, Geophysical Research Letters, 35(5), doi:10.1029/2007gl032244, 2008.
1559
1560 Ustaszewski, K., Schmid, S. M., Fügenschuh, B., Tischler, M., Kissling, E., and Spakman, W.: A map-
1561   view restoration of the Alpine–Carpathian–Dinaridic system for the Early Miocene, Swiss J.
1562   Geosci., 101, 273–294, doi: 10.1007/s00015-008-1288-7, 2008.
1563
1564 Verwater, V. F., Le Breton, E., Handy, M. R., Picotti, V., Najafabadi, A.J., Haberland, C.: Neogene
1565   kinematics of the Giudicarie Belt and eastern Southern Alpine orogenic front (Northern Italy),
1566   Solid Earth, doi: org/10.5194/se-2021-19, 2021, this volume.
1567
1568 van der Meer, D. G., Spakman, W., van Hinsbergen, D. J. J., Amaru, M. L., and Torsvik, T. H.:
1569   Towards absolute plate motions constrained by lower-mantle slab remnants. Nat. Geosci.
1570   3, 36–40, 2010.
1571
1572 van der Meer, D. G., van Hinsbergen, D. J. J., and Spakman, W.: Atlas of the underworld: Slab
1573   remnants in the mantle, their sinking history, and a new outlook on lower mantle viscosity,
1574   Tectonophysics, 723, 309–448, doi.org/10.1016/j.tecto.2017.10.004, 2018.
1575
1576 van Hinsbergen, D. J. J., Torsvik, T. H., Schmid, S. M, Matenco, L. C., Maffione, M., Vissers, R. L .M.,
1577   Gürer, D., and Spakman, W.: Orogenic architecture of the Mediterranean region and kinematic
1578   reconstruction of its tectonic evolution since the Triassic. Gondwana Research 81, 79-229,
1579   https://doi.org/10.1016/j.gr.2019.07.009, 2020.
1580
1581 von Blanckenburg, F., and Davies, J. H.: Slab breakoff: A model for syncollisional magmatism and
1582   tectonics in the Alps, Tectonics, 14, 120-131, doi.org/10.1029/94TC0205, 1995.
1583
1584 Waldhauser, F., Lippitsch, R., Kissling, E., and Ansorge. J.: High-resolution teleseismic tomography of
1585   upper-mantle structure using an a priori three-dimensional crustal model, Geophysical Journal
1586   International, 150, 403–414, doi.org/10-1046/j.1365-246X.2002.01690.x, 2002.
1587
1588 Wortel, M., J., R., and Spakman, W.: Subduction and Slab Detachment in the Mediterranean-
1589   Carpathian Region: Science, 290, 1910-1917, doi: 10.1126/science.290.5498.1910, 2000.
1590
1591 Zahorec, P., Papčo, J., Pašteka, R., Bielik, M., Bonvalot, S., Braitenberg, C., Ebbing, J., Gabriel, G.,
1592 Gosar, A., Grand, A., Götze, H.-J., Hetényi, G., Holzrichter, N., Kissling, E., Marti, U., Meurers, B.,
1593 Mrlina, J., Nogová, E., Pastorutti, A., Salaun, C., Scarponi, M., Sebera, J., Seoane, L., Skiba, P., Szűcs,

1594 E., and Varga, M.: The first pan-Alpine surface-gravity database, a modern compilation that crosses
1595 frontiers. Earth Syst. Sci. Data, 13, 2165–2209, 2021, https://doi.org/10.5194/essd-13-2165-2021
1596
1597 Zhao, L., Paul, A., Guillot, S., Solarino, S., Malusá, M., Zheng, T., Aubert, C., Dumont, T., Schwartz, S.,
1598   Zhu, R., Wang, Q.: First seismic evidence for continental subduction beneath the Western Alps.
1599   Geology, 43; 9, 815–818, 2015. doi:10.1130/G36833.1
1600
1601 Zhao, L., Paul, A., Malusà, M. G., Xu, X., et. al.: Continuity of the Alpine slab unraveled by high-
1602   resolution P wave tomography, Journal of Geophysical Research, Solid Earth, 121(12), 8720–
1603   8737, doi:10.1002/2016jb013310, 2016.
1604
1605